UNIVERSITÀ DEGLI STUDI DI CATANIA

IN CONVENZIONE CON

UNIVERSITÀ DEGLI STUDI DI PALERMO

DOTTORATO DI RICERCA IN

SCIENZA DEI MATERIALI E NANOTECNOLOGIE - XXXI CICLO

VALENTINA LOMBARDO

HIGHLY CONDUCTIVE POLYMER FILMS WITH TUNABLE OPTICAL PROPERTIES OBTAINED BY IN-SOLUTION DOPING OF PEDOT:PSS

TUTOR: PROF. ANTONIO TERRASI

CO-TUTOR: DR. ROSARIA A. PUGLISI

COORDINATORE: PROF.SSA MARIA GRAZIA GRIMALDI

TESI PER IL CONSEGUIMENTO DEL TITOLO DI DOTTORE DI RICERCA

To Jenny

Table of Content

Motivations and Outline

Poly(3,4-ethylenedioxythiophene)-poly(styrene sulfonate), PEDOT:PSS, is one of the most interesting and versatile conductive polymers, CPs. Its intrinsic conductivity and easy tunability of the electrical properties, with a high processability due to fast and low-cost methods of deposition, make this material one of the main protagonists of the organic electronics. In the last decades, an intense scientific production has led scientists toward the understanding of its mechanism of conduction, thus supplying new ways for the improvement of electrical performances. This has paved the way for various technological applications in different fields, from renewable energies to medicine.

Nevertheless, this material still keeps offering new opportunities. For instance, the scientific production has shown a lack about the potentiality of the secondary doping of PEDOT:PSS with sulfuric acid. Indeed, most of the works published in this area, have reported a description of the effects due to post-deposition treatment by H_2SO_4, never lingering on the effective consequences of an in-solution acid doping. Hence, the first aim of this work was to fill this gap by investigating the effects of the direct acidification of PEDOT:PSS solution, finally discovering new chances from this method. In the next chapters, it will be presented a step-by-step study, which not only will elucidate about the mechanism of the secondary doping by sulfuric acid, but new insights and novel use proposals of this material will be also offered.

Chapter 1 will give a background about the organic electronics and conducting polymers, i.e. that family of the material science to which PEDOT:PSS belongs. A short history of the birth of PEDOT will be presented, its first uses in technology and the causes which have led to the production of PEDOT:PSS in the form that we know today. An overview on the conduction mechanism dominating the electric performance will be supplied with some of the most used secondary doping methods. In other words, this chapter will be a guide for understanding the successive explanations, comments and results given in Chapters 2-4.

In Chapter 2, the investigation of annealing influence on the electric response of thin PEDOT:PSS films will be explored. It will be seen that the electrical conductivity of the pristine polymer in not a real intrinsic feature of the material, but it can be related instead to its thickness and its "thermal history". This unexpected behaviour will be explained by the solvent evaporation mechanism and the variation of water content as a consequence of the thermal treatment. A direct influence of the annealing environment and temperature on the electrical performances will be also shown and discussed.

Chapter 3 will introduce the effects of the direct addition of sulfuric acid, showing that it leads to a separation phase of the conducting species from the rest of solution. Films obtained with this procedure will report a higher electrical conductivity with respect to the untreated polymer as well as a good transparency in most of the electromagnetic spectrum. In order to correlate both electrical and optical properties, the Haacke's figure of merit will be supplied for the first time in the history of this material. This parameter will be used for estimating the balance between these two characteristics in order to offer an easier application placement in the wide technological panorama.

Chapter 4 will present that the PEDOT:PSS acidification until its saturation level leads to a highly conductive, flexible paste. It will be supplied a description about the mechanism ruling this process, the thermal and ambient effects related to the annealing conditions and new insights about the morphology and arrangement obtained with this strategy, thus showing the great potentiality offered from this "new face" of PEDOT:PSS .

Finally, the reader will also find a Chapter 5, which offers an example of a possible application of the developed conductive polymer. It will be presented a synthesis protocol to fabricate quasi-1D nanostructures through block copolymer self-assembly (BCP-SA), realized by novel deposition solvents as alternative to toluene, classically used in this process. The effects on the BCP-SA due to the new solvents, i.e. the ethyl acetate and the tetrahydrofuran, will be presented through a study carried by SEM analysis and images elaboration made by a suitable software. The results will show promising outcomes for the polymer solutions obtained with ethyl acetate, in terms of uniformity of geometrical features, ordered areas extension and homogeneity of the pattern obtained, making this chemical a good alternative to the toluene for future perspective.

Chapter 1

Overlook on polymers in the organic electronics world

This Chapter introduces the basic concepts of π-conjugated polymers with a particular emphasis on the material studied in this thesis, the conducting polymer blend PEDOT:PSS. A background about the birth of this widely known material is given in order to well understand the requirements that it has to meet in different fields of the materials science and technology. Insights about the conduction mechanisms which rule the electrical behaviour, are explained and, finally, a summary of the most common secondary doping methods and their effects on the PEDOT:PSS blend is commented.

1.1 – Organic Electronics

The electronic field has been dominated for many years by the physics of the inorganic semiconductors and their production. Silicon, in particular, has been the main protagonist, thanks to its wide availability, moderate manufacturing cost and low toxicity. However, in the last decades, the traditional electronic has been joined by a new branch of the material science: organic electronics. This novel field is based on design, synthesis, characterization and fabrication of small organic molecules or polymers which exhibit appreciable electrical performances. The first clue that soft and plastic materials were overlooking to the electronics was in 1970s, with the discovery that the electrical conductivity of polyacetylene film can be modified of several orders of magnitude by chemical doping [1,2]. From that

moment, organic electronics has introduced and involved new concepts for the modelling and processing of the electronic devices.

The physical principles which rule the transport mechanism in the organic electronics are different with respect to those of the inorganic crystalline semiconductors. Indeed, the electrical charges in soft matters are ruled by the hopping transport mechanism which develops from disordered molecular structures, polaronic nature of the electric charge and the exciton binding energy [3]. These characteristic features, although at the base of the polymer electrical conductivity, cause low charge mobility which thus can be significantly lower with respect to those of crystalline solids. However, one of the greatest advantages of small organic compounds and polymers is the considerable versatility of their physical properties. Indeed, some parameters, such as conductivity and the electrical and optical band gaps, can be finely tuned from time to time by easy chemical modifications. Although they do not achieve the same electrical features of metals and the most common inorganic semiconductors, this potentiality allows the customization of their electrical performances according to their intended use. Aside this versatility, polymer and organic compounds also give very special advantages in their processing. In fact, inorganic materials are obtained by very slow deposition methods and require expensive and complex equipment with high maintenance costs, such as sputtering or thermal evaporation, as well as Chemical Vapour Deposition, Atomic Layer Deposition or Molecular Beam Epitaxy. Vice versa, one of the greatest advantages of conductive polymers and organic compounds is mainly due to their versatile, cost-effective and easy processability. This praises a wide path of choices for deposition methods, industrially scalable and largely cheaper with respect to those used for the inorganic materials. Among the wide variety of techniques, it is worth to remind the most used, such as spin

coating, drop casting, Langmuir-Blodgett, spreading knife, etc. All these approaches lead to thin, uniform and continuous carbon-based films. Interestingly, these methods can be also used on structured surfaces where, because of the presence of some fragile features, hard and aggressive deposition methods, e.g. sputtering, are not recommended.

Unlike crystalline inorganic solids, a special appealing is also due to the mechanical properties achievable by polymers and organic materials. In particular, they overcome the intrinsic brittleness limits of common inorganic oxides, e.g. ITO, since transparent and conductive films with a great robustness and flexibility can be obtained. Thanks to all of these characteristics mentioned above, i.e. chemical and physical versatility, easy manufacturing, low processing-cost and great mechanical features, organic electronics have powerfully become a part of new technologies in the materials science and in consumer products.

1.2 Conducting Polymers

In the very beginning, polymers have caught not only a scientific interest but have also started a new industrial era. This revolution has begun in the 1909, when Belgian chemist Leo Hendrik Baekeland entirely synthesized the first plastic material, belonging to the group of the phenolic resins. A few years later, Baekeland putted in the market this thermosetting plastic with the name of Bakelite. In 1912, the Swiss Jacques Brandenberger produced the cellophane by the viscose, in its turn derived from cellulose. In the 1950s, Bayer definitively established the collaboration between polymer chemistry and industrial chemistry, producing the first synthetic rubber. After about 15 years, many plastic materials

have been produced on industrial scale, including polyvinyl chloride (PVC), used to make pipes, cladding panels and insulating sheaths for electric cables. These polymers mentioned so far have been known and used as resins, textiles and rubbers and in virtue of their insulating properties.

About the conducting polymers, of which there are few traces of their use in 1930 for prevention of the corona discharge, we have to wait until 1977 for discovering that polymers can exhibit very interesting electrical properties and that these can be modified by chemical treatments [2]. This outstanding discovery has brought Mac Diarmid, Heeger and Shirakawa to be awarded the Nobel Prize in Chemistry in 2000. From that moment, an intensive work and many efforts were made for understanding the conduction mechanisms involving in polymers. Several studies have identified that the key of their electrical conductivity lies in their structure.

1.2.1 – Structures and Properties

In order to easily understand the mechanisms which allow charge transport in the polymers, it is worth to begin from the molecular bands formation described by the molecular orbital (MO) theory. It is possible to start by considering the simplest case in which two atoms interact between each other, thus forming a bond. The linear combination between the atomic orbitals of these two interacting atoms arise the formation of a bonding and an antibonding orbital. In the same way, N interacting atoms, where N can be considered infinite, lead to the formation of N molecular orbitals which are split in energy: some of them have energy lower than the initial orbitals, while the others are higher. These sets of overlapping orbitals thus give place to the formation of two energy bands, which are equivalent to the valence and conduction ones normally related to the electronic structure of a

semiconductor. This simple explanation of the electronic bands is strictly related to the molecular structure of an organic material. Indeed, the electrical behaviour is closely related to the specific bonds configuration in the molecule. The formation of a valence and a conduction band takes place in a polymer when a carbon structure exists in which a single C-C bond is alternating with a double one along the polymer chain. In other words, the fundamental requirement for a polymer to be potentially conductive is that it has to have a conjugation between its repetitive units, as shown in Fig. 1.1:

Fig. 1.1: Molecular structure of the polyacetylene, the simplest example of a conductive polymer with a conjugated structure.

This structure can be understood by considering the hybridization process of C-atom. The electronic ground state of a carbon atom can be described as $1s^2 2s^2 2p^2$, but this would suggest that the C atom can form only a pair of bonds with its neighbours, having only two electrons available in its most external shell, Fig. 1.2a. However, our common experience suggests that carbon can form up to four bonds, as in the CH_4 molecule. This happens since the four valence electrons in the most external atomic level of the C atom combine to each other toward hybridized structure when forming covalent bonds. The combination of the external *s* and *p* orbitals leads to three possible configurations, labelled with sp^1, sp^2 and sp^3, which give respectively single, double and triple bonds. In the case of a conjugated polymer, the "electrical repetitive units" are made by 2n+1 atoms with sp^2 hybridization, Fig.1.2b.

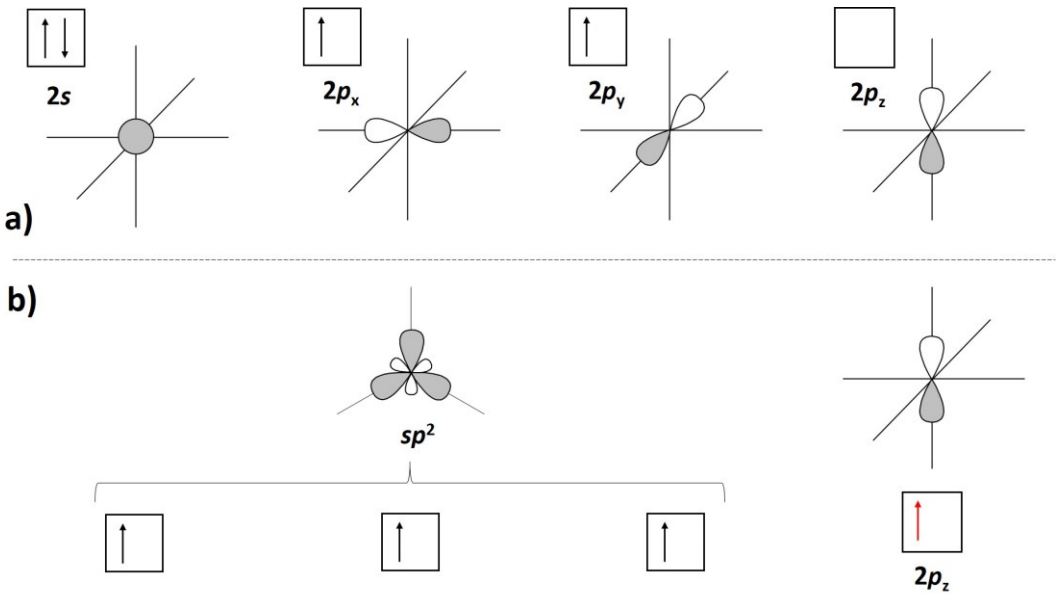

Fig. 1.2: Schematic representation of the hybridization process occurring in C atoms: a) in its ground state, 2*s* and two 2*p* orbitals of the most external shell combine with each other forming b) three hybridized sp^2 orbitals which lay on the same plane, creating three angles of 120° each, while non-hybridized $2p_z$ orbital lays perpendicular to the plane of sp^2.

In this configuration, atoms are covalently bound by σ orbitals and all C atoms lay on the same plane, Fig. 1.3a. These bonds constitute the skeleton of the molecule and do not take part directly to the conduction mechanism. Vice versa, the total or partial overlapping of the non-hybridized p_z orbitals of the sp^2 C atoms form a network of weaker π-bonds, in which electrons are delocalized and can easily move from one atom to neighbours, Fig. 1.3b. In other words, while σ orbitals can be considered the brick of the molecular structure, π electrons are responsible of the electrical conduction phenomenon of the specimen.

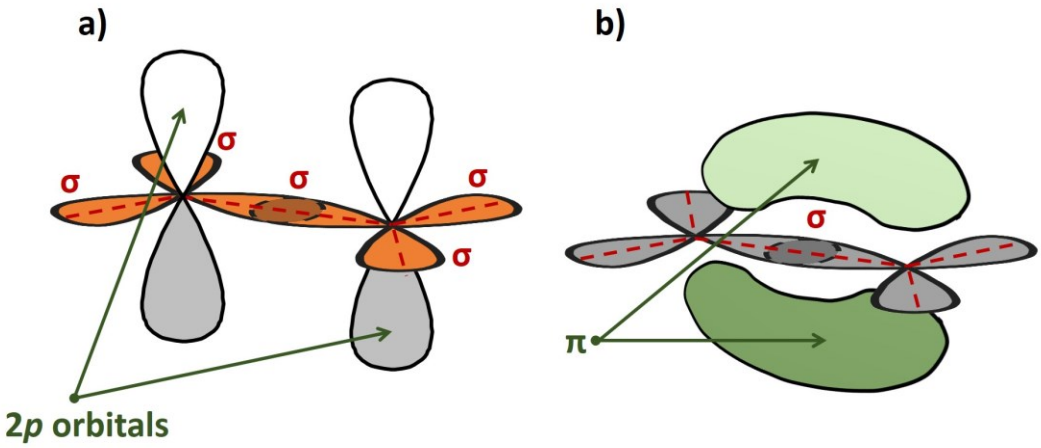

Fig. 1.3: Schematic representation of the in which are evidenced, respectively, a) σ and b) π bonds formed on two sp^2 hybridized C carbons.

According to the Bloch theory, if the bond length between an atom and its neighbours have the same value in all directions, the electron transport properties can be related to a metal-like behaviour. Indeed, the solid formed by the atoms constituting the conductive molecule has half-filled shells which thus determine half-filled bands. However, considering the structure of the polymeric chain described so far, in the simplest case such as the polyacetilene molecule (Fig. 1.1), the backbone is made by alternating single and double bonds. Since the strength of a double bond is higher than single one, the C-C length will be different in the two cases, being shorter in the first. In this way, the final energy of the whole system is minimized and this modification in the molecule structure, in which the length of the bonds is alternatively different, is known as Peierls distortion. This causes a split in energy giving place to two sub-bands: a π valence band, completely occupied and in which the most external level corresponds to the highest occupied molecular orbital (HOMO), and an empty π* conduction band, normally identified with the value of its lowest unoccupied molecular orbital (LUMO). These two

bands are separated by an energy gap, Eg, which can cover several values, most of time in the range between 1.5 and 3.5 eV. In this case, the specific values of these three characteristic features are determined by the structure of the conjugated units, the conjugation length and the atoms constituting the repetitive units. As a general consideration, it is intuitive to say that the more extended the conjugation length is, the smaller the energy gap between HOMO and LUMO in the polymer.

1.2.2 – Polymer Doping

A part the specifics given by the atoms component the polymer and their arrangement into the chain, the energy gap of a pristine π-conjugated macromolecule can be tuned by the doping process. However, this cannot be explained with the mechanism normally associated to the inorganic semiconductors. Indeed, for these latter the doping proceeds by the substitution of an electron-donating or -accepting atom inside the atomic positions of the original crystal lattice. Because of this substitution, the electrical doping of an inorganic semiconductor is basically irreversible. Differently, in the organic materials, it takes place by a completely different path. The main concept of the organic doping is that a given specie is able to accept or to donor electrons to/from the polymer chain but, in the case of the organic materials, the dopants have inter-chains position. Similarly to the inorganic semiconductors, the organic doping can be both n-type (electron donating), or p-type (electron accepting) and it is used for allowing the insulator-to-conductor transition in polymer. Dopants can be charged atoms or molecules and must be able to donor or accept charges to/from the polymer backbone. It is worth to note that, in this case, dopant is not covalently bounded to the polymer, but it interacts to the chain through electrostatic (or Coulomb)

interactions. Instead, when dopant is covalently bound to the chain, the doping is known as self-doping. Describing it in other words, the polymer electrical doping can be understood as a reversible oxidation/reaction process. Generally, this chemical doping can be carried by oxidising (such as Br_2, SbF_5, H_2SO_4) or reducing agents (alkali metals) or via electrochemical reaction, i.e. by applying an appropriate bias to the material. Whatever the doping process is, the charges formation in the polymer chain and then their intra and inter-transport phenomena can be described in the same way: from an electrical point of view, a polymer doping creates new energy levels in between the valence and the conduction bands.

The gap between the localized levels depends on the polymeric system since, according to the electrical structure, it can lead to a bipolaron or soliton charge. Considering, for instance, the oxidation process of the poly-p-phenylene, PPP, in Fig. 1.4, when a less bound electron is subtracted from a p_z orbital, it leaves a radical and a positive charge along the chain. This situation is called polaron, and it is generally accompanied by a structural distortion which results from the π-bonds rearrangement. This last one occurs for allowing the stabilization of the new molecular configuration.

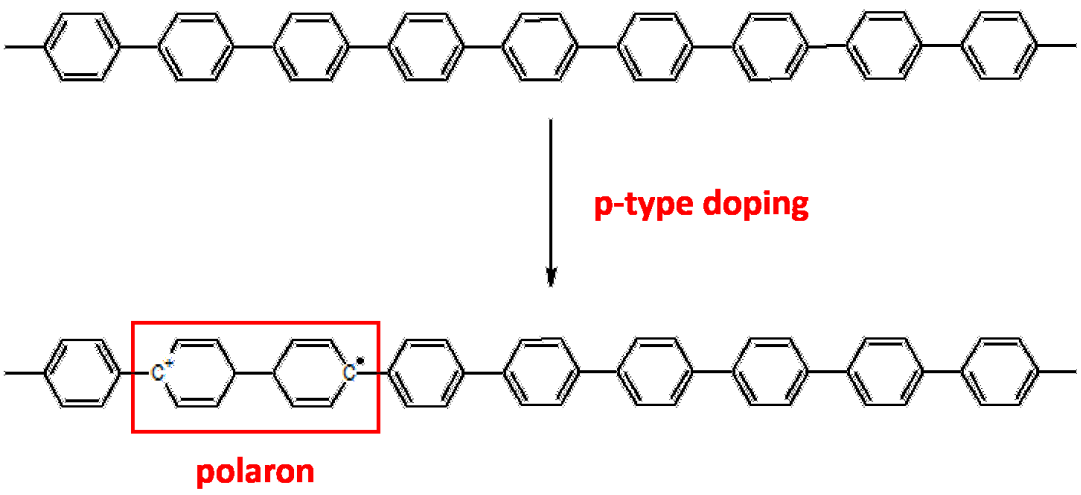

Fig. 1.4: Representation of the p-type doping on a PPP chain which leads to the formation of a polaron, i.e. ion radical associated to the distortion of the molecule and a change in the single-double bonds arrangement.

This new system leads the structure toward a major planarity next to the site in which the charge is generated and it is also accompanied to a local permutation of the alternating single-double bonds. In other words, this new arrangement in the molecule can be described with the coupling between electrons and phonons, which leads to a structural distortion.

As a consequence, this new configuration causes the formation of new energy levels placed symmetrically with respect to the edges of both valence and conduction bands, as schematized in Fig. 1.5.

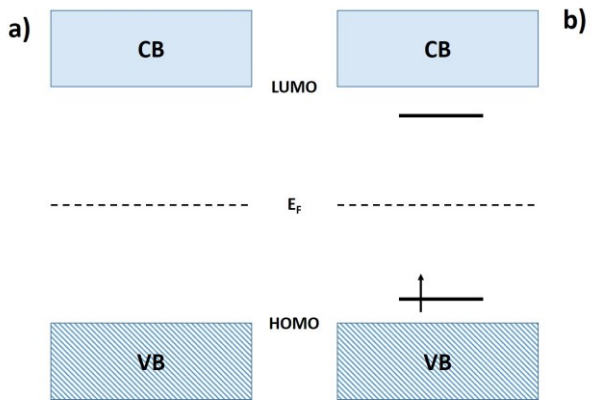

Fig. 1.5: Sketch of the band structure in a polymeric chain in its a) neutral state and b) after the formation of a polaron.

The further oxidation process on the same molecule leads to the formation of a bi-cation and, in this case, two paths are possible: in the first one, a second electron is removed in a new site, i.e. a neutral region of the chain, far away from the first one generated, Fig. 1.6. Alternatively, the second charge is generated very close to the first polaron (Fig. 1.7).

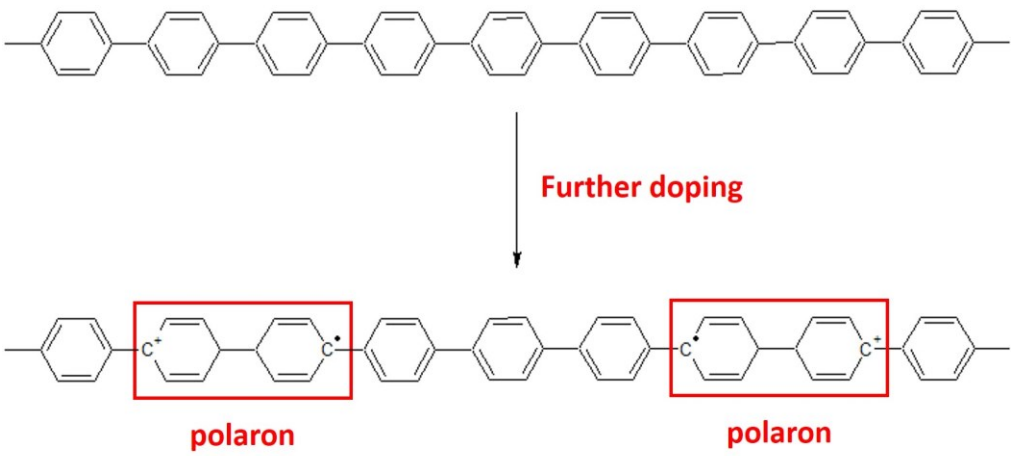

Fig. 1.6: Representation of a further p-type doping on a PPP chain, occurring in a different part of the molecule with respect to the site of the first doping. Two independent polarons are obtained.

In the first case, the two radical-cations do not interact and give place to new energy levels in the E_g, which are degenerate with thoses left from the first polaron, Fig. 1.8a. Vice versa, in the latter condition, the second free electron is removed from the radical already formed, i.e. on the same portion of the molecule in which the first polaron was. In this way, it is possible to observe the formation of a bi-cation that is formed by two positive charges coupled by a lattice distortion. This phenomenon is called electron-phonon coupling and corresponds to a bipolaron.

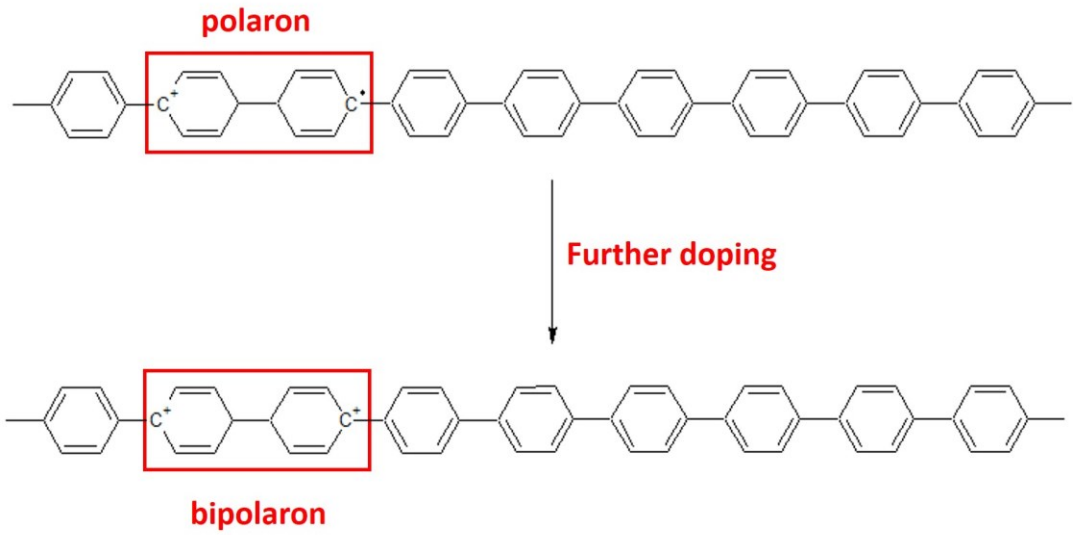

Fig. 1.7: representation of a further p-type doping on a PPP molecule, occurring in the same part of the chain with respect to the first doping event. This leads to the formation of a bipolaron.

This second arrangement gives place to new levels symmetrically placed with respect to the half of the energy gap, farther away from the band edges than the case described above, Fig. 1.8b.

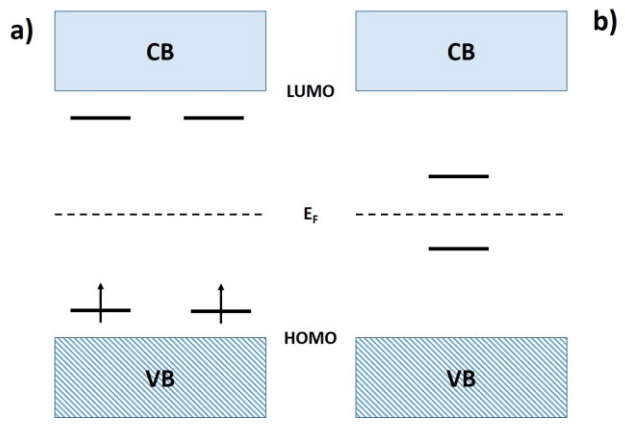

Fig. 1.8: Sketch of the band structure along a polymeric chain after the formation of a) two independent polarons and b) a bipolaron.

The mechanism seen so far describes the p-type doping of conjugated polymer. The same concept can be applied in the case of n-type doping along the chain, but this has the effect of an electron enrichment of the molecule. The new configuration of the bands can be described by new energy states created within the band gap and filled with the introduced negative charges. However, since this discussion is not functional to the topics that will be presented hereinafter, no further details will be given. Instead, the p-type doping is the main concept which involves the polymer studied in this thesis: poly(3,4ethylenedioxythiophene)-poly(styrene sulfonate), PEDOT:PSS.

1.3 – PEDOT:PSS

PEDOT:PSS is a relative young member of the conducting polymers family and one of the most studied and used. It is commercially available in the form of a deep-blue opaque water dispersion and widely available in the chemical market.

The first aqueous dispersion has been initially licenced and commercialized with the trade name of Baytron by Bayer AG, then by Starck, more recently by Heraeus, selling it with the trade name of Clevios, and finally by Sigma-Aldrich (Merck). PEDOT:PSS was also produced for large-scale printing by Agfa, with the trade name of Orgacon [4]. This composite is widely used as a p-type semiconductor [5–7] in different fields, spacing from solar cells, electrochemical cells, devices for energy storage and stretchable electronics [4]. Most of works reported in literature is focused to different procedures for improving the performance of the entire aqueous blend and for understanding the mechanisms which rule its conductivity. However, the history of this material and its physical properties, also involving the electrical conductivity, are more complex.

1.3.1 – Poly(3,4-Ethylenedioxythiophene)

Until early 80s, intense efforts have been made for improving the conductivity of many conjugated polymers, such as polyacetylene, poly(p-phenylene), polyaniline, polypyrrole and polythiophene (Fig. 1.9). This last one had a great appealing thanks to its electrical performances but presented a considerable instability to the environment. Indeed, free C_β in positions 3 and 4 in the structural unit have a high reactivity and give to this macromolecule such an instability to air, moisture and chemical agents.

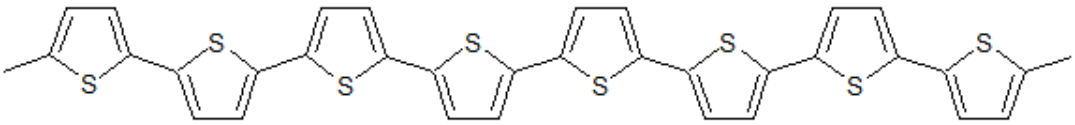

Fig. 1.9: Polythiophene.

In order to improve the environmental stability of this molecule, with maintaining high conductivity, the strategy was to substitute the position C_β with different chemical groups. The most successful product obtained was 3,4-ethylenedioxythiophene [8], EDOT in Fig. 1.10, which represents both the starting monomer and the repetitive unit of PEDOT. Its synthesis from EDOT was reported for the first time in 1988, when Jonas and co-worker deposited their first patent. Here oxidant polymerizations of EDOT to PEDOT arises in presence of some iron salts-based catalyst in acetonitrile [8,9]. The polymerization occurs through both alfa positions and reaction leads to the molecule represented in Fig. 1.10.

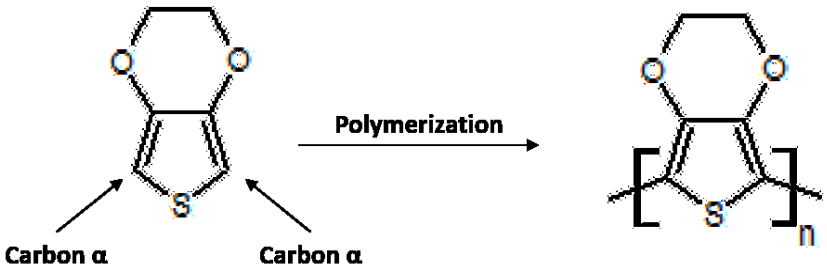

Fig. 1.10: On the left, EDOT molecule is the starting monomer used for the oxidant polymerization of PEDOT, on the right.

Once polymerized, PEDOT was described as a dark blue powder with a conductivity ranging between 5 and 10 S/cm [10]. This reaction product was also insoluble and infusible, thus manifesting a chemical behaviour typically associated to cross-linked polymers. However, in the case of PEDOT, this cross-linkage is forbidden by its own structure since the oxyethylene ring bonded to the C_β prevents any reaction of networking. Therefore, the fact that this powder cannot be melt or re-dispersed in any solvent indicates a great stability, overcoming its ancestor polythiophene and other widely used polymers, such as polypirrole [10]. Seen its

great potentiality, PEDOT was considered a valid alternative to the metals as antistatic coating for preventing damages of breakable electronic components susceptible to high voltage cross [11,12].

1.3.2 – Poly(3,4-Ethylenedioxythiophene)-Poly(Styrene Sulphonate)

Hitherto, the birth of PEDOT and its first use in technology have been seen. However, once polymerized, this material cannot be easily processed. If on one side, the absence of reactivity to both heat and chemical agents awards a very special stability to the environment, on the other hand, the insolubility in most of common solvents affects its processability, thus limiting technological use. In order to overcome this aspect, Jonas et al. developed a way for preparing PEDOT as a water suspension [11,13]. This strategy provides a synthesis path through oxidative polymerization, in which EDOT is made polymerized in presence of polystyrene sulfonic acid in water and in presence of a strong oxidizing agent, e.g. potassium persulfate [14,15]. This approach leads to the common aqueous and well-known poly(3,4-ethylenedioxythiophene)-poly(styrene sulfonate) blend, i.e. PEDOT:PSS, Fig. 1.11.

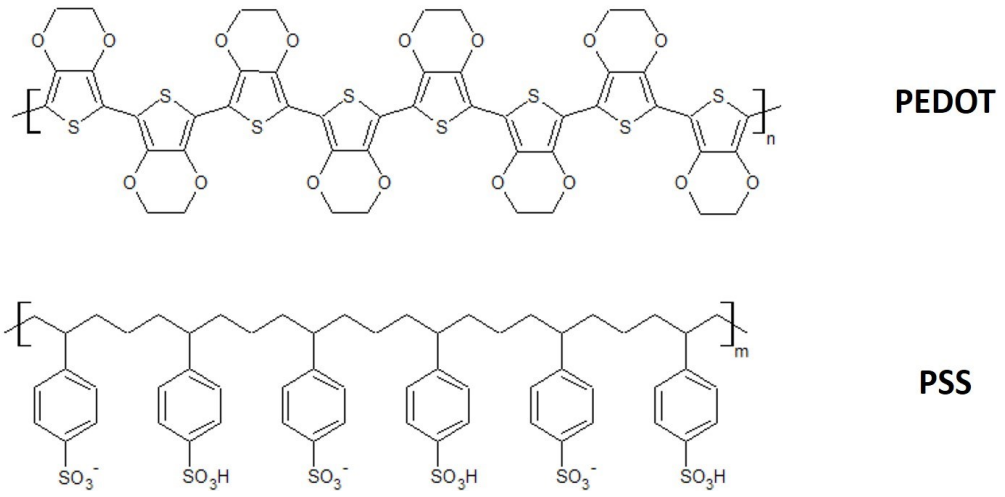

Fig. 1.11: Structure of the two moieties of the poly(3,4-ethylenedioxythiophene)-poly(styrene sulfonate) blend.

The presence of PSS is the key-point of PEDOT processability, since the negative sulfonic groups along PSS chains stabilize the positive charges along the PEDOT molecules. Moreover, the Coulomb interactions established between the styrenic part and PEDOT keep this last one suspended into the aqueous medium.

The overall PEDOT:PSS complex consists of PSS chains with which PEDOT oligomers adhere, coiling up to form a tertiary structure [16–19]. In order to guarantee the right charge-balance between these two species, PSS chains have to be longer and in larger amount with respect to the PEDOT ones. For this reason, the PEDOT/PSS ratio usually is in a range of 1:2 up to 1:20, depending on the intended use, and this suspensions are stable in water for solid content up to 2% wt. [11].

PEDOT:PSS can be easily processed, allowing for the formation of continuous, uniform and smooth conducting thin films on either rigid and flexible substrates. Moreover, PEDOT:PSS films, with thickness in the order of hundreds of

nanometres, exhibit high transmittance in the visible range and even above 90% at 550 nm.

For preparing PEDOT:PSS as thin films, several cost-effective and fast solution-processing techniques can be used, such as spin-coating, doctor blade, spray deposition, inkjet printing, screen printing etc. Nevertheless, if on one side PSS gives a special easiness in the PEDOT:PSS manufacturing, on the other hand it is also the main responsible of the considerable lowering of the overall conductivity of the blend with respect to PEDOT alone. For instance, PEDOT/PSS ratios ranging from 1:2.5 to 1:20 imply conductivities from 1 to 10^{-5} S/cm, respectively [7]. This is not surprising if the dielectric-like behaviour of PSS is considered. When the polymer blend in spread on a surface, both conductive and dielectric species coexist as a solid layer. In this condition, PSS represents an electrical barrier which obstacles the charge transfer from one conductive portion to the others [10,11]. The electrical properties of the PEDOT:PSS aqueous blend are thus related to the PSS content in the original mixture. In general, a major content of the PSS in the blend leads to a less conductive product, but the real mechanisms of the electrical conductivity of PEDOT:PSS blend are still under an intense debate.

The conductivity of PEDOT:PSS composite surely depends on two main features, i.e. the mobility of charge carriers on one side, and the number of available mobile charge carriers on the other one. Stocker and collaborators [7], have reported that the charge carrier density is dependent on the PSS content, thus indicating that the mobility of the carriers plays the major role on the conductivity-dependence. Therefore, PSS would cause a sort of dielectric screening effect between the conductive portions of the global blend. This behaviour gives also some hints about the arrangement and morphology of the polymer blend. According to the literature [7], the in-solution PEDOT:PSS complex consists of PSS chains to which many

shorter PEDOT oligomers attach tightly, forming a stacked arrangement with the styrenic counter-ions. This ensemble forms a tertiary structure with a core of tangled PEDOT:PSS chains embedded in a hydrophilic shell of PSS, in a kind of micelle-like structure [20–23]. This arrangement between the two species is still retained also when the solution is spun onto a substrate [19]. The structure of a PEDOT:PSS film must be intended as formed by grains, sizing in the order of decades of nanometres and with elongated shape [3,24,25]. As reported from Nardes et al. [23,26], these grains arrange themselves in a pancake-like structure in which conducting PEDOT-rich particles are aligned in-plane and embedded in a quasi-continuous, dielectric PSS lamella, as shown in Fig. 1.12.

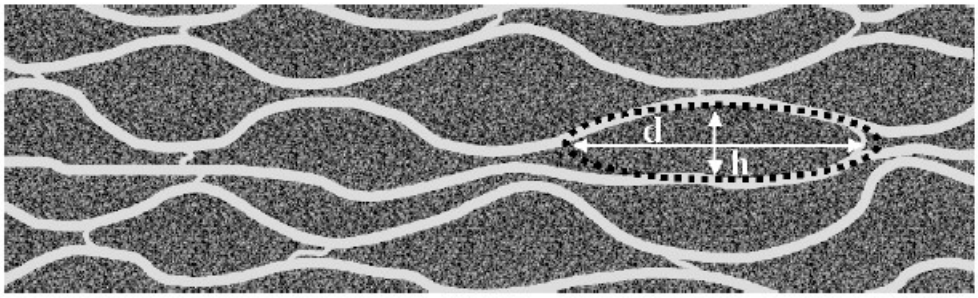

Fig. 1.12: Cross-sectional view of the schematic morphological model for PEDOT:PSS thin films derived from combined STM and X-AFM measurements. PEDOT-rich clusters (dark) are separated by lamellas of PSS (light). The PEDOT-rich lamellas are composed of several pancake-like particles as pictured by the dotted lines. The typical diameter *d* of the particles is about 20–25 nm and the height *h* is about 5–6 nm. Image reproduced from Ref. [23].

The overall electrical conductivity in PEDOT:PSS can thus take place through a percolation path between sites of highly conducting PEDOT:PSS complexes, with a conductivity of 2.3 S/cm, embedded in a matrix PSS-excess with a conductivity of 10^{-3} S/cm. This description is consistent with a hopping transport in a granular

disordered systems described by the Mott and Shklovskii model, in which the electrical conductivity is expressed as a function of the temperature, Equation 1 [23–28]:

$$\sigma(T) = \sigma_0 \exp\left[-\left(\frac{T_0}{T}\right)^a\right]$$

Equation 1

In the Equation 1, T_0 is a characteristic temperature and represents a measure of the potential barrier height that charge carriers have to overcome for conducting [23,26,28]. The pre-factor σ_0 is instead related to the intrinsic conductivity of the grains, the contribution of their size, their mean volume occupied in the material and so on [29]. Finally, the exponent α is the parameter relating to the transport process and can range from 0 to 1. Most critical α values are three, and each one indicates a different conductivity regime. In particular, α=1 indicates a nearest-neighbour hopping type (nn-H), thus meaning a thermally activated process. When grains size decreases, the exponent passes from the unity to almost 0.5 or 0.25. For α= 0.5, it is predicted a charging-energy limited tunnelling (CELT) model, also identified as 1D variable range hopping (1D-VRH), in which carriers tunnel between small conductive grains separated by insulating material. Finally, when α is 0.25, the equation describes a 3D-VRH model. In general, it can thus state that minor value of the α exponent indicates substantially a better conductivity.

Interestingly, the conductivity of the pristine PEDOT:PSS is not isotropic and can be distinguished in two mechanisms. It is found the in-plane conductivity overcomes the vertical one (across the film depth) of several orders of magnitude.

More in detail, while σ along the plane is ruled by the VRH mechanism, along the depth of the film a typical nn-H response is observed [23,26].

Moreover, in PEDOT:PSS thin films the conductivity-response can also be intended as a function of the film thickness and the thermal aging. Film thickness of hundreds of nanometres show a CELT-VRH borderline response also for very long thermal aging carried between 120 and 180°C. Vice versa, very thin film, in the order of 30-50 nm, has a response which falls in the nn-H model, since the film thickness becomes comparable to the grains size. Charges have to move in only one, parallel direction across a mono-layer conductive domains apart from each other by the dielectric medium and the macroscopic effect is a decrease of the electrical conductivity. Vice versa, thicker films contain much more conducting particles which enhance the percolation path, involving not just one layer of domains but also their near neighbours. However, for long thermal treatment at high temperature, conductivity passes from nn-H to CELT because the increase of the charges mobility [25,30].

In light of what explained so far, an intuitive strategy for improving the electrical conductivity of PEDOT:PSS is thus the removal of the dielectric portions, i.e. PSS, that surrounds the conducting PEDOT–PSS grains. Greco et al. [30], for instance, have observed that conductivity improves when free-standing PEDOT:PSS films are released in aqueous medium from their substrate. The solvent-effect which acts for PSS and not for the insoluble PEDOT domains, drags the styrenic chains in solution and leaves the conductive particles on the substrate [15]. This process, which is carried at room temperature, does not allow neither an actual re-arrangement of the conductive chains, which should require external heating, nor an improvement of percolation. Instead, the removal of the dielectric part leads to

the increment of the mobility of charge carriers, which consequently leads to an increase of the in-plane conductivity.

The electrical conductivity of the PEDOT:PSS blend can be also related to the synthesis technique and also to the counter-anion used. Thin PEDOT:PSS films synthesized by the electrochemical polymerization exhibit a conductivity of 80 S/cm, much higher than an analogous product obtained by the oxidative polymerization, which instead shows a σ of 0.03 S/cm [22]. This is because the PEDOT chains formed by the electrochemical polymerization take just the minimum amount of PSS counter-ion needed to attain charge neutralization, while any eventual excess of the styrenic reactant does not interact with the formed film. This mechanism leads to films having a higher concentration of PEDOT with respect to the anionic counter-part. In light of this, the electrochemical polymerization has two main effects. First of all, in the electropolymerized PEDOT:PSS, a single PSS chain interacts electrostatically over its length with many shorter PEDOT chains [21] and, secondly, the distance between adjacent PEDOT chains is small, facilitating the hopping of charges between PEDOT chains. This same effect is also achieved with substituting PSS with a smaller anion counter-part, such as tosylate, which leads to electrical conductivity up to 450 S/cm [21]. Vice versa, the chemically-prepared PEDOT:PSS contains an excess of the counter-anion, which is likely due to the micellar nature of the emulsion. In this case, an excess of PSS possibly surrounds the conductive grains, isolating them from the others [31,32]. In other words, the amount of dielectric part is less in the electrochemical polymerized films than in those blend obtained by chemical oxidative synthesis.

The approaches that were seen so far lead to the improvement of the electrical conductivity of PEDOT:PSS blend. Basically, they do not provide for the

intervention of any other chemicals, but here the main concept for enhancing the electrical performances is just based on the partial removal of the dielectric from polymer films. It should be intuitive that, when the dielectric PSS is partly suppressed from the blend, this leads to a specie which is more similar to the conductive PEDOT. As seen previously, the σ of PEDOT alone reaches values up to some decades of S/cm, and therefore it must be supposed that in the best case in which all the dielectric is gone, the film conductivity must return these values. However, in some cases the conductivity can also be one order of magnitude higher [21]. This suggests that a PEDOT counter-anion in the blend, regardless of whether it is PSS or another specie, has a part in the improvement of the charge carrier mechanism. For instance, when PSS is partly substituted by tosylate, which is also a dielectric, the electrical performance of the PEDOT-based film improves. This suggests that, a part the effects due to the shielding caused by the PSS, when a chemical is added to the polymer blend it causes some modification, leading also to the electrical improvement. This effect is related to the so called "secondary doping" mechanism.

1.3.3 – Secondary Doping of PEDOT:PSS

As seen at the beginning, standalone PEDOT films can carry electricity by themselves, and for this reason it is considered as one of the few intrinsic conductive polymers. However, as mentioned in the previous sections, PSS does not only take insoluble PEDOT chains dispersed in water, but also stabilize the polaronic charges on it by establishing some electrostatic interactions. For this role of balancing-charges anion, PSS is considered as a dopant of PEDOT. Seen that PEDOT:PSS blend does not praise a high conductivity, in the last decades the

scientific production has been filled with a wide plethora of works finalized to the improvement of its electrical performance. Most of time, this purpose is reached through the addition of a new chemical to the pristine PEDOT:PSS solution or film. The consequent increase of conductivity is due to the effect of a secondary dopant. According to the definition given by Mac Diarmid and Epstein, a secondary dopant is "an apparently 'inert' substance including a further increase in conductivity of a primarily doped conjugated polymer. It differs from a primary dopant in that the newly enhanced properties may persist even upon complete removal of the secondary dopant" [1]. Many works have involved the use of organic solvents treatment in the PEDOT:PSS solution or as post-deposition treatment. In 2002, Kim et al. found that PEDOT:PSS film conductivity can be increased by the addition of some organic solvents, such as dimethyl sulfoxide (DMSO), N,N-dimethyl formamide (DMF), and tetrahydrofuran (THF) [33]. Among these, DMSO has led to the best results for the improvement of PEDOT:PSS film conductivity, causing an increase of over two orders of magnitude. This promising result moves the attention toward a wide choice of polar organic solvents, i.e. glycerol, sorbitol, methoxyethanol, diethylene glycol, dimethyl sulfate, xylitol and so on. Ethylene glycol (EG) and glycerol also have given significant improvements in the PEDOT:PSS film conductivity [6,33–41]. Jönsson et al. [19] reported the effects of the addition of sorbitol, N-methyl-2-pyrrolidone and isopropanol, also suppling an explanation for the increased film conductivity. They explained that any excess of PSS is "cleaned off" from the surface of the PEDOT:PSS grains distributed in the film, because of the solvent-effect between the external PSS shell of the grains and the chemical. This partly suppresses the "dielectric shielding effect", improving the connection between the conducting grains and hence a better pathway for charge transport. Sorbitol, in particular, does not only improves the film conductivity but also enhances the

stability of the PEDOT:PSS films to the humidity. This effect is explained by an increased packaging of PEDOT:PSS grains, which reduces the tendency to take up water from the air [42]. Interestingly, the enhancement in the electrical performances is related not only to the in-solution effect of solvents, but also when the secondary doping is carried by polar organic chemicals on the deposited film. In particular, this post-deposition treatment leads to interesting results in the case of secondary doping made by EG and DMSO [43]. Post-deposition treatment gives a special advantage in the secondary doping carried by low boiling point solvents, which act efficiently as dopants in post deposition treatment. For instance, methanol moves the PEDOT:PSS film conductivity from 0.3 to 1362 S/cm [44],

It is worth to note that an effective improvement of conductivity is reached when dopants contains more than one polar group in its structure, while a significant increase of σ cannot be related to the dielectric constant, ε, of the chemical [43,45]. About this, for instance, for compounds like acetonitrile, nitromethane, and methyl alcohol, no conductivity enhancement is observed. This result gives an important clue about the doping mechanism provided by secondary dopants, since the organic compounds that do enhance the conductivity significantly have a common feature: they have at least two groups in their structure. In this case, dopant acts like a "bridge" between the two moieties of the blend and leads to a micro-segregation phase. This has the effect to segregate the dielectric PSS, while conductive PEDOT-base portions approach to each other, improving percolation [43,45–47]. Whatever the solvent used for the secondary doping, it is considered to change the lateral charge motion from a three-dimensional (3D) to a quasi 1D variable range hopping behaviour [7,48]. As seen in the previous section, the exponent α in the Equation 1 indicates the regime in which the polymer is carrying charges. Pristine PEDOT:PSS exhibits α=0.5, which is related to a 1D VRH behaviour. Instead, the

addition of polar organic solvent changes the conduction mechanism and turns α value from 0.5 to 0.25, thus leading from 1D to a 3D VRH regime. This is finally manifested in a remarkable increase of σ. However, Ouyiang et al. [43] give also another interpretation of the increased conductivity. Raman analysis of both a pristine and EG-treated films shows a change in the PEDOT-fingerprint band located between 1400 and 1500 cm^{-1}, Fig. 1.13a. This variation is attributed to a change in the PEDOT-chain conformation. Indeed, in the pristine polymer, the benzoid structure dominates, thus determining a prevalence of random coils on a linear conformation. In the presence of EG dopants, Raman reveals a shift of characteristic C_α=C_β band toward higher values, indicating that the quinoid structure prevails onto the benzoid one, as show in the Fig. 1.13b. At a structural level, this means that the EG addition to the aqueous PEDOT:PSS solution pushes the equilibrium toward the linear conformation of the conductive chains, and thus decrease the percentage of the coil-like ones, causing a transition from polarons to bipolarons. The electron spin resonance (ESR) also reveals that, when coils expand in more linear conformation, roughly half of the polarons pair to bipolarons, thus resulting in a major doping level and delocalization of the charges along PEDOT.

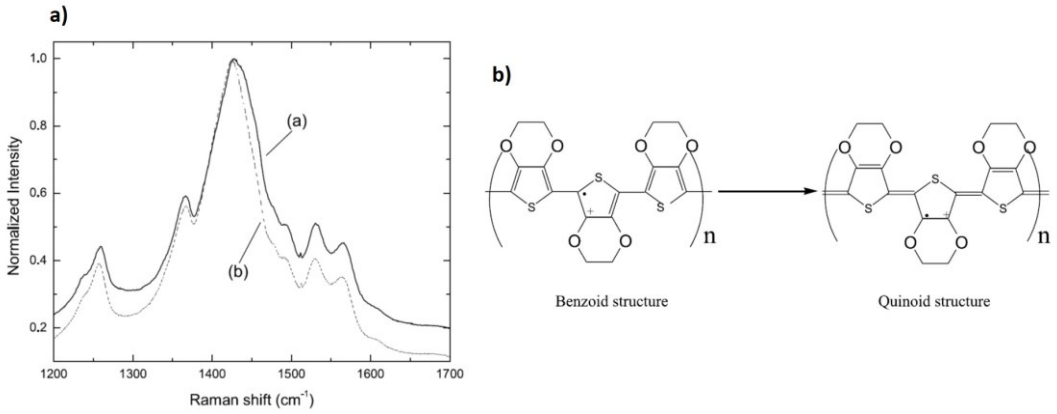

Fig. 1.13: a) Raman spectra of (a) PEDOT:PSS and (b) EG-PEDOT:PSS film under 632.8 nm laser excitation and b) Scheme of transformation of the PEDOT chain from the benzoid to the quinoid structure. The 'dot' and 'plus' represents the unpaired electron and positive charge on the PEDOT chain, respectively. Picture printed from Ref. [43].

Aside the secondary doping carried by organic solvents, acid treatment deserves a special regard. Similarly to secondary doping with organic polar and non-polar solvents, acid doping can be carried both in PEDOT:PSS solution or as a post-deposition method. Small amount of diluted sulfuric acid leads to an enhancement of conductivity of about 1400 times with respect the pristine blend, moving the σ value from 0.07 S/cm to 100 S/cm. However, the same results are not reached when hydrochloric acid is used on the pristine polymer solution and any significant increase of the conductivity is not observed. In this case, the final pH is probably far from the optimal value for making effective the secondary doping [49], which is identified for pH values ranging between 0 and 3 [50]. Despite the neat improvement of the electrical performance reached with the direct acidification of the pristine polymer solution, post-deposition methods are considered the best approaches for the acid secondary doping. In fact, Xia et al. [51] have obtained PEDOT:PSS thin films exhibiting a final conductivity 3065 S/cm, similar to what

measured on ITO. This value was reached with three consecutive addition of 1 M H_2SO_4 aqueous solution on an annealed polymer film. Kim and co-workers [52] have also reported an even better performance, achieving the outstanding σ value of 4380 S/cm. This outcome was related to an acid-promoted crystallization of the conductive part of the polymer blend, which neatly improves the percolation along the film. Nevertheless, this result has actually different contributions. The acid addition on the aqueous pristine PEDOT:PSS solution leads to the water dissociation of the sulfuric acid, which produce HSO_4^-, coming from the first strong dissociation, and SO_4^{2-}, provided by the second, and also to the autoprotolysis which instead establishes an equilibrium with $H_3SO_4^+$ and HSO_4^-. These new counter-ions in the aqueous blend creates a new charge-balance between PEDOT and PSS, which are partly separated by the establishment of new electrostatic interactions. In this case, the increase of conductivity can be explained in a more classical way, relating it to the enhancement of both carrier concentration and mobility, accompanied also to a significant structural and morphological re-arrangement of the entire film. This last one, in particular, is carried out by the formation of ordered and highly dense PEDOT:PSS nanofribrils.

Analogous effect relatively to the improvement of the electrical performance was also achieved by the addition of mild and weak organic acid, such as oxalic acid, malonic acid, methanesulfonic acid, acetic acid, propionic acid and so on [51,53,54].

It is clear now that the acid treatment of the PEDOT:PSS basically leads to the increase of conductivity because of the enhancement of the charge carriers along the PEDOT chains, which thus increases the doping level. Indeed, while free sulfonic groups in the PSS chains can retain only one negative charge each one, in the case of sulfuric acid, for one molecule at least two counter anions are generated,

and one of this i.e. SO_4^{2-}, is also able to balance two positive charges [55]. This means that, while PSS can interact with just one positive charge, i.e. polaronic state in PEDOT chain, counter-anions with two or more negative charges increase the probability to produce bipolaron carriers in PEDOT specie. The final effect of this new balance is the increase of bipolaron population, which consequently leads to the enhancement of the doping-level and thus the final conductivity.

1.4 – Research Perspective

Hitherto, it has been shown the great potentiality offered by PEDOT:PSS and some of the characteristics which arouse the scientific interest in the research and technology.

Despite the enormous production on this material, some aspects still need to be addressed. In particular, during these studies it was considered appropriate to clarify some features about the secondary doping of PEDOT:PSS made by H_2SO_4.

For this reason, most of the efforts have been pointed to understand the effects of this doping strategy, exploring its consequences and giving them some insights and interpretations. In the next Chapters, the reader will attend to a gradual evolution of this study and the results obtained, starting from some investigation carried on the pristine polymer up to the results to which acid doping by H_2SO_4 can lead. In this route, it will take advantage of what obtained by electrical and morphological characterizations and consequent interpretations, in order to give a step-by-step explanation about the results achieved and how to exploit the materials obtained.

1.5 – Bibliography

[1] A.G. MacDiarmid, A.J. Epstein, The concept of secondary doping as applied to polyaniline, Synth. Met. 65 (1994) 103–116. doi:10.1016/0379-6779(94)90171-6.

[2] H. Shirakawa, E.J. Louis, S.C. Gau, C.K. Chiang, C.R. Fincher, Y.W. Park, A.G. Macdiarmaid, A.J. Heeger, Electrical Conductivity in Doped Polacetylene, Phys. Rev. Lett. 39 (1977) 1098–1101.

[3] A.M. Nardes, On the conductivity of PEDOT: PSS thin films, 2007. doi:http://dx.doi.org/10.6100/IR631615.

[4] K. Sun, S. Zhang, P. Li, Y. Xia, X. Zhang, D. Du, F.H. Isikgor, J. Ouyang, Review on application of PEDOTs and PEDOT:PSS in energy conversion and storage devices, J. Mater. Sci. Mater. Electron. 26 (2015) 4438–4462. doi:10.1007/s10854-015-2895-5.

[5] C. Liu, F. Jiang, M. Huang, R. Yue, B. Lu, J. Xu, G. Liu, Thermoelectric performance of poly(3,4-Ethylenedioxy-thiophene)/ poly(Styrene sulfonate) pellets and films, J. Electron. Mater. 40 (2011) 648–651. doi:10.1007/s11664-010-1494-8.

[6] L.U. Bao-yang, L.I.L. Ó, Å ñ ±) , 25 (2008) 2202–2205.

[7] T. Stöcker, A. Köhler, R. Moos, Why does the electrical conductivity in PEDOT:PSS decrease with PSS content? A study combining thermoelectric measurements with impedance spectroscopy, J. Polym. Sci. Part B Polym. Phys. 50 (2012) 976–983. doi:10.1002/polb.23089.

[8] B.G. Heywang, F. Jonas, New , Very Stable Conducting Polymers **, 4 (1992) 116–118.

[9] M. Dietrich, J. Heinze, G. Heywang, F. JonasEP. 339340 (1989), Bayer AG, (n.d.).

[10] F. Jonas, POLYMERS, 39 (1994) 1345–1347.

[11] F. Jonas, Z.F. Uerdingen, B. Ag, W. Krafft, A. Ag, 100, 169-173 (1995), 173 (1995) 169–173.

[12] F. Jonas, B. Ag, Z.B. Zentrale, © Elsevier Sequoia / Printed in The Netherlands, 43 (1991) 831–836.

[13] Jonas, F.; Krafft, W. (Bayer AG) European Patent EP 440 957, March 10, 1991. "New polythiophene dispersions, their preparation and their use," EP 440 957, n.d.

[14] M. Lefebvre, Z. Qi, D. Rana, P.G. Pickup, Chemical Synthesis , Characterization , and Electrochemical Studies of Poly (styrene-4-sulfonate) Composites, (1999) 262–268.

[15] O. Pyshkina, A. Kubarkov, Poly (3 , 4-ethylenedioxythiophene): Synthesis and Properties, 21 (2010) 51–54.

[16] G. Li, P.G. Pickup, Ion Transport in a Chemically Prepared Polypyrrole/Poly(styrene-4-sulfonate) Composite, J. Phys. Chem. B. 103 (1999) 10143–10148. doi:10.1021/jp9914727.

[17] U. Lang, E. Muller, N. Naujoks, J. Dual, Microscopical investigations of PEDOT:PSS thin films, Adv. Funct. Mater. 19 (2009) 1215–1220. doi:10.1002/adfm.200801258.

[18] S. Kirchmeyer, K. Reuter, Scientific importance, properties and growing applications of poly(3,4-ethylenedioxythiophene), J. Mater. Chem. 15 (2005) 2077–2088. doi:10.1039/b417803n.

[19] S.K.M. Jönsson, J. Birgerson, X. Crispin, G. Greczynski, W. Osikowicz, A.W. Denier van der Gon, W.R. Salaneck, M. Fahlman, The effects of solvents on the morphology and sheet resistance in poly(3,4-ethylenedioxythiophene)-polystyrenesulfonic acid (PEDOT-PSS) films, Synth. Met. 139 (2003) 1–10. doi:10.1016/S0379-6779(02)01259-6.

[20] A.M. Higgins, S.J. Martin, P.C. Jukes, M. Geoghegan, R.A.L. Jones, S. Langridge, R. Cubitt, S. Kirchmeyer, A. Wehrum, I. Grizzi, Interfacial structure in semiconducting polymer devices, J. Mater. Chem. 13 (2003) 2814–2818. doi:10.1039/b304990f.

[21] G. Zotti, S. Zecchin, G. Schiavon, F. Louwet, L. Groenendaal, X. Crispin, W. Osikowicz, W. Salaneck, M. Fahlman, Electrochemical and XPS studies toward the role of monomeric and polymeric sulfonate counterions in the synthesis, composition, and properties of poly(3,4-ethylenedioxythiophene), Macromolecules.

36 (2003) 3337–3344. doi:10.1021/ma021715k.

[22] X. Crispin, S. Marciniak, W. Osikowicz, G. Zotti, a W.D.V. a N.D.E.R. Gon, F. Louwet, M. Fahlman, L. Groenendaal, F.D.E. Schryver, W.R. Salaneck, Stability of Poly (3 , 4-ethylene dioxythiophene)– Poly (styrene sulfonate): A Photoelectron Spectroscopy Study, Polymer (Guildf). 41 (2003) 2561–2583. doi:10.1002/polb.10659.

[23] A.M. Nardes, M. Kemerink, R.A.J. Janssen, J.A.M. Bastiaansen, N.M.M. Kiggen, B.M.W. Langeveld, A.J.J.M. Van Breemen, M.M. De Kok, Microscopic understanding of the anisotropic conductivity of PEDOT:PSS thin films, Adv. Mater. 19 (2007) 1196–1200. doi:10.1002/adma.200602575.

[24] E. Vitoratos, S. Sakkopoulos, E. Dalas, N. Paliatsas, D. Karageorgopoulos, F. Petraki, S. Kennou, S.A. Choulis, Thermal degradation mechanisms of PEDOT:PSS, Org. Electron. Physics, Mater. Appl. 10 (2009) 61–66. doi:10.1016/j.orgel.2008.10.008.

[25] E. Vitoratos, S. Sakkopoulos, E. Dalas, N. Paliatsas, K. Emmanouil, P. Malkaj, S.A. Choulis, Correlation between thickness, conductivity and thermal degradation mechanisms of PEDOT:PSS films, AIP Conf. Proc. 1203 (2010) 178–181. doi:10.1063/1.3322407.

[26] A.M. Nardes, M. Kemerink, R.A.J. Janssen, Anisotropic hopping conduction in spin-coated PEDOT:PSS thin films, Phys. Rev. B - Condens. Matter Mater. Phys. 76 (2007) 1–7. doi:10.1103/PhysRevB.76.085208.

[27] B. I. Shklovskii, A. L. Efros, Electronic Properties of Disordered Semiconductors, Springer, Berlin 1984, (n.d.).

[28] N. Mott, E. A. Davis, Electronic Processes in Non-Crystalline Materials,Clarendon, Oxford 1979, (n.d.).

[29] E. Vitoratos, An analysis of DC conductivity in terms of degradation mechanisms induced by thermal aging in polypyrrole/polyaniline blends, Curr. Appl. Phys. 5 (2005) 579–582. doi:10.1016/j.cap.2004.06.024.

[30] F. Greco, A. Zucca, S. Taccola, A. Menciassi, T. Fujie, H. Haniuda, S. Takeoka, P.

Dario, V. Mattoli, Ultra-thin conductive free-standing PEDOT/PSS nanofilms, Soft Matter. 7 (2011) 10642–10650. doi:10.1039/c1sm06174g.

[31] G. Greczynski, T. Kugler, W.R. Salaneck, Characterization of the PEDOT-PSS system by means of X-ray and ultraviolet photoelectron spectroscopy, Thin Solid Films. 354 (1999) 129–135. doi:10.1016/S0040-6090(99)00422-8.

[32] S. Ghosh, J. Rasmusson, O. Inganäs, Supramolecular Self-Assembly for Enhanced Conductivity in Conjugated Polymer Blends: Ionic Crosslinking in Blends of Poly(3,4-ethylenedioxythiophene)-Poly(styrene sulfonate) and Poly(vinylpyrrolidone), Adv. Mater. 10 (1998) 1097–1099. doi:10.1002/(SICI)1521-4095(199810)10:14<1097::AID-ADMA1097>3.0.CO;2-M.

[33] J.Y. Kim, J.H. Jung, D.E. Lee, J. Joo, Enhancement of electrical conductivity of poly(3,4-ethylenedioxythiophene)/poly(4-styrene sulfonate) by a change of solvents, Synth. Met. 126 (2002) 311–316. doi:10.1016/S0379-6779(01)00576-8.

[34] J. Ouyang, C.W. Chu, F.C. Chen, Q. Xu, Y. Yang, High-conductivity poly(3,4-ethylenedioxythiophene):poly(styrene sulfonate) film and its application in polymer optoelectronic devices, Adv. Funct. Mater. 15 (2005) 203–208. doi:10.1002/adfm.200400016.

[35] C. Liu, B. Lu, J. Yan, J. Xu, R. Yue, Z. Zhu, S. Zhou, X. Hu, Z. Zhang, P. Chen, Highly conducting free-standing poly(3,4-ethylenedioxythiophene)/ poly(styrene sulfonate) films with improved thermoelectric performances, Synth. Met. 160 (2010) 2481–2485. doi:10.1016/j.synthmet.2010.09.031.

[36] J. Ouyang, Y. Yang, Conducting polymer as transparent electric glue, Adv. Mater. 18 (2006) 2141–2144. doi:10.1002/adma.200502475.

[37] H. Shi, C. Liu, J. Xu, H. Song, B. Lu, F. Jiang, W. Zhou, G. Zhang, Q. Jiang, Facile fabrication of pedot:pss/polythiophenes bilayered nanofilms on pure organic electrodes and their thermoelectric performance, ACS Appl. Mater. Interfaces. 5 (2013) 12811–12819. doi:10.1021/am404183v.

[38] J.P. Thomas, L. Zhao, D. McGillivray, K.T. Leung, High-efficiency hybrid solar

cells by nanostructural modification in PEDOT:PSS with co-solvent addition, J. Mater. Chem. A. 2 (2014) 2383–2389. doi:10.1039/c3ta14590e.

[39] Q. Wei, M. Mukaida, Y. Naitoh, T. Ishida, Morphological change and mobility enhancement in PEDOT:PSS by adding co-solvents, Adv. Mater. 25 (2013) 2831–2836. doi:10.1002/adma.201205158.

[40] J.P. Thomas, K.T. Leung, Defect-minimized PEDOT:PSS/planar-si solar cell with very high efficiency, Adv. Funct. Mater. 24 (2014) 4978–4985. doi:10.1002/adfm.201400380.

[41] B.D. Martin, N. Nikolov, S.K. Pollack, A. Saprigin, R. Shashidhar, F. Zhang, P.A. Heiney, Hydroxylated secondary dopants for surface resistance enhancement in transparent poly(3,4-ethylenedioxythiophene)-poly(styrene sulfonate) thin films, Synth. Met. 142 (2004) 187–193. doi:10.1016/j.synthmet.2003.09.005.

[42] A.M. Nardes, M. Kemerink, M.M. de Kok, E. Vinken, K. Maturova, R.A.J. Janssen, Conductivity, work function, and environmental stability of PEDOT:PSS thin films treated with sorbitol, Org. Electron. Physics, Mater. Appl. 9 (2008) 727–734. doi:10.1016/j.orgel.2008.05.006.

[43] J. Ouyang, Q. Xu, C.W. Chu, Y. Yang, G. Li, J. Shinar, On the mechanism of conductivity enhancement in poly(3,4- ethylenedioxythiophene):poly(styrene sulfonate) film through solvent treatment, Polymer (Guildf). 45 (2004) 8443–8450. doi:10.1016/j.polymer.2004.10.001.

[44] D. Alemu, H.Y. Wei, K.C. Ho, C.W. Chu, Highly conductive PEDOT:PSS electrode by simple film treatment with methanol for ITO-free polymer solar cells, Energy Environ. Sci. 5 (2012) 9662–9671. doi:10.1039/c2ee22595f.

[45] H. Shi, C. Liu, Q. Jiang, J. Xu, Effective Approaches to Improve the Electrical Conductivity of PEDOT:PSS: A Review, Adv. Electron. Mater. 1 (2015) 1–16. doi:10.1002/aelm.201500017.

[46] D. Alemu Mengistie, P.C. Wang, C.W. Chu, Effect of molecular weight of additives on the conductivity of PEDOT:PSS and efficiency for ITO-free organic solar cells, J. Mater. Chem. A. 1 (2013) 9907–9915. doi:10.1039/c3ta11726j.

[47] W. Zhang, B. Zhao, Z. He, X. Zhao, H. Wang, S. Yang, H. Wu, Y. Cao, High-efficiency ITO-free polymer solar cells using highly conductive PEDOT:PSS/surfactant bilayer transparent anodes, Energy Environ. Sci. 6 (2013) 1956–1964. doi:10.1039/c3ee41077c.

[48] A.M. Nardes, R.A.J. Janssen, M. Kemerink, A morphological model for the solvent-enhanced conductivity of PEDOT:PSS thin films, Adv. Funct. Mater. 18 (2008) 865–871. doi:10.1002/adfm.200700796.

[49] I. Cruz-Cruz, M. Reyes-Reyes, R. López-Sandoval, Formation of polystyrene sulfonic acid surface structures on poly(3,4-ethylenedioxythiophene): Poly(styrene sulfonate) thin films and the enhancement of its conductivity by using sulfuric acid, Thin Solid Films. 531 (2013) 385–390. doi:10.1016/j.tsf.2012.12.050.

[50] O. Solids, S. Barbara, S. Barbara, Transport properties of poly(3,4-ethylenedioxythiophene)/ poly(styrene sulfonate), 94 (1998) 173–177.

[51] Y. Xia, K. Sun, J. Ouyang, Solution-processed metallic conducting polymer films as transparent electrode of optoelectronic devices, Adv. Mater. 24 (2012) 2436–2440. doi:10.1002/adma.201104795.

[52] N. Kim, S. Kee, S.H. Lee, B.H. Lee, Y.H. Kahng, Y.R. Jo, B.J. Kim, K. Lee, Highly conductive PEDOT:PSS nanofibrils induced by solution-processed crystallization, Adv. Mater. 26 (2014) 2268–2272. doi:10.1002/adma.201304611.

[53] J. Ouyang, Solution-processed pedot:pss films with conductivities as indium tin oxide through a treatment with mild and weak organic acids, ACS Appl. Mater. Interfaces. 5 (2013) 13082–13088. doi:10.1021/am404113n.

[54] Y. Xia, J. Ouyang, Significant conductivity enhancement of conductive poly(3,4-ethylenedioxythiophene): Poly(styrene sulfonate) films through a treatment with organic carboxylic acids and inorganic acids, ACS Appl. Mater. Interfaces. 2 (2010) 474–483. doi:10.1021/am900708x.

Chapter 2

Study of the influence of thermal treatment conditions on PEDOT:PSS films

Several works made on PEDOT:PSS were mostly addressed to the improvement of the electrical features of this polymer, which usually exhibits a conductivity of about 1 S/cm in its pristine form. However, since in most of standard procedures, post-deposition thermal treatments are required, it is worth to shade light about the best conditions of this processing step. The comprehension of the role played by the annealing conditions on the electrical conductivity of pristine PEDOT:PSS films are extremely useful for their optimization. In this Chapter, both roles of the temperature and annealing atmosphere on the conductivity of PEDOT:PSS films are investigated.

2.1 - Introduction

PEDOT:PSS has found an increasing interest in the scientific community thanks to its properties such as a good ambient stability, an excellent processability and good versatility of both electrical and optical properties. More than others, these last two features have given to PEDOT:PSS a huge popularity in several fields including, for example, the photovoltaics [1-6]. In parallel, seen its great

potentiality, most of the scientific efforts were addressed to the improvement of the intrinsic characteristics of this polymer blend, leading also to good results in terms of electrical performance [7,8]. However, another part of the studies relative to PEDOT:PSS was hardly pointed to the identification of the conduction mechanisms and their relation with the external ambient conditions. Regarding the thermal budget supplied to thin PEDOT:PSS films, different theories were formulated about the mechanism ruling the charge transport into the film. First studies and chemical characterizations of pristine polymer solution have presented PEDOT:PSS as chemically and thermally stable. For instance, some thermogravimetric analysis has proven that the first degradation step of the polymer chains occurs at very high temperature, i.e. 350C°, and on the load of the styrenic part [9]. However, from an electrical point of view, different works have shown an influence of both temperature and duration of the thermal treatment which, depending on the condition applied, can have beneficial effects on the conductivity on one side or can eventually affect it [10,11].

In order to clarify the behaviour of the PEDOT:PSS due to the post-deposition standard thermal treatment, it was reported in this Chapter a systematic study about the conductivity-response of thin polymer films to different annealing atmospheres, i.e. low (0.01 mbar) and ambient pressure, and temperatures, exploring a range from 80 up to 200°C. The purpose of this study was to identify the competitive mechanisms which contribute to the change of the electrical conductivity and thus comprehend the role played by the solvent removal, atmosphere and heating. Moreover, the results that will be discussed in the next sections lay the foundation to some of the considerations and results that will be described and explained in the successive Chapters.

2.2 – Sample Preparation

PEDOT:PSS thin films can be made by different techniques and methods. Among the others, spin coating is a fast approach which offers a cost-effective, easy and reproducible method for thin layer preparation on flat substrates.

Even if further details about this technique are supplied in the Appendix A, it will be here provided a brief description about the deposition method used in this Chapter. The spin coating technique is based on the essential concept which a solution dropped onto a given substrate is spread in all directions when support is undergone to a rotation. For high spinning speed, centrifugal forces squeeze the drop of solution down to the surface and toward the edges of the substrate. When initial acceleration and deposition spin speed are opportunely chosen, the coverage of the substrate by the solution must appears continuous and uniform at the naked eye along all directions. In all experiments performed, the initial acceleration of spin coater was kept at a fixed value. Vice versa, spin speed was changed time by time and it will be specified in each case. The maximum spin coater speed is 6000 rpm, and the deposition velocities ranged between 1000 and 5000 rpm. Aside these two parameters already mentioned, duration of the deposition was also determined. The goal is to obtain a dry surface sample at the end of the spin coating, since the substrate's rotation must lead to a total or almost complete removal of the solvent. For this reason, the deposition time used for all samples here reported was set to 5 minutes. Shorter times were not used because the samples still appear wet. On the other hand, since longer deposition times are not desirable from the perspective of fast preparation procedure, time of deposition longer than 5 minutes were avoided. In parallel to the different deposition velocities, the effects of both ambient and

temperatures of post-deposition annealing were also investigated. In particular, the environment used for the annealing was atmospheric air and vacuum (i.e. 0.01 mbar). Temperature explored were 80 and 100°C in the first case while 100, 150°C and 200°C were used in the second one. The experiment matrix, showing all the different synthesis conditions explored, is reported below in Fig. 2.1

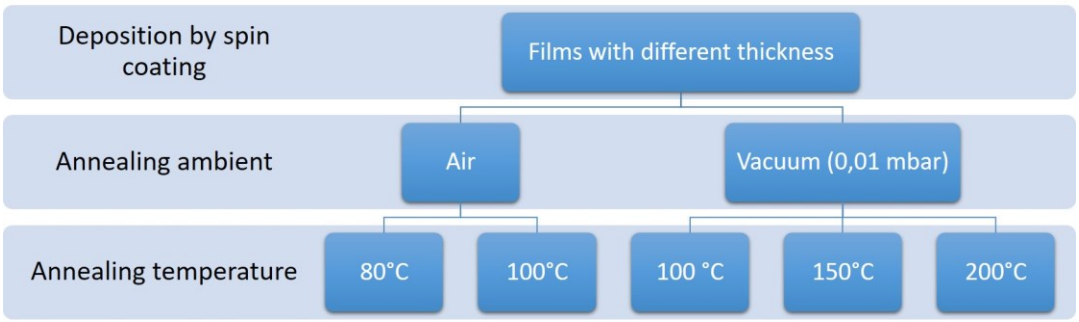

Fig. 2.1: Summary of the processing conditions explored in this Chapter.

High conductive PEDOT:PSS (Sigma-Aldrich), 1.1% w/w and PEDOT to PSS content in ratio 1:2.5, was used for these purposes, as received and without any further purification. Prior of each deposition, pristine PEDOT:PSS aqueous solution was kept under a gentle stirring for 15 minutes at room temperature in order to homogenize the water suspension. Glass square substrates sizing from 1 cm to 1.5 cm were obtained by cutting Corning 2947 glass slides and were used as supports. Before each deposition, substrates undergone to sonication for 5 minutes in acetone, isopropyl alcohol and water respectively, and finally dried under nitrogen flow. Immediately before spin coating, the substrates were pre-heated at 80°C for 1 minute to allow for the evaporation of any residual traces of wetness. Deposition was made by pipetting few microliters of the pristine polymer on the

substrate, which was then spun at several spin speeds, for 5 minutes each. Finally, thermal treatment was carried out for 10 minutes in air (80 and 100°C) or vacuum at 0.01 mbar (100, 150 and 200°C).

2.3 – Effects Related to the Annealing Conditions

After each deposition and annealing treatment, the film thickness was measured by spectroscopic ellipsometer J.A.Wollam V-Vase, using diffraction index, n = 1.55, as reported from the supplier. Fig. 2.2 reports the film thickness measured for samples deposited at different spin speed within a range of 1500 and 5000 rpm and annealed in different conditions, in particular air atmosphere at 80 and 100°C, and vacuum oven at 100, 150 and 200°C, as in Fig. 2.2a and b respectively.

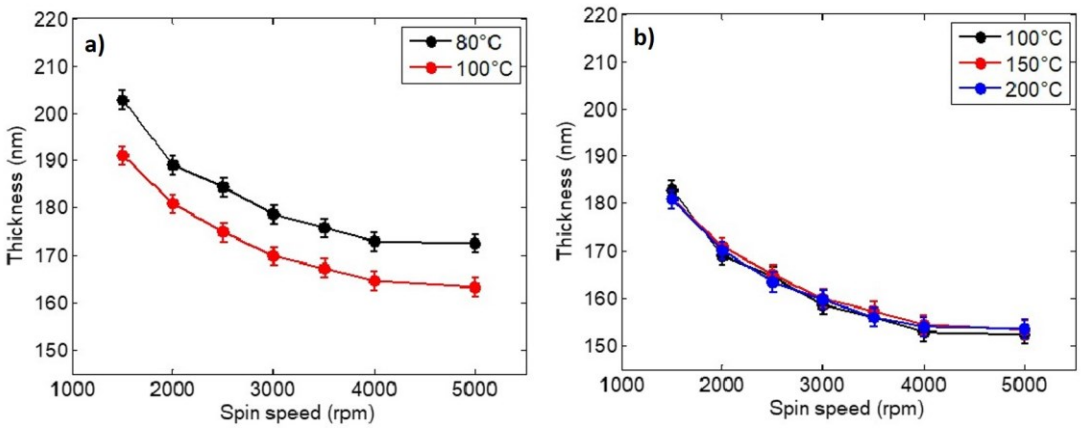

Fig. 2.2: Graphs of thickness of PEDOT:PSS films as a function of the deposition speed. a) the results for two samples treated at 80 and 100°C in air for 10 minutes are reported; b) three PEDOT:PSS films annealed at three different temperatures, 100, 150 and 200°C for 10 minutes in vacuum chamber (0.01 mbar).

As shown in the graphs, film thickness has a dependence on three parameters:

1. Thickness is clearly correlated to the spin speed of deposition. The higher the spin velocity, the lower the film depth. This effect is a peculiarity due to the deposition technique used (and better described in the relative Appendix A);
2. The environment in which the thermal treatment is carried has an influence on the general trend of the curve. Indeed, samples annealed in air show higher thickness trend with respect to those ones measured for samples treated in vacuum chamber;
3. Temperature also plays a role on the film thickness obtained when the annealing is performed in air at ambient pressure. Indeed, films treated at 80°C show thickness of about 10 nm higher than those ones annealed at 100°C. This same consideration cannot be applied to the samples annealed at low pressure, Fig. 2.2b. In this latter case, films deposited at the same velocity reach comparable thickness between each other, showing a general trend lower than those ones annealed in air.

In light of these results, it seems clear that the annealing conditions have a role in the shrinkage effect of the PEDOT:PSS films due to the solvent removal. Indeed, water, i.e. the solvent in which the polymer blend is suspended, is mostly removed during the spin coating but part of it still remains embedded into the polymer film at the end. The successive annealing treatment leads to a further removal of the entrapped water thus causing a decrease in the film thickness. When the annealing is carried in air, the solvent evaporation must compete with the external ambient pressure which counteracts on it. In this case, the annealing carried at 100°C allows

a faster solvent removal with respect to those samples heated at lower temperature, i.e. 80°C, Fig. 2.2a. Differently, when the thermal treatment is made in vacuum condition, temperature does not play the main role anymore. Indeed, its variation does not lead to any substantial changes in the film thickness obtained, and curves appear almost overlapped between each other, Fig. 2.2b. In this case, the general thickness trend appears lower than the previous one because of a more effective solvent evaporation due to the low pressure in the chamber. A schematic representation of what explained so far is give in the Fig. 2.3.

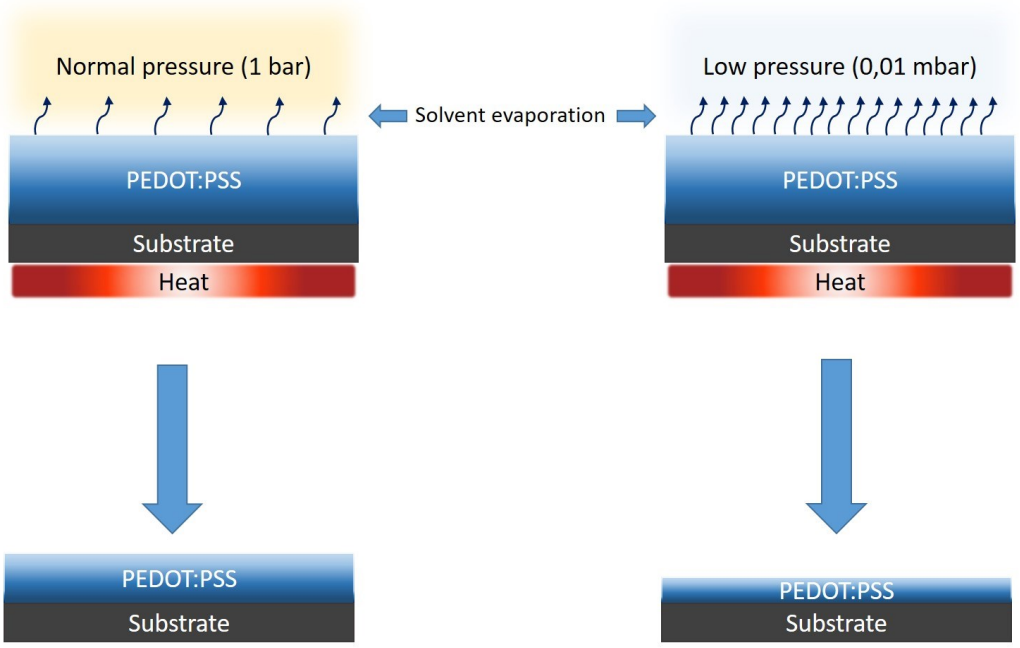

Fig. 2.3: Schematic sketch of the film-shrinkage mechanism related to the annealing environment. PEDOT:PSS film thickness is emphasized for an easier understanding.

As expected, the decrease of the film thickness leads to an increase in the material transparency. Fig. 2.4 shows the transmittance percentage (T%) of PEDOT:PSS films annealed in air atmosphere at 80°C for 10 minutes measured with

spectroscopic ellipsometer J.A.Wollam V-Vase. Films were spun on glass substrate at different speeds, thus leading to the thickness listed in the legend. This acquisition was obtained by measuring the intensity of the light transmitted for an incident laser beam normal to the sample surface. As mentioned above, a difference of 30 nm of thickness causes a decrease in the transparency of the polymer film which is more accentuate when the incident wavelength increases. This is in agreement with the blue colour of the PEDOT:PSS solution and films, which suggests a greater light absorption at longer wavelengths. This effect becomes more evident for thicker films.

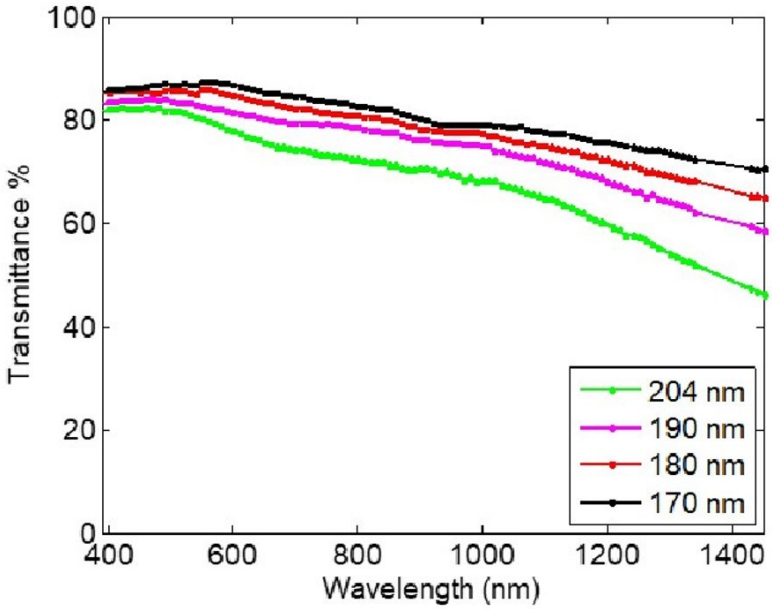

Fig. 2.4: Direct transmittance %, obtained by setting the incident light spot perpendicularly to the sample surface, for different PEDOT:PSS film thickness as a function of incident wavelength.

2.4 – Sample Morphology

In order to understand if the different film thickness and different annealing conditions have some kind of influence on the morphology of the PEDOT:PSS film, SEM analysis in-plane view was used for characterizing the external surface of the polymer layer. Fig. 2.5 shows three different PEDOT:PSS films with their three corresponding thickness, annealed in vacuum chamber at 200°C for 10 minutes. As it is possible to see, no relevant variations in the morphology of the polymer layer are observed by changing the deposition speed. The surface appears substantially flat, without any specific structure or pattern.

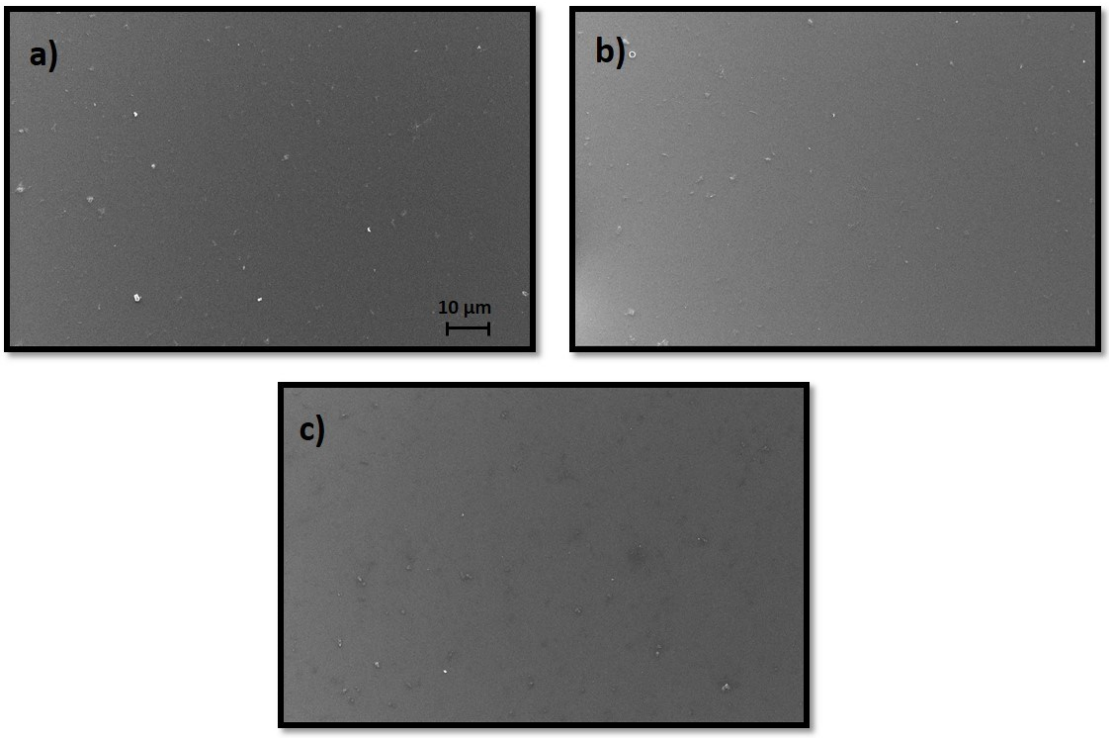

Fig. 2.5: SEM images acquired in-plan view for three samples annealed at 200°C at low pressure (0.01 mbar) for 10 minutes. Samples are deposited at three different spin speeds reaching thickness of a) 180, b) 165 and c) 150 nm respectively.

Small pins with brighter contrast with respect to the surrounding background can be attributed to particulate coming from the external ambient. Analogously, SEM analysis were also performed for samples prepared in different annealing environment.

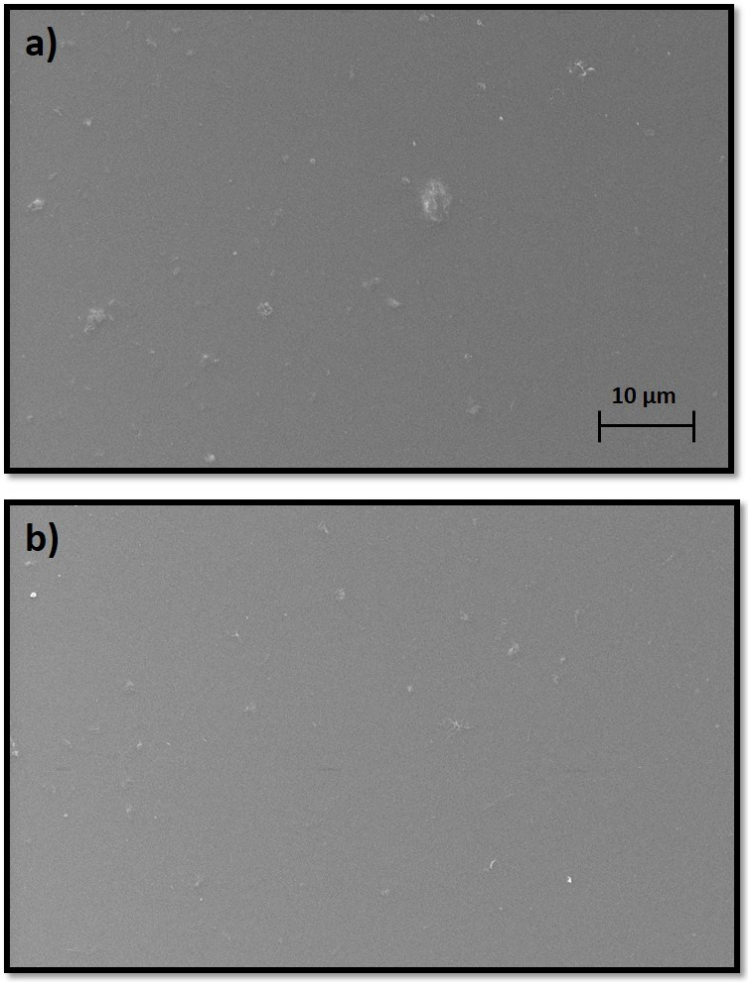

Fig. 2.6: SEM image acquired in-plan comparing samples undergone to different ambient conditions: a) sample spun at 1500 rpm on glass and annealed in air at

100°C for 10 minutes; b) PEDOT:PSS film deposited at 1500 rpm of glass and then treated at 100°C for 10 minutes at pressure of 0.01 mbar.

Fig. 2.6 shows two samples deposited at the same velocity and for which the annealing was performed at 100°C in two different atmospheres, air and vacuum in Fig. 2.6a and b respectively. Again, the surface appears flat and without any specific pattern. Some agglomerates discernible in the case of sample treated in air seem to be reduces when film is heated at low pressure. In fact, it is reasonable to think that vacuum can have such "cleaning effect" on the samples, removing or desorbing part of the particulate randomly present on the polymer surface.

2.5 – Electrical Characterization

The electrical performances of PEDOT:PSS films and their response relatively to its thermal treatment were carried by the Four Point Probe technique (4PP). As better described in the Appendix B, 4PP allows the measurements of the thin-films sheet resistance from which conductivity can be then extrapolated. While for most of measurements normally performed on metals or inorganic semiconductors, such as Si, metal probes can in most of the cases directly be put in physical contact with the sample, in the case of soft matter, as polymers, some precautions are required for preserving the organic film, since they can be easily scratched by the probe tips. For instance, in the Fig. 2.7 it is shown a scuff made by steel tweezers on the surface of a PEDOT:PSS film.

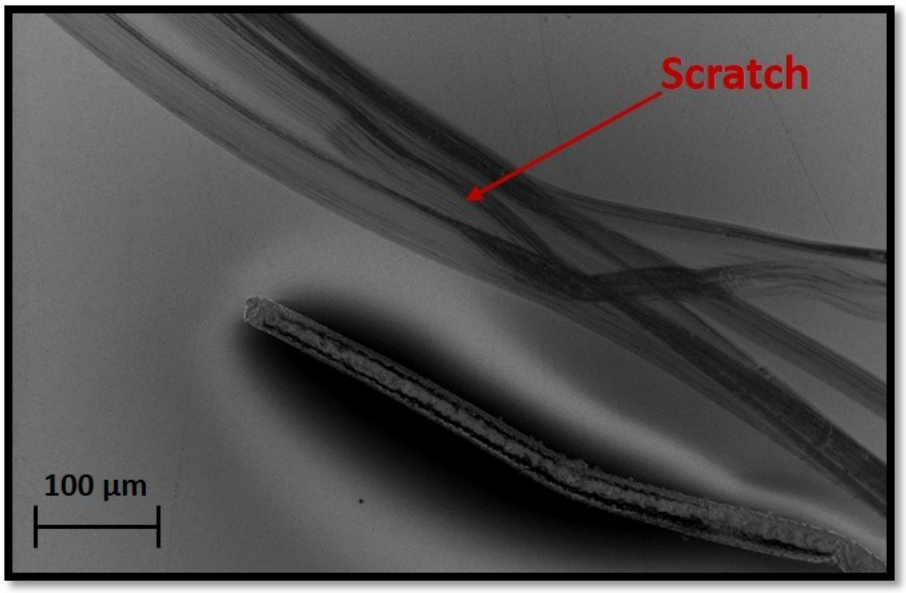

Fig. 2.7: Scratch on a PEDOT:PSS thin film made by steel tweezers.

Therefore, in order to perform the 4PP measurements on PEDOT:PSS films, it was decided to deposit four collinear silver dots on the polymer surface.

Four silver dots obtained with 600 µm of diameter, 1 mm edge-edge distance and 600 nm, were sputtered through a shadow mask on 1 x 1 cm samples using Quorum Q300TD performing at 50mA in a $5x10^{-3}$ bar vacuum chamber. Fig. 2.8a reports a schematic representation of the 4PP set up with using silver dots, while Fig. 2.8b shows a SEM image of a pair of Ag dots deposited onto a PEDOT:PSS film. Silver is one of the most used metals with which PEDOT:PSS is interfaced within most of devices. For the purposes of this work, Ag was chosen in virtue of the fact that this polymer/metal interface exhibits an Ohmic behaviour, which is in line with the scopes of our characterization (Fig. 2.9). Indeed, the PEDOT:PSS/Ag interface manifests the suitable band alignment between the metal Fermi's level

and the HOMO-LUMO gap of the polymer, thus allowing its use in most of configurations of hybrid or organic solar cells [12].

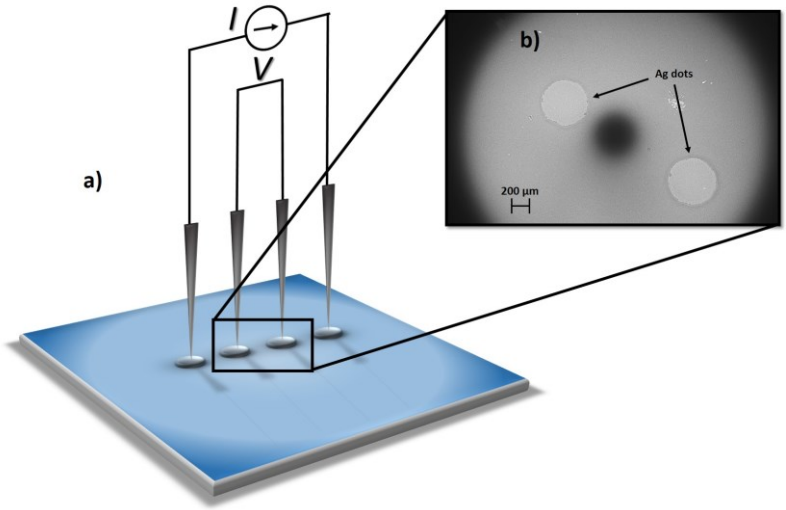

Fig. 2.8: a) schematic representation of the 4PP set up using four collinear Ag dots as metal contacts for avoiding damages on the polymer film and b) SEM image acquired in-plan view showing the central pair of Ag dots sputtered on a PEDOT:PSS thin film.

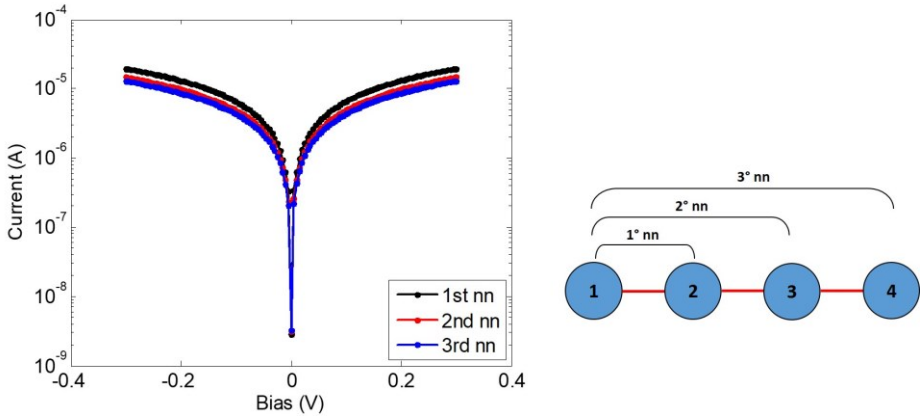

Fig. 2.9: I-V curves acquired by the two-points probe for testing the Ohmic behaviour in the PEDOT:PSS/Ag interface. The three different curves in the graph correspond

to the I-V acquired with positioning the probes on the next neighbours (#nn) dots according to the configuration shown in the schematic on the left side.

Results obtained from the 4PP measurements on the PEDOT:PSS thin films, also in relation with the different thermal treatments performed, are shown and discussed in the following.

Fig. 2.10 reports the sheet resistance as a function of thickness of PEDOT:PSS films annealed in air at 80 and 100°C, Fig. 2.10a and b respectively. Graphs show that R_{sh} decreases with increasing the film thickness, since, for the same material, the amount of sample investigated by the probes is larger for thicker films than for thinner ones and, for the first ones the contribution coming from the bulk increases. In the graph shown in the Fig. 2.10, the comparison between samples is made through films obtained by deposition carried at the same spin speed. However, better comparison of these results is given in Fig. 2.11, where conductivity is shown for the samples annealed in air at 80 and 100°C (Fig. 2.11a and b, respectively).

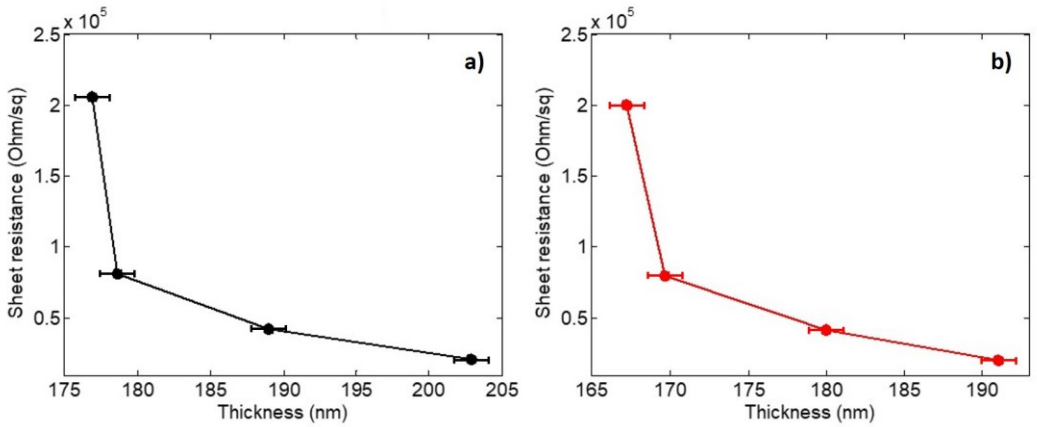

Fig. 2.10: Sheet resistance values reported as function of four different thicknesses of the polymer films. Samples reported for each graph are obtained by depositing the

initial solution at the same spin speeds. PEDOT:PSS were both annealed in air for 10 minutes at a) 80°C and b) 100°C.

The electrical conductivity, σ, calculated from the corresponding sheet resistance according to the formulas reported in Appendix B, is a parameter which intrinsically depends on the material and not on the layer thickness. This preliminary consideration suggests that, whatever is the depth sampled in the layer, σ should be constant. However, as reported in the Fig. 2.11, a dependence between the electrical conductivity and the sample thickness exists.

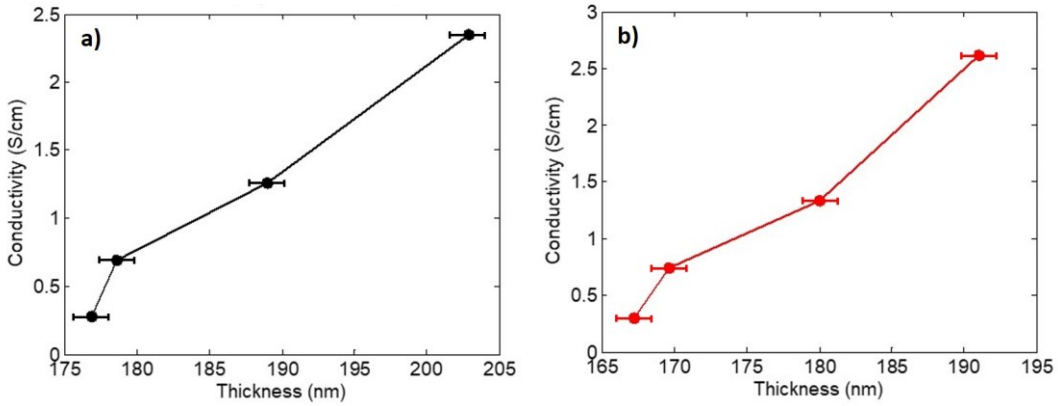

Fig. 2.11: Conductivity values reported as function of four different thicknesses of the polymer films obtained. PEDOT:PSS films annealed in air for 10 minutes at a) 80°C and b) 100°C.

In particular, thicker samples show a higher conductivity with respect to thinner ones. This result is in agreement with what Sakkopoulos et al. have already reported [13]. The PEDOT:PSS polymer blend is composed of conductive grains. The increment of conductivity with the thickness is explained with the fact that in a deeper layer, more conductive grains can accommodate, thus improving the chargers' path, as schematized in the Fig. 2.12.

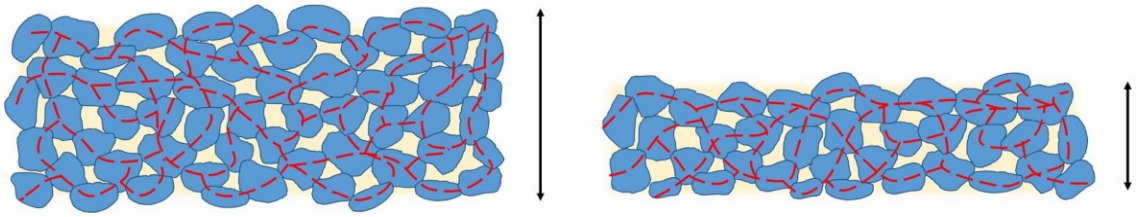

Fig. 2.12: Schematic sketch of the charging path as function of the conductive polymer grains related to the film thickness.

Aside the effect due to the amount of grains on the conduction mechanism, temperature also has role in the conductivity of PEDOT:PSS. Indeed, as shown in the Fig. 2.11, films treated at 100°C show a better conductivity with respect to those samples annealed at lower temperature. This result suggests that the amount of water eventually retained into the film plays a role on its conductivity. As already discussed in the section 2.3 of this Chapter, for the same annealing time, higher temperature allows a faster water evaporation, which thus leads to a shrinkage of the polymer film. This probably approaches the conductive portions of the polymer blend and improves the charge transport mechanism by increasing the percolation path between domains [14], as represented in the Fig. 2.13.

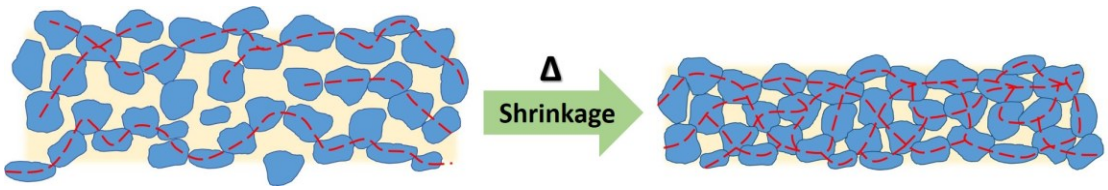

Fig. 2.13: Schematic representation of the shrinkage effect due to the annealing. Heating removes entrapped solvent inside the polymer film causing its thinning and approaching the conductive grains.

Fig. 2.14 shows the a) sheet resistance and b) the relative electrical conductivity for samples annealed at low pressure and three different temperatures, 100, 150 and 200°C.

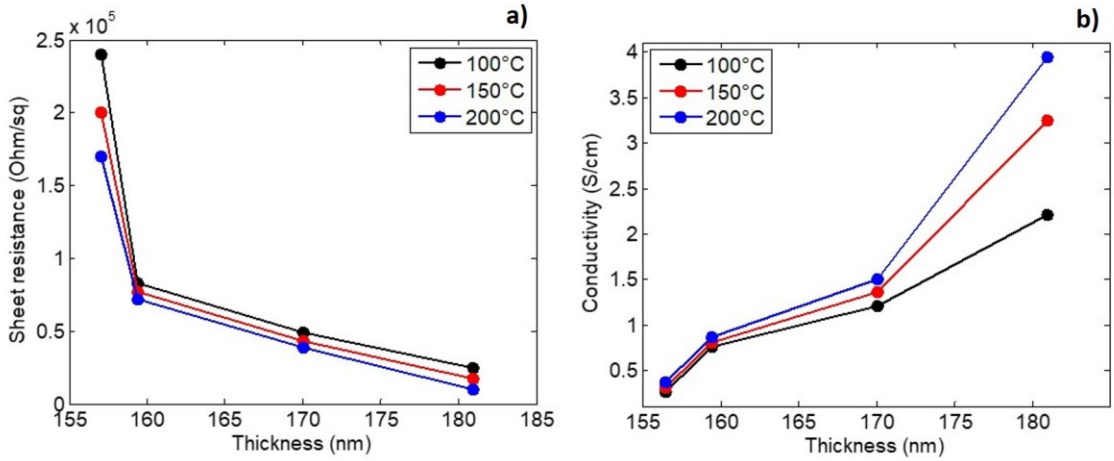

Fig. 2.14: PEDOT:PSS samples deposited at different velocities and annealed at three different temperatures (100, 150, 200°C) for 10 minutes in vacuum chamber (0.01 mbar). Graphs show respectively, a) sheet resistance and b) corresponding electrical conductivity as function of film thickness.

As already mentioned in the section 2.3, samples annealed in vacuum reach a comparable final thickness between each other for the same deposition speed used. Thanks to this similarity and for a better comparison of the results obtained, the value of thickness for each point is thus plotted as the average between thicknesses of samples obtained at the three annealing temperatures. Also in this case, the reduction in the conductivity due to the films thinning caused by the higher deposition velocities can be still considered valid, since a relation between σ and the film thickness is still observed, as shown in Fig. 2.14b. For 170-180 nm-thick samples, an effect due to the temperature is still observed and can be attributed again to the removal of small amount of solvent. Instead, for sample having a

thickness between 150 and 160 nm, the effect due to the temperature disappears. Probably, this is due to a threshold thickness-value for which the solvent evaporation in not more predominant, and film reaches its minimum depth value. Therefore, here the improvement of the electrical performance must be attributed to a better re-arrangement given from the conductive chains which probably increase the percolative path of charges [15-18].

A direct comparison between the results shown in Fig. 2.11 and Fig. 2.14 cannot be made because, as already explained, thickness of films deposited at the same speed is not comparable between samples in different annealing atmospheres. Therefore, from all the sample prepared, those polymer films having the same thickness were chosen for comparing the conductivity obtained.

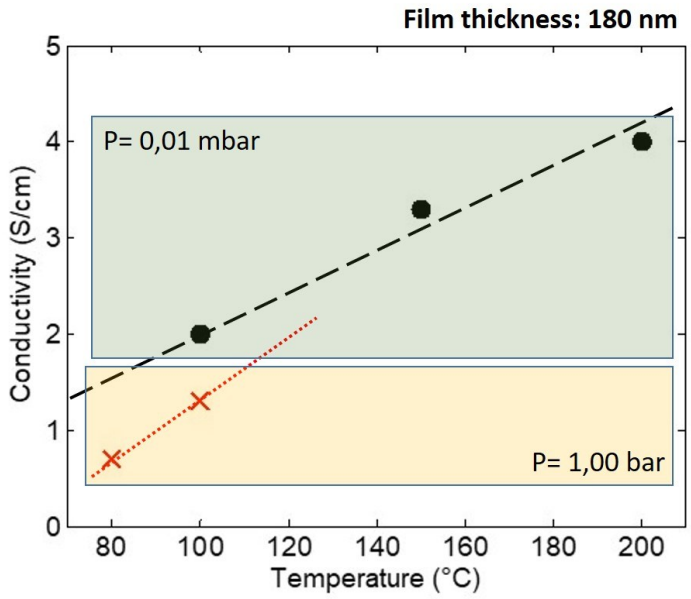

Fig. 2.15: Conductivity as function of annealing temperature for 180 nm-thick samples undergone to different annealing atmospheres. Black dots in the green area refer to the samples annealed in vacuum chamber, while red crosses in yellow rectangular correspond to those treated at ambient pressure.

Fig. 2.15 recapitulates what was herein discussed, showing the conductivity obtained for samples having the same thickness and annealed in different environments and temperatures. The general trend shows that conductivity improves with the increase of the annealing temperature, while better electrical performances are achieved for a thermal treatment carried at low pressure. Here again, there are two main effects playing the major role in the PEDOT:PSS conduction, i.e. heating on one side and environment on the other. An annealing carried for short time, i.e. 10 minutes, leads to a conductivity enhancement with the temperature, which is related to an improvement of the crystallinity between the conductive grains in the film blend [15,19,20]. For the same treatment duration, higher temperature supplies more thermal budget with respect to the lower ones. This allows the organization of the conductive grains in more regular and crystalline structures, eventually increasing the charge conductive path in the polymer film [16,21]. This effect is finally manifested with the increase of conductivity. For what concerning the surrounding ambient of the annealing, low pressure atmosphere leads to better results than those achieved at 1 bar. Indeed, in this latter case, the main cause for explaining lower conductivity is relative to some external "contaminants", such as moisture and atmospheric oxygen [19], that finally affect the film conductivity.

2.6 – Conclusions

In this Chapter, the effect related to the annealing atmosphere and temperature on PEDOT:PSS thin films was investigated, founding that both of them can play an

important role in the conduction mechanism. It was found that electrical conductivity has always a dependence on the film thickness. This behaviour, which is normally anomalous for most of inorganic compounds, was explained by the fact that thicker films, which thus have a higher content of polymer grains, exhibits a more effective conductive path which thus increase the global conductivity of the polymer film. On the other side, PEDOT:PSS film thickness has also shown a relation with both ambient and temperature of post-deposition thermal treatment. It was observed that, for the same annealing time and temperature, heating performed in vacuum chamber at a pressure of 0.01 mbar leads to a faster solvent evaporation with respect to the one performed at atmospheric pressure. This effect was noticed through the reduction of the film thickness after each annealing treatment. Finally, a relation between PEDOT:PSS film conductivity and the annealing condition was found. It was shown that, for the same film thickness, electric performances improve when the annealing is carried in vacuum. These observations were found to be in agreement with the grains-conduction mechanism previously described by other authors for different conditions of annealing and film thickness.

2.7 – Bibliography

[1] S.J. Lee, H. Pil Kim, A.R. Bin Mohd Yusoff, J. Jang, Organic photovoltaic with PEDOT:PSS and V2O5mixture as hole transport layer, Sol. Energy Mater. Sol. Cells. 120 (2014) 238–243. doi:10.1016/j.solmat.2013.09.009.

[2] B. Xu, S.A. Gopalan, A.I. Gopalan, N. Muthuchamy, K.P. Lee, J.S. Lee, Y. Jiang, S.W. Lee, S.W. Kim, J.S. Kim, H.M. Jeong, J.B. Kwon, J.H. Bae, S.W. Kang, Functional solid additive modified PEDOT:PSS as an anode buffer layer for enhanced photovoltaic

performance and stability in polymer solar cells, Sci. Rep. 7 (2017) 1–13. doi:10.1038/srep45079.

[3] S. Jäckle, M. Liebhaber, C. Gersmann, M. Mews, K. Jäger, S. Christiansen, K. Lips, Potential of PEDOT:PSS as a hole selective front contact for silicon heterojunction solar cells, Sci. Rep. 7 (2017) 1–8. doi:10.1038/s41598-017-01946-3.

[4] S.J. Lee, B.S. Kim, J.Y. Kim, A.R.B.M. Yusoff, J. Jang, Stable organic photovoltaic with PEDOT:PSS and MoOX mixture anode interfacial layer without encapsulation, Org. Electron. Physics, Mater. Appl. 19 (2015) 140–146. doi:10.1016/j.orgel.2015.01.028.

[5] Z. Hu, J. Zhang, Z. Hao, Y. Zhao, Influence of doped PEDOT:PSS on the performance of polymer solar cells, Sol. Energy Mater. Sol. Cells. 95 (2011) 2763–2767. doi:10.1016/j.solmat.2011.04.040.

[6] A. Savva, E. Georgiou, G. Papazoglou, A.Z. Chrusou, K. Kapnisis, S.A. Choulis, Photovoltaic analysis of the effects of PEDOT:PSS-additives hole selective contacts on the efficiency and lifetime performance of inverted organic solar cells, Sol. Energy Mater. Sol. Cells. 132 (2015) 507–514. doi:10.1016/j.solmat.2014.10.004.

[7] Z. Zhu, C. Liu, J. Xu, Q. Jiang, H. Shi, E. Liu, Improving the electrical conductivity of PEDOT:PSS films by binary secondary doping, Electron. Mater. Lett. 12 (2016) 54–58. doi:10.1007/s13391-015-5272-x.

[8] Y. Han, Enhanced electrical properties of PEDOT:PSS via synergistic effect, Soft Mater. 16 (2018) 31–36. doi:10.1080/1539445X.2017.1387151.

[9] L. Yue, S. Wang, X. Zhao, L. Zhang, Nano-silicon composites using poly(3,4-ethylenedioxythiophene): poly(styrene sulfonate) as elastic polymer matrix and carbon source for lithium-ion battery anode, J. Mater. Chem. 22 (2012) 1094–1099. doi:10.1039/c1jm14568a.

[10] E. Vitoratos, An analysis of DC conductivity in terms of degradation mechanisms induced by thermal aging in polypyrrole/polyaniline blends, Curr. Appl. Phys. 5 (2005) 579–582. doi:10.1016/j.cap.2004.06.024.

[11] E. Vitoratos, S. Sakkopoulos, E. Dalas, N. Paliatsas, D. Karageorgopoulos, F. Petraki, S. Kennou, S.A. Choulis, Thermal degradation mechanisms of PEDOT:PSS, Org. Electron. Physics, Mater. Appl. 10 (2009) 61–66. doi:10.1016/j.orgel.2008.10.008.

[12] N. Duraisamy, G. Ponniah, J. Jo, K.-H. Choi, Structural and Electrical Properties of Ag Grid/Poly(3,4-ethylenedioxythiophene):Poly(styrene sulfonate) Coatings for Diode Application Through Advanced Printing Technology, J. Nanosci. Nanotechnol. 13 (2013) 5957–5963. doi:10.1166/jnn.2013.7542.

[13] E. Vitoratos, S. Sakkopoulos, E. Dalas, N. Paliatsas, K. Emmanouil, P. Malkaj, S.A. Choulis, Correlation between thickness, conductivity and thermal degradation mechanisms of PEDOT:PSS films, AIP Conf. Proc. 1203 (2010) 178–181. doi:10.1063/1.3322407.

[14] F. Greco, A. Zucca, S. Taccola, A. Menciassi, T. Fujie, H. Haniuda, S. Takeoka, P. Dario, V. Mattoli, Ultra-thin conductive free-standing PEDOT/PSS nanofilms, Soft Matter. 7 (2011) 10642–10650. doi:10.1039/c1sm06174g.

[15] A.M. Nardes, M. Kemerink, M.M. de Kok, E. Vinken, K. Maturova, R.A.J. Janssen, Conductivity, work function, and environmental stability of PEDOT:PSS thin films treated with sorbitol, Org. Electron. Physics, Mater. Appl. 9 (2008) 727–734. doi:10.1016/j.orgel.2008.05.006.

[16] A.M. Nardes, M. Kemerink, R.A.J. Janssen, Anisotropic hopping conduction in spin-coated PEDOT:PSS thin films, Phys. Rev. B - Condens. Matter Mater. Phys. 76 (2007) 1–7. doi:10.1103/PhysRevB.76.085208.

[17] A.M. Nardes, R.A.J. Janssen, M. Kemerink, A morphological model for the solvent-enhanced conductivity of PEDOT:PSS thin films, Adv. Funct. Mater. 18 (2008) 865–871. doi:10.1002/adfm.200700796.

[18] A.M. Nardes, M. Kemerink, R.A.J. Janssen, J.A.M. Bastiaansen, N.M.M. Kiggen, B.M.W. Langeveld, A.J.J.M. Van Breemen, M.M. De Kok, Microscopic understanding of the anisotropic conductivity of PEDOT:PSS thin films, Adv. Mater. 19 (2007) 1196–1200. doi:10.1002/adma.200602575.

[19] E. Vitoratos, S. Sakkopoulos, N. Paliatsas, K. Emmanouil, S.A. Choulis, Conductivity Degradation Study of PEDOT:PSS Films under Heat Treatment in Helium and Atmospheric Air, Open J. Org. Polym. Mater. 2 (2012) 7–11. doi:10.4236/ojopm.2012.21004.

[20] A.M. Nardes, On the conductivity of PEDOT: PSS thin films, 2007. doi:http://dx.doi.org/10.6100/IR631615.

[21] A.M. Nardes, M. Kemerink, R.A.J. Janssen, J.A.M. Bastiaansen, N.M.M. Kiggen, B.M.W. Langeveld, A.J.J.M. Van Breemen, M.M. De Kok, Microscopic understanding of the anisotropic conductivity of PEDOT:PSS thin films, Adv. Mater. 19 (2007) 1196–1200. doi:10.1002/adma.200602575

.

Chapter 3

In-solution doping of PEDOT:PSS by sulfuric acid

Secondary doping made by sulfuric acid is one the most common approach for increasing the electrical conductivity of PEDOT:PSS. Most of works reported in literature, however, use this chemical as a post-deposition dopant, while no mention is given about the effects of the direct acidification of a pristine PEDOT:PSS solution with H_2SO_4. In this Chapter, this lack in the scientific production is filled by a systematic study of the effects due to the direct acidification of PEDOT:PSS with sulfuric acid. Polymer films with different acid content were obtained by spin coating and characterized after deposition and aging. Sheet resistances as low as 40 Ohm/sq, with an average transmittance of ≈75% in the visible range, were obtained and samples doped with this method also showed good aging resistance. These results have identified this in-solution doping method as a novel, efficient and easy strategy for improving the electrical performance of PEDOT:PSS.

3.1 - Introduction

Commercially available PEDOT:PSS is supplied with different electrical and optical specifications. As known from literature, its optical and electrical characteristics are ruled by opposite trends [1, 2–10], making difficult to obtain a good compromise. In order to increase the PEDOT:PSS electrical conductivity,

several chemicals, such as organic solvents [10–12], alcohols [13–15], polyols [16–19], surfactants [20–22] and inorganic acids [17,23–26] are proposed, by using an in-solution secondary doping approach. The direct addition of the dopant to the PEDOT:PSS aqueous solution is indeed the most used method for doping by organic solvents and surfactants. In some cases, it is also reported that the use of some chemicals, such as isopropyl alcohol, can lead to the recovery of the initial electrical properties of a years-aged PEDOT:PSS [15]. High resistive PEDOT:PSS films have been also improved by specific post-deposition annealing treatments, like for instance by changing the temperature [16,27], duration [28] and environment [16]. Acid casting on the annealed PEDOT:PSS films is another very common doping alternative in the post-deposition class strategies [24,29]. Secondary doping can be either carried out by dipping the polymeric film into acid solutions [23,25] or by the exposition of the undoped films to acid vapour [26]. Nevertheless, these approaches cannot be thought on an industrial scale because of the large amounts of chemicals required, long times of thermal treatments and poor reproducibility. Moreover, there is no mention in the literature about the effect of the acidic doping when run directly to the PEDOT:PSS aqueous solution. Finally, even if it is known that doping by acids improves the PEDOT:PSS films conductivity [23–26], no optical properties and their correlation with the electrical ones are reported.

In this Chapter, the main purpose has been to investigate the effect of the in-solution acidification with H_2SO_4 of the PEDOT:PSS solution on the optical and electrical properties of the doped films. The layers were obtained by easy and fast spin-coating deposition, which meets those requirements of cost-effectiveness, reproducibility and short manufacturing time. These features allow for the overcoming of limits of drop casting and vapour exposure techniques. For this

purpose, three concentrations of sulfuric acid, 0.3, 0.7 and 1% wt., have been examined. Doped PEDOT:PSS films have been characterized by EDX, Raman analysis, optical and electron microscopy, four point probe analysis and direct transmittance measurements, in the as deposited conditions and after three weeks aging. Haacke's figure of merit [30] have been calculated for the first time for doped PEDOT:PSS, giving an estimation of the balance between the electrical and optical properties. The results obtained have demonstrated good electrical and optical properties of the doped samples together with appreciable stability to aging, thus suggesting that the novel "in-solution" method represents an efficient, easy, low cost strategy for preparing conductive PEDOT:PSS films.

3.2 – Sample Preparation

High conductive grade PEDOT:PSS aqueous solution (Sigma Aldrich), 1.1% wt. and PEDOT to PSS content in ratio 1:2.5, and high purity sulfuric acid, H_2SO_4 (96%, Basf), were used as received and without any further purification. Glass square substrates sizing from 1 cm to 1.5 cm were obtained by cutting Corning 2947 glass slides and were used for the electrical and optical characterizations, while square c-Si <100> samples of 1 cm side were used for morphological and chemical analysis. Substrates were cleaned by sonication in acetone, isopropyl alcohol and deionized water for 5 minutes each and finally dried under nitrogen flow. In the case of the c-Si substrate, immediately before each polymer deposition on it, native silicon oxide of few nanometres was removed by wet etching in a 5% HF water solution for 1 minute at room temperature in order to allow a better adhesion to the underlying substrate. Pristine PEDOT:PSS was taken under a gentle stirring for 15 minutes at room temperature before each use, in order to

homogenize the colloidal suspension. Treated PEDOT:PSS solutions were prepared by adding H_2SO_4 directly into the pure suspension, obtaining three different acid concentrations of 0.3, 0.7 and 1% wt. Strong shaking of the acidified PEDOT:PSS solutions was required in order to obtain a uniform dispersion before each deposition. Therefore, undoped and treated PEDOT:PSS films were deposited by spin coating at 1500 rpm for 5 minutes on Si and glass substrates, pre-heated at 80°C for 1 minute. Samples were then annealed in an oven for 10 minutes under vacuum conditions (0.01 mbar) at 100, 150 and 200°C. Low magnification images were acquired by optical microscope on the chemical liquid sources and on the deposited films. The electrical resistivity was measured by using the Four Point Probe technique with a collinear configuration. In order to perform electrical measurements, four silver collinear dots were used as metallic contacts to avoid scratching of the polymer layers by the four tungsten probes, according to a strategy and a design already reported in Chapter 2. The metallic circular dots were obtained by sputtering silver through a shadow mask with holes of 600 μm of diameter and 1 mm edge-edge distance. Silver dots with 600 nm of thickness were obtained on the 1 x 1 cm samples by sputtering in a Quorum Q300TD system at 50mA in a $5x10^{-3}$ bar. The silver contacts were always sputtered at the centre of each sample in order to avoid any edge-effect during the electrical measurements. Probe spacing-effect and any further correction factor were taken in regard when sheet resistance was calculated for each sample (see Appendix B for further details). Optical characterizations consisted on the acquisition of the direct transmittance measurements carried by spectroscopic ellipsometer J.A.Wollam V-Vase (Vertical Variable Angle Spectroscopic Ellipsometer) in the range from 190 nm to 2100 nm. Experimental setup is assembled with a 75W lamp source, a monochromator and an optic fibre before the sample and a Si/InGaAs detector placed on the back of the sample. Morphological characterization was performed

by a field emission Scanning Electron Microscope equipped with energy dispersive X-ray (EDX) microanalysis system. Raman spectra were acquired in the backscattering mode using a 632.8 nm laser source.

3.3 – Effect of the Addition of H_2SO_4 to PEDOT:PSS

Commercially available PEDOT:PSS aqueous solution normally appears as a dark blue, homogeneous and viscous suspension. The addition of pure sulfuric acid directly to the pristine polymer leads to the formation of dark blue, immiscible agglomerates. This sort of precipitate, once formed, is immiscible also when heating, vigorous stirring and even sonication are applied. Moreover, this behaviour does not have a threshold related to the concentration of the acid directly dropped, since it is easily recognizable also when very low amounts of H_2SO_4 are used.

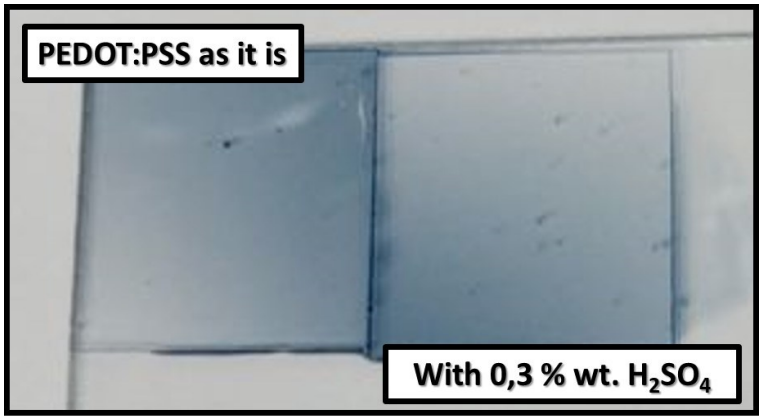

Fig. 3.1: Optical image of PEDOT:PSS aqueous solutions, pristine one (on the left), and with 0.3 % wt. of H_2SO_4 directly added to the polymer blend (on the right). Some

dark blue dots are recognizable in both solutions, meaning that some precipitation effect is manifested.

Fig. 3.1 shows the pristine PEDOT:PSS solution and that one enriched of 0.3 % wt. of acid. It must be noted that, since PEDOT:PSS is naturally deep-dark blue, the precipitates formed after acid addition are not easy to be distinguished from the rest of solution. For this reason, both suspensions are observed putting a drop of each solution between a microscope glass slide and a coverslip. As it is possible to see, blue agglomerates are discernible. Moreover, as shown in the Fig. 3.2, the agglomerates density increases with increasing the acid concentration.

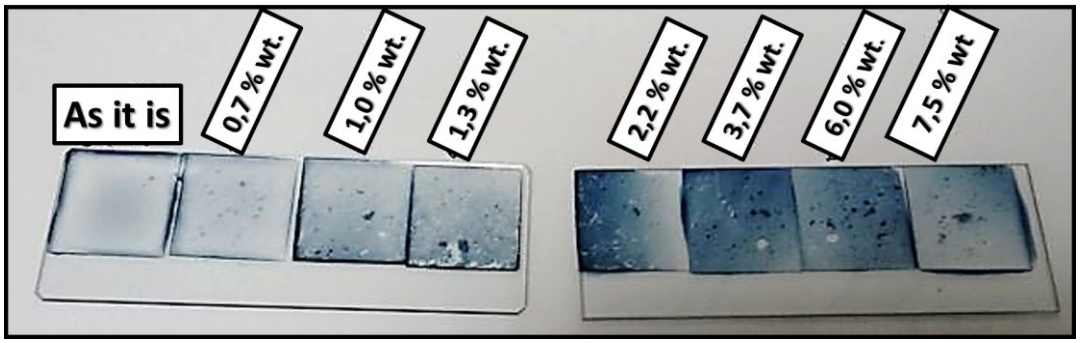

Fig. 3.2: Optical image of different PEDOT:PSS solutions with different acid-content. Image is acquired by placing a drop of each solution between two microscope glass slides. The first sample on the left corresponds to the pristine PEDOT:PSS solution, which is taken as reference.

For the purposes of this work, and in the next sections, only three acid-content solutions will be taken in regard, in particular 0.3, 0.7 and 1 % wt. of H_2SO_4. Fig. 3.3a-d show more in detail the analogues solution already seen above with a magnification of 100X: in the undoped PEDOT:PSS, no micrometre agglomerates or particles are observed in an area of about 4 mm^2 (Fig. 3.3a). Vice versa, for the

0.3% wt. solution, PEDOT:PSS shows the formation of agglomerates with size of hundreds of micrometres (Fig. 3.3b). For further additions of sulfuric acid, the treated PEDOT:PSS has a higher viscosity with respect to the pristine solution and the agglomerates density increases (Fig. 3.3c and d). Solutions with >>1% wt. of acid present "solid" blue polymeric agglomerates and a colourless, transparent supernatant. Further details and results about this latter case will be well discussed and addressed in the Chapter 4. Here instead, to avoid further precipitation, acid contents higher than 1% wt. have not been considered. After spin coating and annealing, the agglomerates present in the liquid are still clearly visible on the sample surface (Fig. 3.3e-d), showing the same characteristics of those already described for the solution phase.

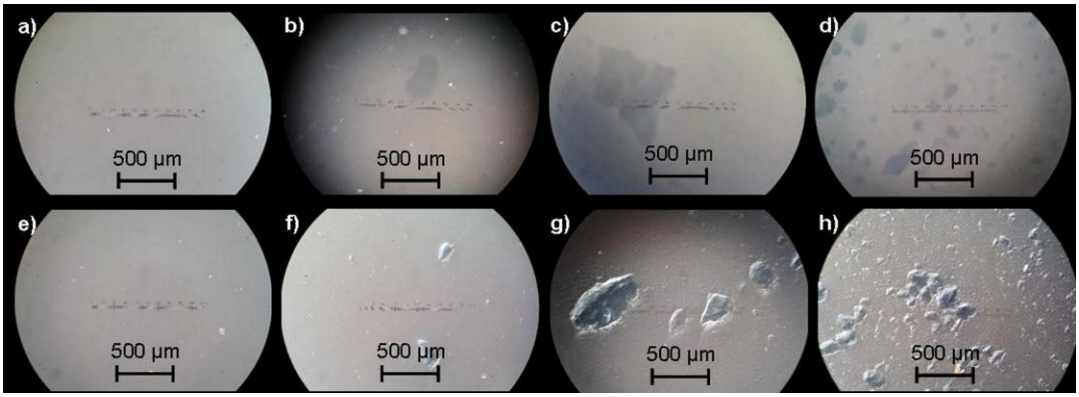

Fig. 3.3: Optical microscope images of samples spun at 1500 rpm on glass substrates and annealed at 200°C with different acid concentrations, respectively: e) 0%, f) 0.3% wt., g) 0.7% wt. and h) 1% wt. Glimpsing line at the centre of each image corresponds to the marker of the optical microscope.

To the naked eye, the substrate area for the low doping case appears as a uniform blue film, while, by increasing the acid concentration, both density and size of

agglomerates increase. A schematic representation of the samples obtained after doping, deposition and annealing is give in the Fig. 3.4.

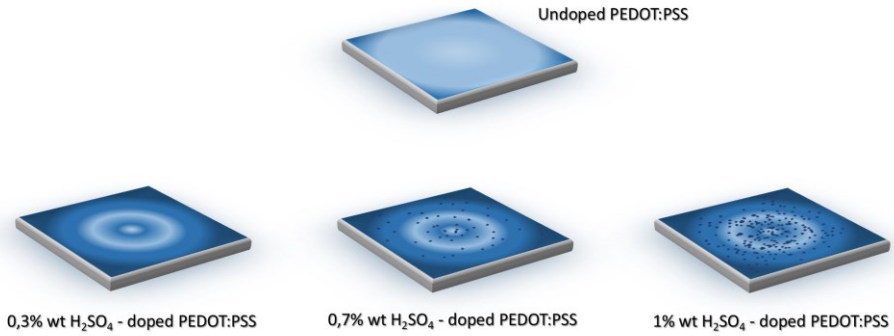

Fig. 3.4: Sketch of samples obtained after spin coating deposition of the undoped PEDOT:PSS and of three different acid-contents solutions.

Due to the presence of the agglomerates it is important to investigate the surface roughness, in order to understand if they play a role on the surface morphology. Due to their large size, standard surface characterization techniques, such as atomic force microscopy, cannot be used to investigate the thickness inhomogeneities of the film. For this reason, optical microscopy was used to estimate the surface morphology conditions and the roughness. By adjusting the microscope focus and referring to its calibrated z-axis, it was possible to observe that the agglomerates protrude from the surrounding areas and that the height difference was of some of micrometres, in the case of much larger agglomerates. A more fine analysis of the surface of the samples was made by the SEM in tilted mode. About this, Fig. 3.5 shows a cross section SEM image of 1% wt. doped PEDOT:PSS film. The image reported offers a general overview of the surface morphology. It is possible to see an extended film with a thickness of 180-200 nm, indicated as matrix, with

embedded the agglomerates a few microns high. This analysis confirms the preliminary data obtained by optical microscopy.

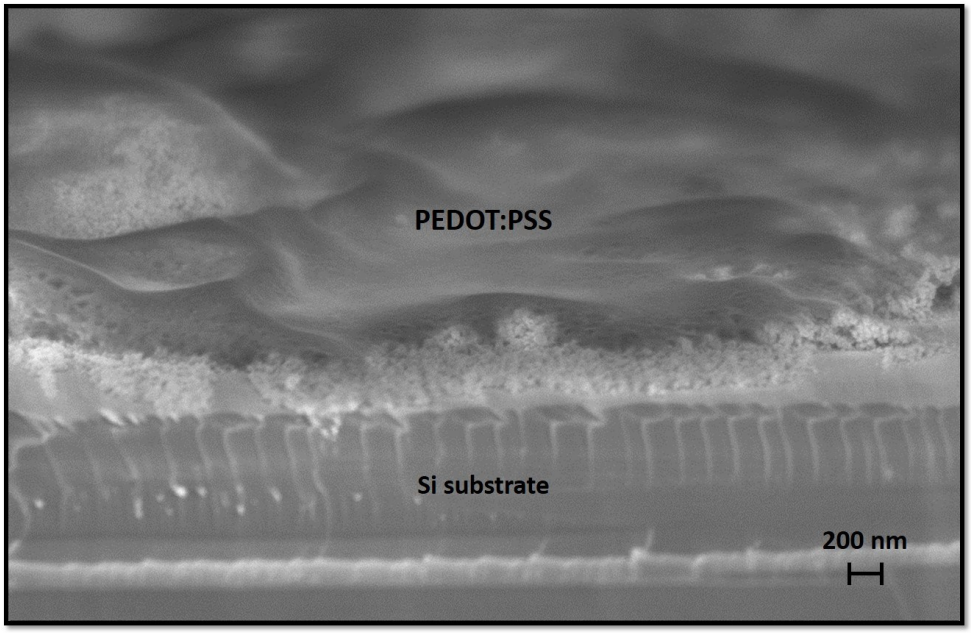

Fig. 3.5: Cross-section SEM image acquired on a PEDOT:PSS film, doped with 1% wt. of H_2SO_4, spun on c-Si substrate and annealed in vacuum at 200°C for 10 minutes. Image acquired with stage tilted at 14°.

Some interesting observations can be made by analysing the matrix more in detail. Fig. 3.6a shows a cross section SEM image of a zone of the doped film in which only few agglomerates are detected with a size of some hundreds of nanometres while the inset in the Fig. 3.6b shows a zoomed portion of the sample. Here, it is possible to see that the polymer layer is composed by some particles sized some tens of nanometres which are present everywhere along the film depth. Each of this particle has been attributed to the basic unit of the precipitate, as well as the conductive grain of which the polymer blend is made [31-33]. Indeed, it is

supposed that the agglomerates formation in the PEDOT:PSS solution starts probably from these aggregates which stay suspended in aqueous medium. When the acid content is gradually increased, these small aggregates join with each other, thus giving place to some bigger agglomerates which reach the size of several hundred of microns (schematic representation in Fig. 3.6c).

Further details about the reaction mechanism and interpretation about the particles' composition will be supplied in the next Chapter.

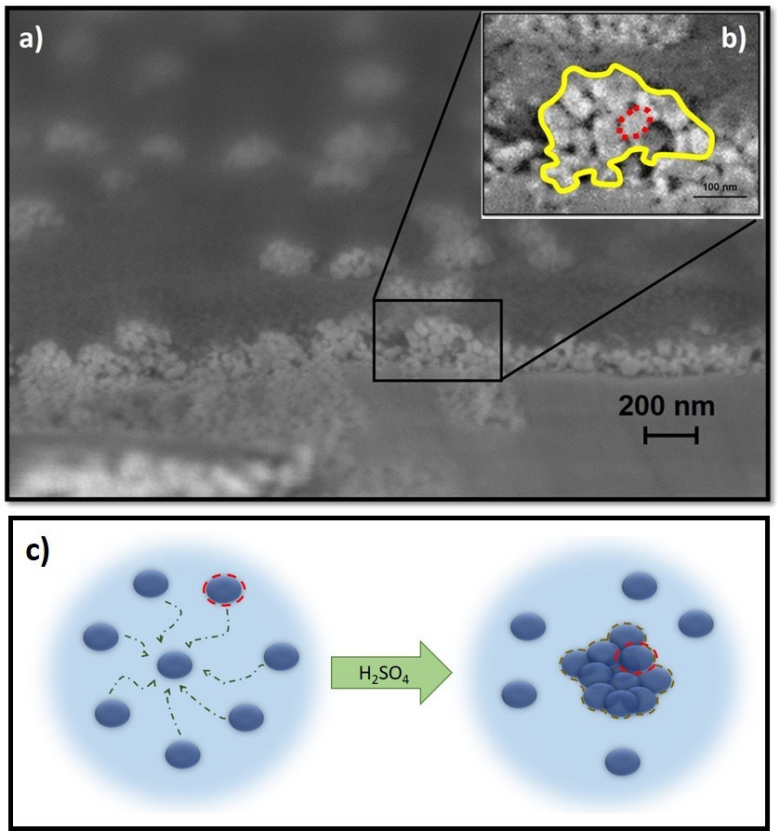

Fig. 3.6: (a) Scanning electron microscopy in cross view of a PEDOT:PSS film doped with 1% wt. of sulfuric acid, deposited by spin coating at 1500 rpm for 5 min on Si substrate and annealed at 200°C for 10 min in vacuum chamber (0.01 mbar). The inset shown in figure (b) is a detail of the sample, where a particle composing the polymer blend is indicated by the red dashed line and the agglomerate is evidenced

by the yellow continuous one. (c) Hypothetical scheme of reaction between PEDOT:PSS and sulfuric acid. The acid addition causes a change of the solubility of both PEDOT and PSS, which in its turn causes the precipitation of the grains made by the polymer blend. Particles thus collapse and separate from the rest of solution.

3.4 – Electrical Characterization

For the electrical characterization, four-point probes (4PP) measurements were performed on the undoped and the three doped samples. These measurements were run immediately after the polymer deposition and metallic dots formation and hereinafter they will be identified as "fresh" samples. Seen the morphological characteristics of the doped films, the electrical measurements return the average conductivity, since the total sample length investigated by 4PP corresponds to about 5 mm, i.e. much larger than the largest observed agglomerate. However, a statistical analysis on three samples for each annealing temperature explored (100, 150 and 200°C) was conducted. On each one, 16 Ag pads were deposited according to the scheme in the Fig.3.7:

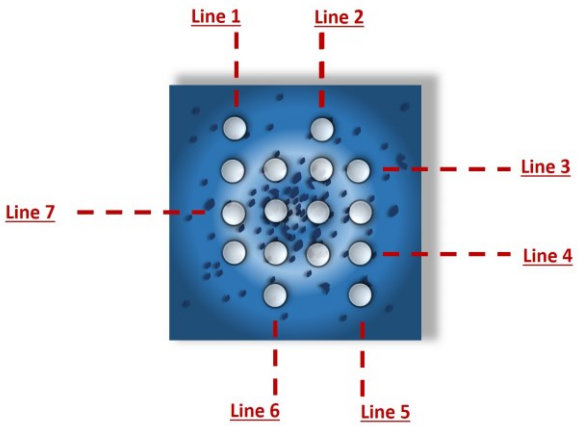

Fig. 3.7: Scheme of Ag dots on a film of PEDOT:PSS doped with 1% wt. of H_2SO_4. Line 7 represents the main row of dots, i.e. those placed at the centre of the square sample.

According to the scheme of Fig. 3.7, on each sample a complete set of measurements will give seven values of sheet resistance. Fig. 3.8 reports the values obtained for each set prepared at different annealing temperatures:

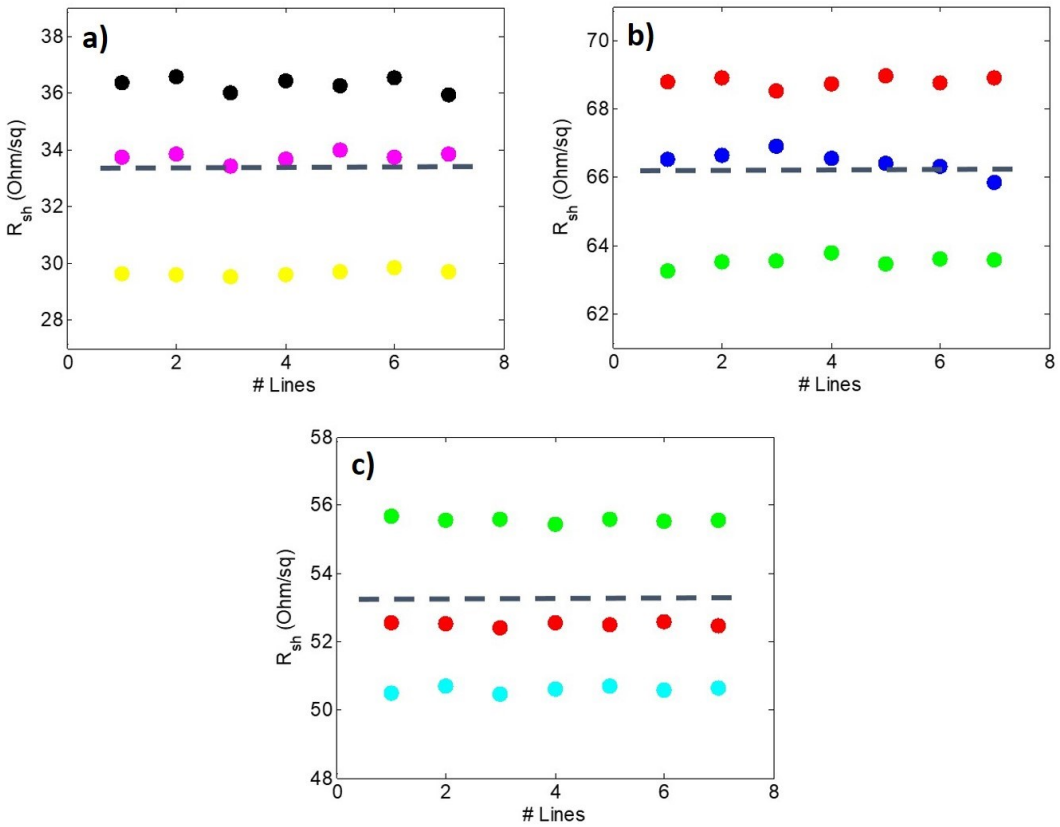

Fig. 3.8: Sheet resistance values found for each row of metal pads aligned as in the scheme shown in Fig. 7. Each colour used in a graph above represents a sample. Dashed line represents the value of sheet resistance averaged on three twin samples. Measurements are performed on samples annealed in vacuum at a) 100, b) 150 and c) 200°C.

According to the Fig. 3.8, it is seen that, for many 4PP measurements on different parts of the same sample and on twin ones, R_{sh} values are always comparable and

within an error bar of 2-3 Ohm/sq, calculated as standard deviation, and thus the sheet resistance value acquired on sample's centre (corresponding to line 7 in scheme) can be considered representative to the effective electrical behaviour of doped films**.**

After these forewords, the next considerations concern the comparison in term of sheet resistance between samples with different acid-contents and three annealing temperatures.

Fig. 3.9a shows the R_{sh} response of fresh samples as a function of the three H_2SO_4 concentrations for the three annealing temperatures, 100, 150 and 200°C. Results show that the sheet resistance slightly decreases when the annealing temperature is increased from 100 to 200°C, showing a moderate dependence on it (see Fig. 3.9b to see in detail the variation of R_{sh} of 1% wt. doped sample as a function of different annealing temperatures).

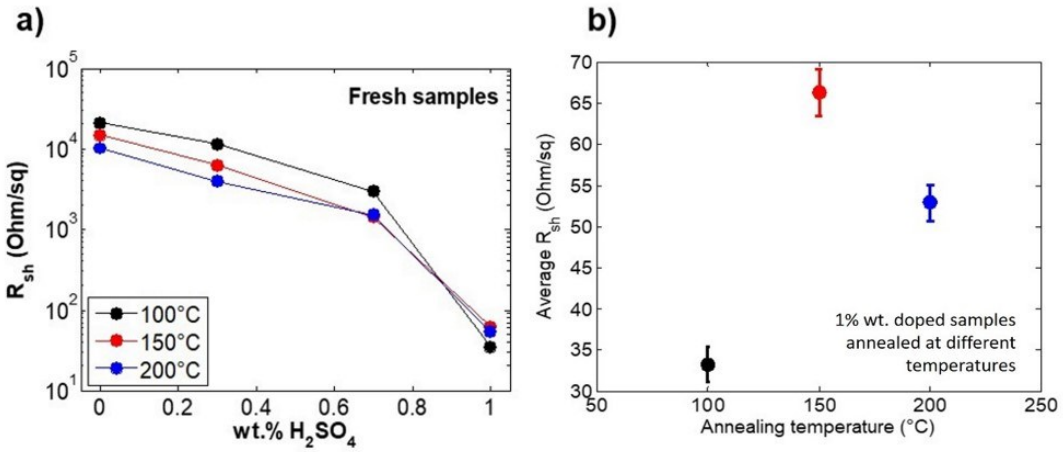

Fig. 3.9: a) Sheet resistance values for samples with different acid contents (0, 0.3, 0.7 and 1% wt.) and three different annealing temperatures (100, 150, 200°C). Data acquired immediately after the polymer deposition and metallic dots formation (fresh samples); b) R_{sh} in linear scale of 1% wt. doped samples reported as a function of the annealing temperatures.

This moderate effect could be attributed to a re-arrangement of the polymeric chains during the annealing, or more likely, to a more efficient removal of water. Indeed, higher temperature leads to a faster aqueous phase evaporation, thus inducing an easier inter-charge transfer and inter-chain hopping.

A remarkable effect on the sheet resistance is seen with the variation of the acid content: a decrease of two orders of magnitude of R_{sh} is observed when the acid content changes from 0 to 1% wt. and the best result is obtained for the sample annealed at 100°C.

In order to verify if an aging effect plays an influence on the electrical response, both untreated and treated samples have been monitored up to forty days. In Fig. 3.10 aging curves will be reported only for samples with the four acid concentrations used and annealing carried at 100° C in vacuum. In the same graph it is also shown the comparison between a “old” PEDOT:PSS solution, aged of 2 years, and a new one, which means open and used for the purposes of this work within the successive two months.

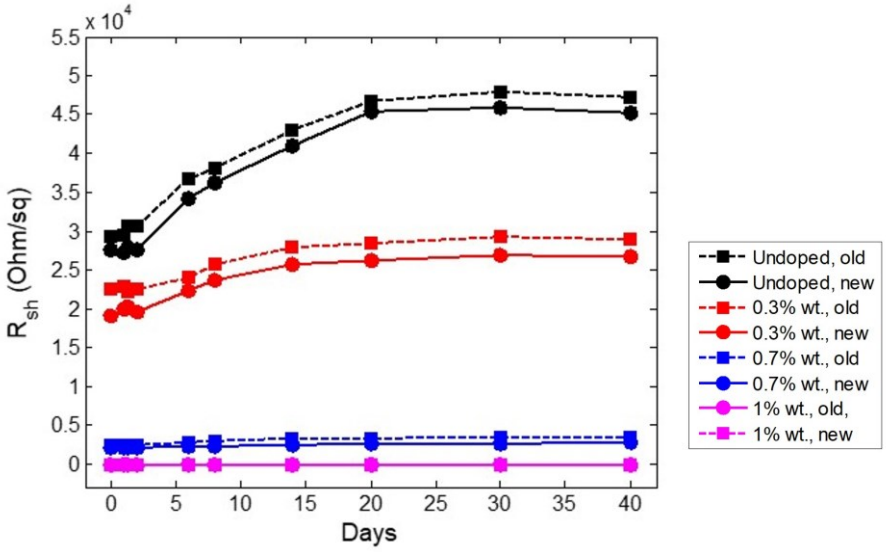

Fig. 3.10: Aging graph acquired by monitoring the sheet resistance of four samples with different acid contents and annealed in vacuum (0.01 mbar) at 100°C. Squares and dashed lines correspond to those samples prepared by a PEDOT:PSS solution aged of 2 years. Dots and solid lines represent the samples obtained from a new solution which was open and used for this purpose within 2 months. Percentages in the side legend indicate the H_2SO_4 content in each solution expressed as % wt.

As it is possible to see from the graph in Fig. 3.10, the undoped sample manifests the more intense variation of the sheet resistance calculated. Indeed, its value starts around 30 kOhm/sq and reaches 45 kOhm/sq after 40 days. For doped samples, instead, it is still possible to assist to a modification in the electrical response due to the aging effect, but this time, the variation of the R_{sh} value decreases with increasing the acid content. In the case of the most doped sample, the variation in the whole range of time explored is basically negligible. This effect suggests that the sulfuric acid addition helps for preserving from the aging, and this influence depends on its percentage. Moreover, this aging-preserve effect is not influenced by the oldness of the initial solution used. Indeed, what was discussed so far can be applied both to the case of the aged and new solution of PEDOT:PSS. The relevant

consequence in both cases is that, the two curves relative to the solutions overlap for higher acid concentrations. In other words, this means that the oxidative action due to the acid is able to compensate the aging-effect of the solution, thus "restoring" its conductivity, which eventually coincide with that one of the fresh-opened solution.

After these results, the 4PP were indeed performed on both untreated and treated samples annealed at 100, 150 and 200°C, after storing in air at 20°C for 20 days. This time for monitoring these samples was chosen since, as seen in the Fig. 3.10, after 20 days sheet resistance values tend to stabilize in each case, and no further, relevant variations are observed between 20^{th} and 40^{th} days of aging. For simplicity, these 20 days-aged films measurements will be indicated hereafter as "aged" samples. The results are reported in Fig. 3.11 in which Fig. 3.11a shows the R_{sh} values measured for fresh sample (as reported in Fig. 3.9a), while Fig. 3.11b reports the sheet resistance measured on 20 days-aged samples. In this last one, R_{sh} trends seem to be not affected by the aging, showing a similar decrease with the acid concentration as that observed in the fresh samples. However, from the comparison between the fresh and aged cases, Fig. 3.11a and Fig. 3.11b, it is observed that, while for the undoped films the aging effect leads to 50% increase of the sheet resistance with respect to the corresponding fresh samples, the most doped films show a small increase of the R_{sh}.

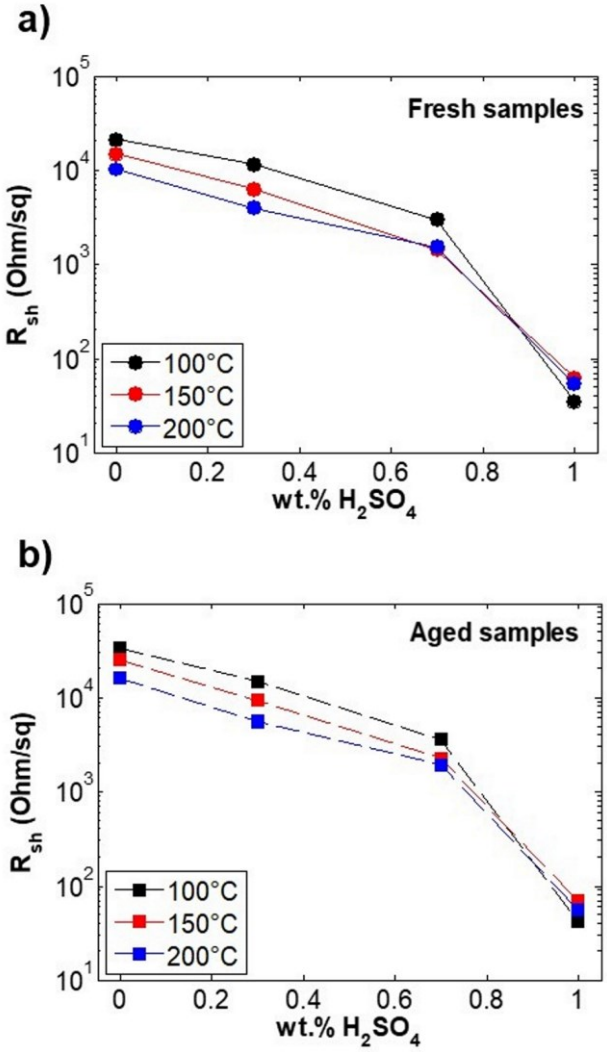

Fig. 3.11: Sheet resistance values for samples with different acid contents (0, 0.3, 0.7 and 1% wt.) and three different annealing temperatures (100, 150, 200°C): a) results acquired immediately after the polymer deposition and metallic dots formation (fresh samples) and b) after 20 days (aged samples).

Summarizing these results, it was observed that in the fresh samples the lowest R_{sh} is reached for the highest acid content and the lowest annealing temperature. However, when the aging effect is examined, it is shown that the 1% wt. H_2SO_4

sample annealed at 200°C has the minimum deterioration, since the sheet resistance presents a variation of only 3.7% after 20 days. The electrical response observed so far can be related to a chemical modification of the polymers caused by the acidification of the solution. Indeed, when the acid content increases into the PEDOT:PSS solution, the protonation grade of PSS also enhances and makes weaker the Coulomb interactions between PEDOT and PSS and this causes the separation process. Under massive precipitation conditions, the PEDOT forms conductive domains of different sizes ranging from several hundred of microns down to a few microns, separated by PSS. When a thin film is deposited starting from a solution with these characteristics, it reproduces the high density agglomerate conditions of the starting solution. Numerous PEDOT domains form a conductive path through hopping transport mechanisms, which is thus manifested by the reduction of the electrical resistance of the material.

Since the sheet resistance is not an intrinsic feature of the material, but it depends on the thickness of the layer, it cannot complete alone the electrical characterizations of the samples described so far. In order to complete this study, the electrical conductivity of both undoped and doped samples was also calculated. This starts from the films thickness acquired by ellipsometer measurements, acquired on an area of about 3.14 mm^2, i.e. the ellipsometer laser spot probe area (≈1 mm diameter). The film thickness, averaged on this area, as a function of the acid content is reported in the Fig. 3.12. Error bar was calculated as standard deviation of thickness values found on different samples.

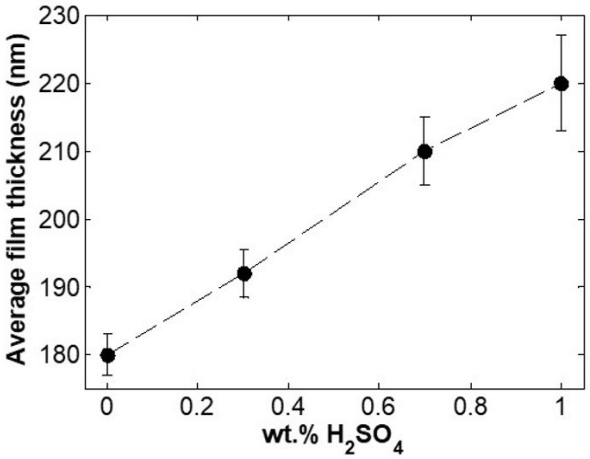

Fig. 3.12: Average film thickness obtained by ellipsometer measurements and reported as a function of the acid amount used for doping. Error bar is calculated as standard deviation of thickness values found on different samples.

The average thickness ranges between 180 and 220 nm. The electrical conductivity was thus calculated from these values and those of the sheet resistance reported above and for both fresh and aged samples (Fig. 3.13a and b, respectively). As expected from the sheet resistance, samples with an acid content of 1% wt. manifest the best electrical performance. The electrical conductivity reaches values in the order of 10^3 S/cm, while finer variations can be related to the annealing temperature used.

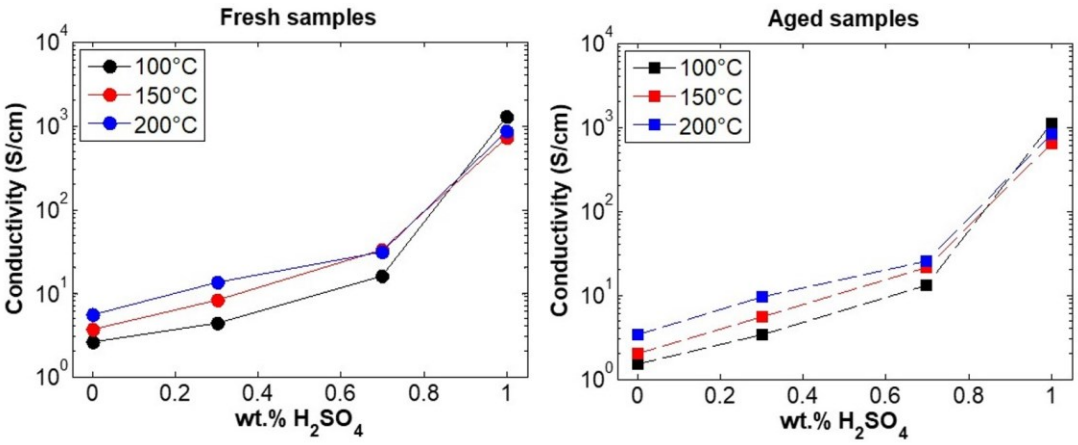

Fig. 3.13: Electrical conductivity obtained for each sample as a function of the acid percentage used for the different annealing temperatures used. Values of σ are reported for fresh and aged samples in left and right graphs respectively.

3.5 – Optical Characterization

The optical properties of the doped PEDOT:PSS were investigated in order to estimate the transparency of the deposited films. Direct transmittance spectra were acquired with spectroscopic ellipsometer in vertical configuration by exploring a wavelength range from 190 to 2100 nm. However, only 380-1470 nm range was reported. Fig. 3.14a shows the transmittance, T, of fresh doped and undoped samples annealed at 200°C and the highest T values are reached between 400 and 500 nm in each case.

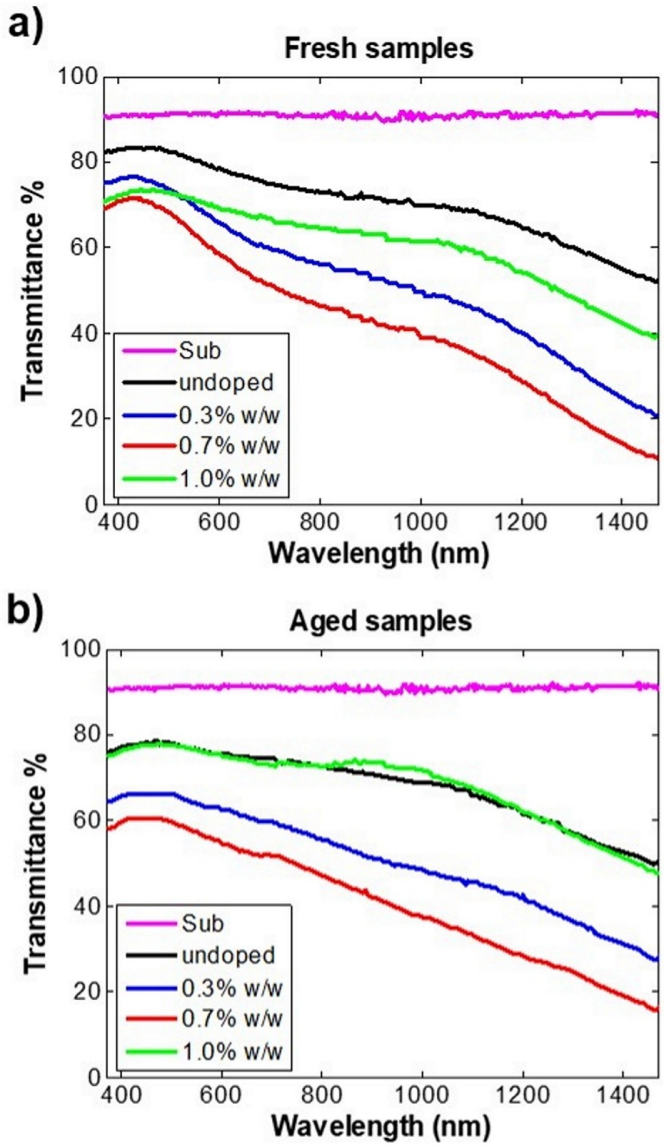

Fig. 3.14: Direct transmittance measurements in 380-1470 nm range for PEDOT:PSS films with different acid contents (0, 0.3, 0.7 and 1% wt.) annealed at 200°C. a) Fresh and b) 20 days-aged samples. Note that all the transmittance curves were not normalized to the glass substrate transmittance, which is reported in the graphs as the magenta curve.

It is seen that, when the acid concentration ranges between 0 and 0.7% wt., the transmittance values decrease with the increase of the dopant content. This is in agreement with the well-known opposite optical and electrical trends which show that with increasing the conductivity, the optical transmittance worsens [1-9].

On this trail, the highest acid-content sample would be expected to show the worst optical properties by a strong reduction of T. However, for the 1% doped sample, the transmittance unexpectedly increases in both the fresh and aged cases (green curve in Fig. 3.14a and b). By performing a statistical survey on several 1% wt. - H_2SO_4 treated samples, the average T results to be ranging from 70 to 80% for each film. This large fluctuation of the average transmittance is caused by the morphological inhomogeneity due to the agglomerates on the surface which have a lateral size comparable with the laser spot of the ellipsometer. Only in this case the agglomerates on the PEDOT:PSS surface can affect the optical transmittance on a local scale, but the average T% still shows high values. Seen the complexity of the surface morphology in the case of 1% wt. doped films, a statistical analysis of the direct transmittance on different spots of the sample was performed. For this analysis, the direct transmittance was acquired on five different spots of a sample, according to the scheme reported in Fig. 3.15.

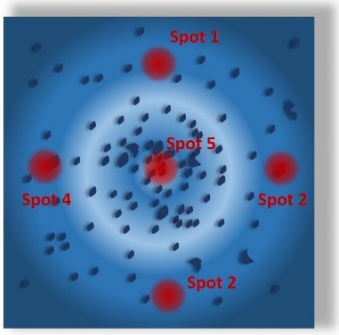

Fig. 3.15: Schematic representation of the sample and of the 5 positions where the optical transmittance measurements were performed.

The results of these five measurements are reported in the Fig. 3.16a. As it is possible to see, they range between 70 and 80% within 400 and 1000 nm. The T value averaged along these measurements is reported as the green curve in the Fig. 3.16b, showing that the transmittance is about 75% between 400 and 500 nm, as it was already observed in the Fig. 3.14.

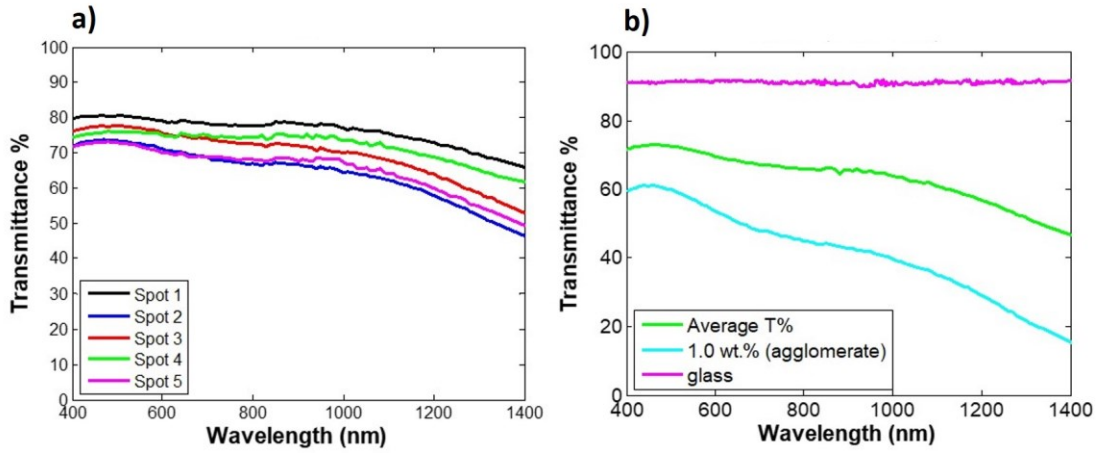

Fig. 3.16: a) Optical transmittance measurements obtained in five different spots on 1% wt. doped sample, according to scheme in Fig. 3.6; b) green curve represents the average of the measurements reported in Fig.3.16a, while ciano curve corresponds to the T measured onto one of the large agglomerates.

However, if the laser beam source is placed exactly on a large agglomerate with lateral size of a few hundreds of microns, i.e. with a lateral size comparable to the laser source spot diameter (about 1 mm), as schematized in Fig. 3.17, a significant decrease of the transmittance with respect to its average value is observed (ciano curve in Fig. 3.16b).

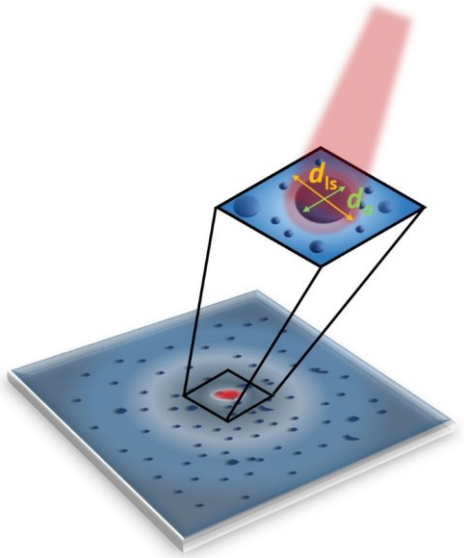

Fig. 3.17: Scheme of T measurement by ellipsometer onto one of the largest agglomerates.

This behaviour is expected since dark blue agglomerates likely manifest an optical absorption in the red region, in agreement with a decrease of the T at long wavelengths. Moreover, as it was already discussed in the previous section, it is observed that the agglomerates cause an increase of the local thickness of the polymeric film which decreases the quantity of light passing through. However, this effect is negligible because the large agglomerates are very small with respect to the sample size, which is 1.5 cm. Moreover, since the agglomerates are spread everywhere on the surface, the optical properties of a film have to be expressed only as a global feature obtained by the statistical survey. Since the T value obtained in different points of the sample has provided an average transmittance of about 75%, as seen above, it means that the inhomogeneities and agglomerates are negligible with respect to the size of the sample in terms of optical transparency.

3.6 – Figure of Merit

It is well known that the electrical and optical properties of the doped PEDOT:PSS follow opposite trends [1-9]. Nevertheless, since this material is often used for those applications where both properties are needed to be controlled, Haacke et al. have formulated a Figure of Merit (FOM), defined as T^{10}/R_{sh}, in order to weight both the contributions of the electrical and optical characteristics. Therefore, the FOM is here used to give an estimation of both properties for undoped and doped samples. Fig. 3.19a reports the FOM calculated between 380 and 1470 nm. For the lowest acid content film, even if there is a slight reduction of the sheet resistance (Fig. 3.8a), a stronger deterioration of the optical transmittance is observed with respect to the untreated film (Fig. 3.13a). For this reason, FOM calculated for the 0.3% wt. sample shows a reduction with respect to the undoped one from 500 nm onwards. Vice versa for the 0.7% wt. sample, FOM shows a good improvement with respect to the reference, since the sheet resistance is one order of magnitude less than the untreated film. Therefore, in this case, the reduction of T is accompanied by a clear benefit for the electrical properties. A remarkable result is obtained for the sample with 1% wt. of acid, since it shows the highest and constant FOM value. This result is due to a sheet resistance percentage change of 99.7% with respect to the untreated film, while transmittance still reaches 70% along most part of the spectrum. Moreover, it is worth to note the FOM resulting for the corresponding aged samples (Fig. 3.19b): films with an acid content of 0.3 and 0.7% wt. show a slight deterioration, while the highest acid content sample still shows a flat curve which has almost unchanged values from those ones of the fresh film.

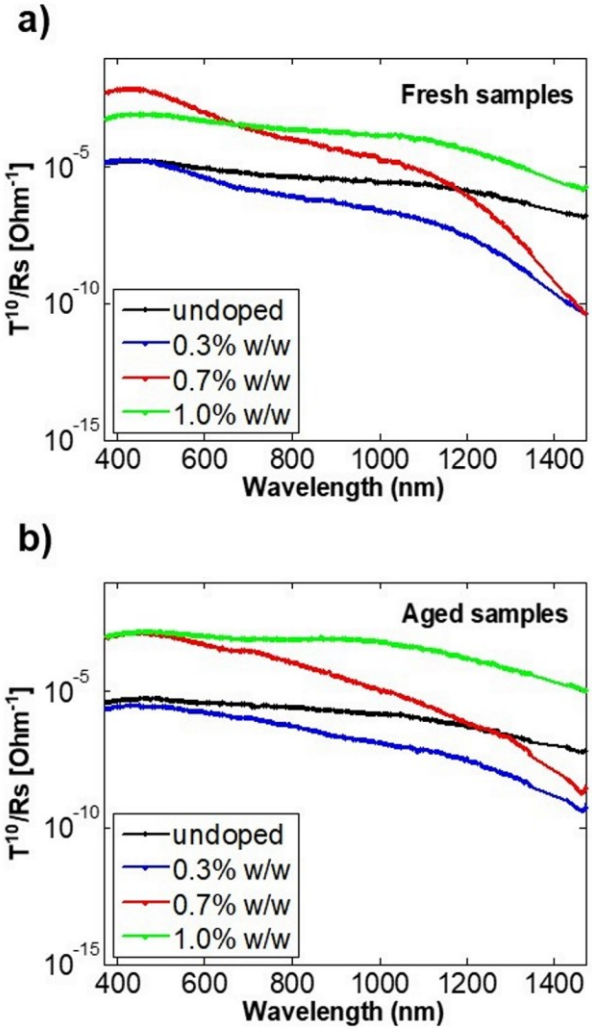

Fig. 3.18: Figure of Merit calculated for a) fresh and b) aged samples.

3.7 – Morphological and Chemical Characterization

SEM analysis was used in order to characterize the morphology of the undoped and doped films. For the untreated PEDOT: PSS, the surface appears homogenous and

smooth (see Chapter 2). EDX analysis relative to the K-lines of Si, S, C, and O has reported that the S/C weight ratio (%) is around 0.03 and it does not depend neither on the size of the area examined, nor on the spot investigated, since the sample is compositionally and morphologically homogeneous. In the case of the highest doped sample, the agglomerates observed through the optical microscope are revealed by SEM as darker areas on a brighter background (Fig. 3.19a). They do not show sharp edges and present a lateral size of hundred micrometres, while the height variation is hard to be directly evaluated by such analysis, as previously discussed in section 3.3. EDX analysis has been performed on both dark and bright areas and the resulting chemical maps relative to the K-lines of Si, S, C, and O are reported in Fig. 3.19b-e respectively. Table 1 reports the %weight found for each element in bright (spectrum 1) and dark (spectrum2) areas. In the dark regions the signal intensities of S, C and O increase, along with the S/C ratio and S/O ratio, indicating an enrichment in the S content, whereas a strong reduction of the Si signal is observed as evidenced in the maps of Fig. 3.19c and Fig. 3.19b respectively. This result can be explained with the increase of the local thickness in correspondence of the agglomerates, as found by optical microscope analysis and discussed in section 3.3. It is worth noting that a statistical survey made on different doped samples and in different dark and bright areas shows that S/C wt. ratio ranges between 0.23 up to 0.45 in the first and 0.07 in the latter ones. Even if an absolute quantitative analysis of the elements is not easily achieved by SEM-EDX without suitable calibration samples, it is possible to make some considerations about the sulphur/carbon relative ratio. The S/C ratio increment in both matrix and agglomerates with respect to the undoped film can be addressed to the increase of the S-content due to the use of sulfuric acid as secondary dopant. Moreover, the chemical characteristic of immiscibility [34] of the so obtained dark blue agglomerates leads to make the hypothesis that they are made, or at least

enriched, of PEDOT chains, which thus prevail on the PSS counterpart. Moreover, it was already reported, that the increment of the S/C ratio is attributed to a major content of PEDOT specimen with respect to the styrenic one. The considerations made so far are also supported by the decrease of the R_{sh} already seen in the section 3.2. Indeed, the presence of the PEDOT-rich agglomerates obtained by the acidification of the initial solution form a conductive path through hopping transport mechanisms when spun onto the substrate.

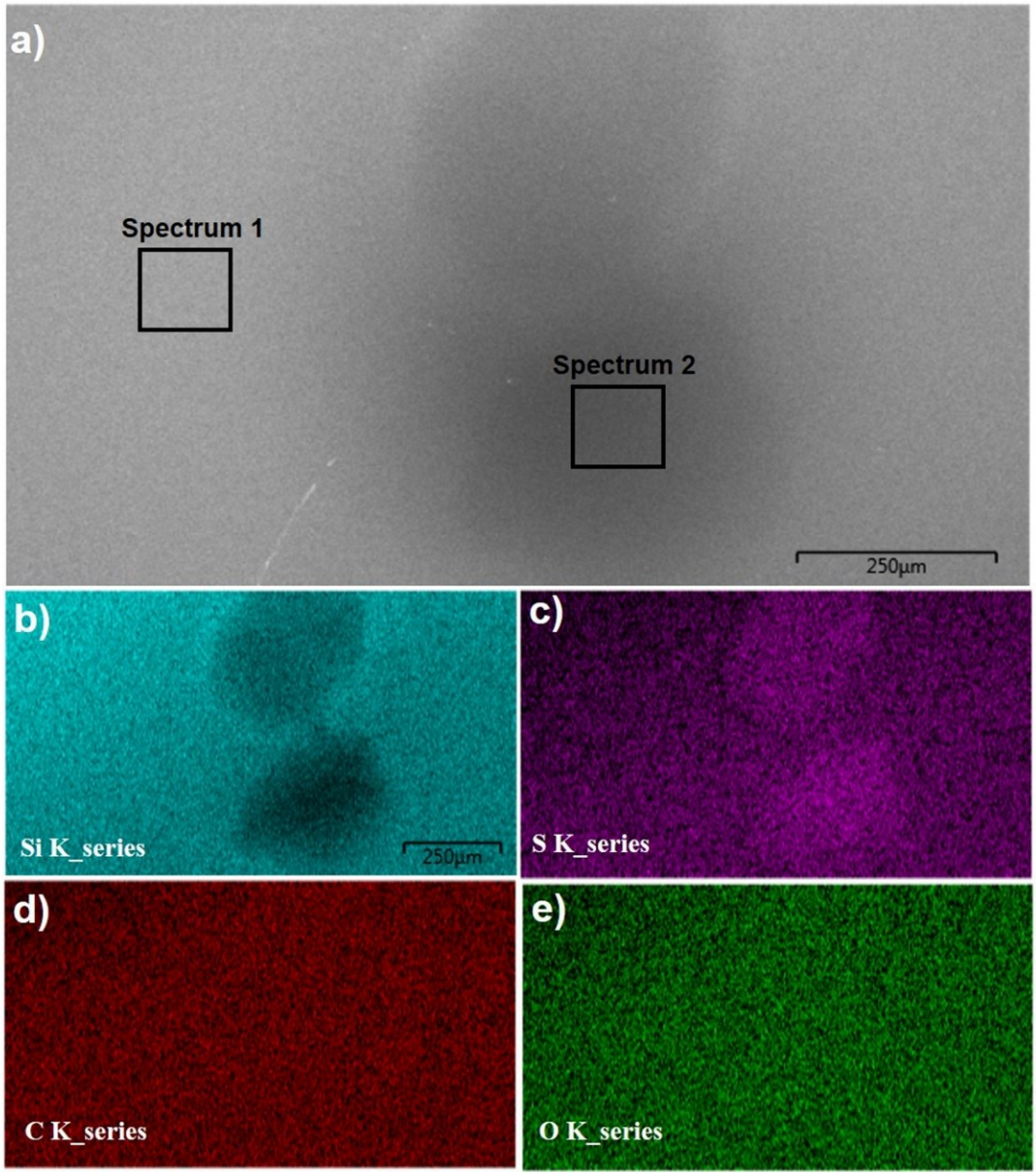

Fig. 3.19: a) SEM image of 1% wt. H_2SO_4-PEDOT:PSS annealed at 200°C. Darker areas correspond to the agglomerates observed through optical microscopy and the brighter regions correspond to the matrix of the polymeric film. SEM-EDX maps of the same sample area of b) Si K series, c) S K series, d) C K series and e) O K series respectively.

Spectrum 1			**Spectrum 2**		
Element	Wt. %	Wt. % Sigma	Element	Wt. %	Wt. % Sigma
C	43.58	0.40	C	53.14	0.29
O	9.40	0.18	O	17.19	0.20
Si	43.92	0.33	Si	17.13	0.13
S	3.10	0.06	S	12.36	0.11

Table 3.1: SEM-EDX analysis of the elemental content (%weight) in two different regions of the same sample (1% wt. H_2SO_4-PEDOT:PSS annealed at 200°C), as indicated in Fig.19a (spectrum 1 and spectrum 2)

3.8 – Raman Analysis

In order to investigate the chemical composition of the deposited layers, Raman spectra were performed both on undoped and 1% wt. doped PEDOT:PSS samples annealed at 200°C. These polymeric films were deposited on monocrystalline Si substrate and the analysis was performed using a laser source with 632.8 nm as the excitation wavelength. Silicon Raman spectrum was also acquired as reference and reported in Fig. 3.20.

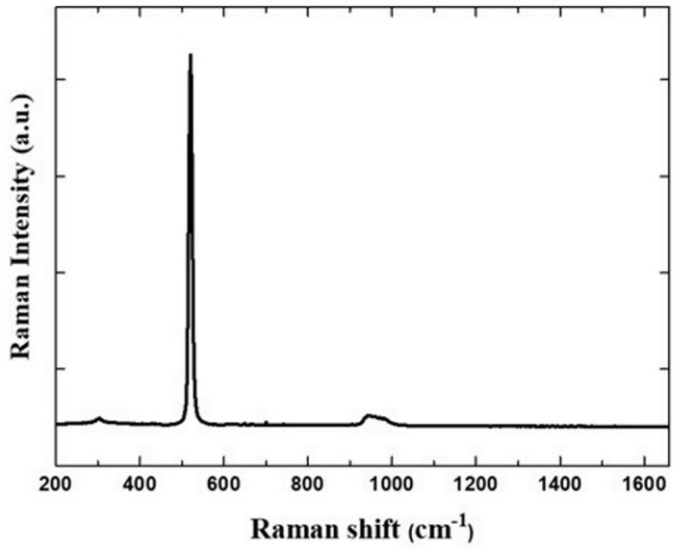

Fig. 3.20: Raman spectrum of silicon substrate acquired with an excitation wavelength of 633 nm. Signal at 521 cm^{-1} is due to the optical modes of the c-Si and is characteristic of silicon. Second order modes related to Si are close to 1000 cm^{-1}, while combined transverse and longitudinal modes are placed around 300 cm^{-1}.

The typical first-order Raman scattering of monocrystalline Si, which appears as a Lorentzian line shape at 521 cm^{-1} [35] was observed in all prepared samples. In this respect, the other signals at ≈300 cm^{-1} and those ones in the 930 and 960 cm^{-1} range, respectively due to some transverse and longitudinal modes and to second order of c-Si, will not be taken in consideration in the following argumentation. All PEDOT:PSS spectra were acquired by setting the laser power source at ≈1.4mW. This choice is made in order to avoid any modification of polymeric films under laser beam irradiation. Fig. 3.21a reports the optical image of 1% wt. doped H_2SO_4-PEDOT:PSS annealed at 200°C deposited on Si. Fig. 3.21b reports the associated Raman imaging map obtained at a frequency between 1400 and 1480 cm^{-1}, showing that sample surface appeared extremely inhomogeneous, presenting light and black regions of several micrometers in size. For shedding light on the

chemical composition of both film and agglomerates, vibrational spectra (Fig. 3.21c) were acquired in the two regions, corresponding to the matrix of film (bright region in the map) and agglomerates (dark region), and were reported respectively as blue and red curves. In the same figure, Raman spectrum of undoped PEDOT:PSS was also recorded (green curve). All curves were normalized by the intensity of the band placed at 989 cm^{-1} (marked with a double asterisk) characteristic of the oxyethylene ring deformation in PEDOT films. Spectral signals attribution is quite in agreement with those ones reported in the literature [28]. Most of the signals shown are related to the PEDOT chain and they can be identified as: the asymmetric C_α=C_β stretching between 1563 and 1532 cm^{-1}, while at 1431 cm^{-1} a large band appears as a fingerprint of the PEDOT and it is associated to the symmetric stretching of the C_α=C_β. Band at 1369 cm^{-1} is related to the stretching of the C_β=C_β, while band at 1260 cm^{-1} is attributed to the inter-ring stretching of the C_α=C_α and the region included between 1080-1160 cm^{-1} hosts the C-O-C deformation. Signals at 989 and 579 cm^{-1} are characteristic to the oxyethylene ring breathing and 701 cm^{-1} band is due to the C-S-C deformation. The band appeared at 438 cm^{-1} is the only signal which can be attributed to the PSS chain since it is related to the SO_2 bending that can only come from the sulfonic group of the styrenic chain. In light of this, it is possible to make an estimation of the relative quantities of PEDOT and PSS for each curve. In order to evidence any change in the PEDOT:PSS films after doping, for each curve**,** signals related to the oxyethylene ring breathing of PEDOT (989 cm^{-1}) and the SO_2 bending (438 cm^{-1}) of PSS were considered to calculate the integrated intensity ratio I_{438}/I_{989} reported in Table 2. Hence, agglomerates show an I_{438}/I_{989} ratio slightly lower than that one of the light region, suggesting a slight reduction of the PSS or, in other words, an increase in the amount of the PEDOT counterpart. Unless any further local compositional inhomogeneity within the agglomerates, this result is quite in

agreement with that one obtained by considering the increase of %wt. signals of S, C and O in the EDX analysis shown in the previous section. Therefore, both these analysis lead to the conclusion that agglomerates correspond to a local, thicker and dark blue region where a slight enrichment of PEDOT chains is supposed. Moreover, it is worth to note that the band centred at 1431 cm^{-1} shows a relative higher intensity in the agglomerate spectrum with respect to the light region. This can be attributed to two different causes: an increment in the local concentration of PEDOT, which strengthens the observation of EDX and the discussion above, or, as an alternative, can be due to a rearrangement of the C_α=C_β and C_β =C_β portions related to a modification in the electronic structure [28,36].

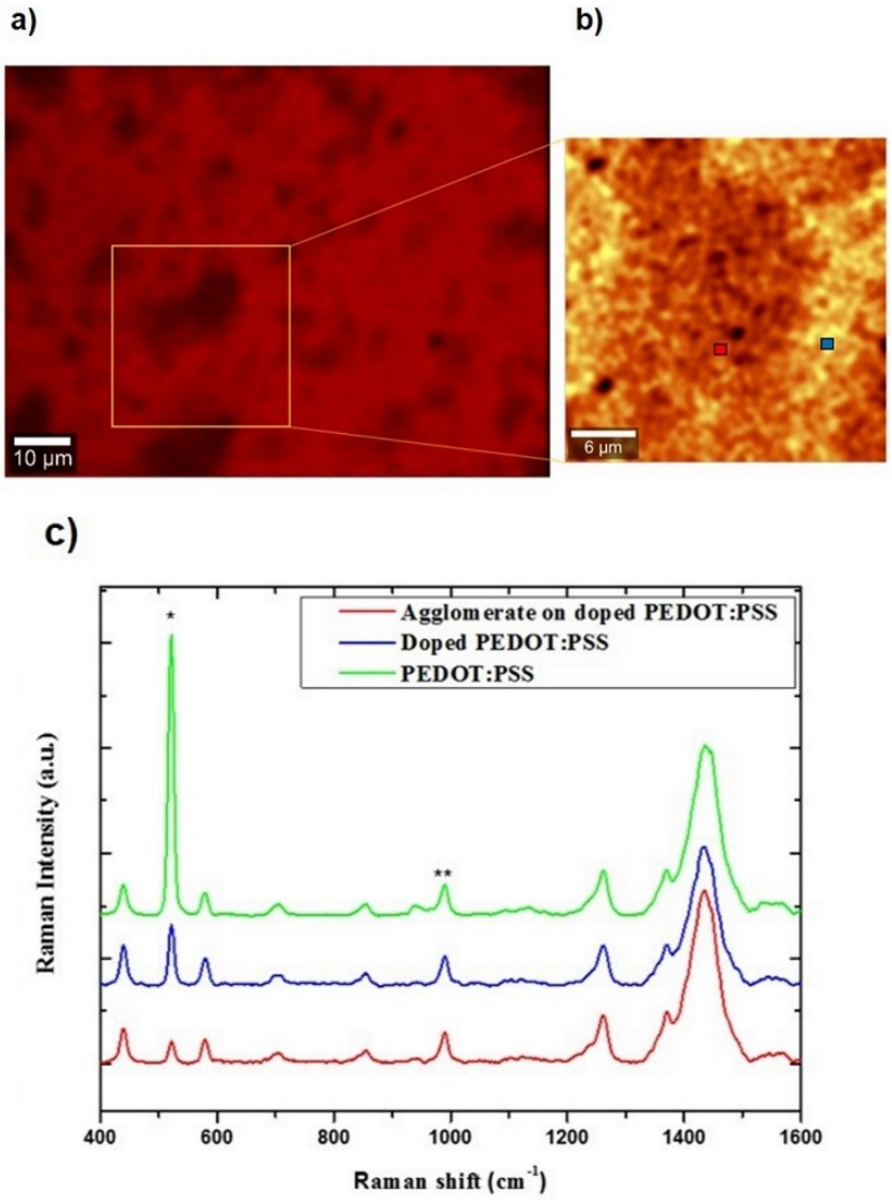

Fig. 3.21: (a) Optical image 1% wt. doped H_2SO_4-PEDOT:PSS annealed at 200°C (light region) deposited on Si; (b) Raman map of intensity between 1400–1480 cm^{-1} and (c) corresponding Raman spectra excited at λ_{ext}=632.8 nm, with red and blue curves showing dark agglomerates and light region, instead the green curve was recorded on undoped PEDOT:PSS. The three

curves are normalized for the intensity of the signal at 989 cm^{-1} (**). In all spectra the vibrational feature of monocrystalline silicon is also visible (*).

Raman Curve	PSS to PEDOT relative ratio (I_{439}/I_{989})
Agglomerate	1,19
Polymeric film	1,48
Undoped	1,07

Table 3.2: Intensities ratio between the 439 cm^{-1} signal, related to SO_2 bending of PSS, and the 989 cm^{-1} band, attributed to the breathing of the oxyethylene ring of the PEDOT for the undoped sample and two different regions (matrix and agglomerate) of the 1% wt. doped H_2SO_4-PEDOT:PSS sample.

These results strongly suggest that the addition of H_2SO_4 directly to the aqueous PEDOT:PSS solution leads to the formation of dark blue and immiscible agglomerates. It is also observed that this precipitation effect increases with increasing the acid concentration and they are probably due to the protonation of the anionic group on the styrenic chains [24]. This has the effect to strongly reduce the coulomb interactions between the anionic groups of the PSS and the positive charges along PEDOT chains, and the solvatation effect for the first ones prevails. In this way, conductive agglomerates enriched of PEDOT are formed and dispersed in the aqueous media. When this suspension is spun on the substrate, the film obtained still keeps the characteristics of the solution blend and therefore, the final polymeric film is made by dark blue conductive agglomerates embedded in a PSS matrix. This segregation phase, in which PEDOT domains partly exclude the

dielectric PSS [37], lead to the formation of a conducting path through a hopping transport mechanism which is finally manifested by a reduction of the electrical resistance of the material.

3.9 - Conclusions

For the first time the effect of the direct addition of the sulfuric acid to PEDOT:PSS aqueous solution on the polymer electrical and optical properties has been studied. The characterization has shown that the 1% wt. H_2SO_4 doped films annealed at 200°C in vacuum conditions exhibited sheet resistance as low as 40 Ohm/sq, with a reduction of over 99% with respect to the corresponding undoped sample. The measured average transmittance in the same case ranged between 70 and 80%. For the first time the figure of merit was calculated for these films and showed that the case with the highest conductivity produced the best compromise also in terms of transparency. The electrical optimization has been attributed to the PEDOT-enriched agglomerates, which form after the doping procedure by phase separation from the PSS species, and increase the conductive path of the whole polymeric sheet through hopping transport mechanisms. The study also demonstrated that the H_2SO_4 doped samples after aging exhibit a worsening of the sheet resistance only by 3.7%, unlike the undoped samples that worsened by 50%, thus making the doped polymer less susceptible to the aging process. Although improvements in the fabrication of transparent conductive PEDOT:PSS doped by this novel in-solution method are still necessary to obtain an optimal material, this method demonstrates to represent a promising alternative to overcome the restrictions that transparent conductive polymers still present.

3.10 - Bibliography

[1] V. Scardaci, R. Coull, J.N. Coleman, Very thin transparent, conductive carbon nanotube films on flexible substrates, Appl. Phys. Lett. 97 (2010) 2008–2011. doi:10.1063/1.3462317.

[2] E. Ritz, Y.L. Wu, J. Hong, D. Andruczyk, T.S. Cho, D.N. Ruzic, Atmospheric pressure dielectric barrier discharge (DBD) for post-annealing of aluminum doped zinc oxide (AZO) films, Surf. Coatings Technol. 251 (2014) 64–68. doi:10.1016/j.surfcoat.2014.04.004.

[3] B.J. Kim, S.H. Han, J.S. Park, Sheet resistance, transmittance, and chromatic property of CNTs coated with PEDOT:PSS films for transparent electrodes of touch screen panels, Thin Solid Films. 572 (2014) 68–72. doi:10.1016/j.tsf.2014.08.015.

[4] X. Yu, D. Zhang, P. Wang, R. Murakami, B. Ding, X. Song, THE OPTICAL AND ELECTRICAL PROPERTIES OF ZnO/Ag/ZnO FILMS ON FLEXIBLE SUBSTRATE, Int. J. Mod. Phys. Conf. Ser. 06 (2012) 557–562. doi:10.1142/S2010194512003777.

[5] L.E. Nore, Synthesis and measurement of the optical and electrical properties of polyaniline and polypyrrole thin films, 59 (2013) 147–151.

[6] M. Thirumoorthi, J. Thomas Joseph Prakash, Structure, optical and electrical properties of indium tin oxide ultra thin films prepared by jet nebulizer spray pyrolysis technique, J. Asian Ceram. Soc. 4 (2016) 124–132. doi:10.1016/j.jascer.2016.01.001.

[7] K.P. Sibin, N. Swain, P. Chowdhury, A. Dey, N. Sridhara, H.D. Shashikala, A.K. Sharma, H.C. Barshilia, Optical and electrical properties of ITO thin films sputtered on flexible FEP substrate as passive thermal control system for space applications, Sol. Energy Mater. Sol. Cells. 145 (2016) 314–322. doi:10.1016/j.solmat.2015.10.035.

[8] M. Mazur, D. Kaczmarek, J. Domaradzki, D. Wojcieszak, S. Song, F. Placido, Influence of thickness on transparency and sheet resistance of ITO thin films, Conf. Proc. -

8th Int. Conf. Adv. Semicond. Devices Microsystems, ASDAM 2010. (2010) 65–68. doi:10.1109/ASDAM.2010.5666348.

[9] J. Kim, W.J. da Silva, A.R. bin Mohd Yusoff, J. Jang, Organic devices based on nickel nanowires transparent electrode, Sci. Rep. 6 (2016) 19813. doi:10.1038/srep19813.

[10] Y. Xia, J. Ouyang, PEDOT:PSS films with significantly enhanced conductivities induced by preferential solvation with cosolvents and their application in polymer photovoltaic cells, J. Mater. Chem. 21 (2011) 4927. doi:10.1039/c0jm04177g.

[11] Y. Xia, H. Zhang, J. Ouyang, Highly conductive PEDOT:PSS films prepared through a treatment with zwitterions and their application in polymer photovoltaic cells, J. Mater. Chem. 20 (2010) 9740. doi:10.1039/c0jm01593h.

[12] J. Luo, D. Billep, T. Waechtler, T. Otto, M. Toader, O. Gordan, E. Sheremet, J. Martin, M. Hietschold, D.R.T. Zahn, T. Gessner, Enhancement of the thermoelectric properties of PEDOT:PSS thin films by post-treatment, J. Mater. Chem. A. 1 (2013) 7576. doi:10.1039/c3ta11209h.

[13] W. Zhang, X. Bi, X. Zhao, Z. Zhao, J. Zhu, S. Dai, Y. Lu, S. Yang, Isopropanol-treated PEDOT:PSS as electron transport layer in polymer solar cells, Org. Electron. 15 (2014) 3445–3451. doi:10.1016/j.orgel.2014.09.026.

[14] D. Alemu, H.-Y. Wei, K.-C. Ho, C.-W. Chu, Highly conductive PEDOT:PSS electrode by simple film treatment with methanol for ITO-free polymer solar cells, Energy Environ. Sci. 5 (2012) 9662. doi:10.1039/c2ee22595f.

[15] G. Namkoong, E.M. Younes, T.M. Abdel-Fattah, E.M. El-Maghraby, A.H. Elsayed, A.H. Abo Elazm, Aging process of PEDOT:PSS dispersion and robust recovery of aged PEDOT:PSS as a hole transport layer for organic solar cells, Org. Electron. Physics, Mater. Appl. 25 (2015) 237–244. doi:10.1016/j.orgel.2015.06.049.

[16] J. Huang, P.F. Miller, J.S. Wilson, A.J. De Mello, J.C. De Mello, D.D.C. Bradley, Investigation of the effects of doping and post-deposition treatments on the conductivity,

morphology, and work function of poly(3,4- ethylenedioxythiophene)/poly(styrene sulfonate) films, Adv. Funct. Mater. 15 (2005) 290–296. doi:10.1002/adfm.200400073.

[17] Y.H. Kim, C. Sachse, M.L. MacHala, C. May, L. Müller-Meskamp, K. Leo, Highly conductive PEDOT:PSS electrode with optimized solvent and thermal post-treatment for ITO-free organic solar cells, Adv. Funct. Mater. 21 (2011) 1076–1081. doi:10.1002/adfm.201002290.

[18] X. Crispin, F.L.E. Jakobsson, A. Crispin, P.C.M. Grim, P. Andersson, A. Volodin, C. van Haesendonck, M. Van der Auweraer, W.R. Salaneck, M. Berggren, The Origin of the High Conductivity of Poly(3,4-ethylenedioxythiophene)−Poly(styrene sulfonate) (PEDOT−PSS) Plastic Electrodes, Chem. Mater. 18 (2006) 4354–4360. doi:10.1021/cm061032+.

[19] S. Timpanaro, M. Kemerink, F.J. Touwslager, M.M. De Kok, S. Schrader, Morphology and conductivity of PEDOT/PSS films studied by scanning-tunneling microscopy, Chem. Phys. Lett. 394 (2004) 339–343. doi:10.1016/j.cplett.2004.07.035.

[20] W. Zhang, B. Zhao, Z. He, X. Zhao, H. Wang, S. Yang, H. Wu, Y. Cao, High-efficiency ITO-free polymer solar cells using highly conductive PEDOT:PSS/surfactant bilayer transparent anodes, Energy Environ. Sci. 6 (2013) 1956. doi:10.1039/c3ee41077c.

[21] Z. Li, W. Meng, J. Tong, C. Zhao, F. Qin, F. Jiang, S. Xiong, S. Zeng, L. Xu, B. Hu, Y. Zhou, A nonionic surfactant simultaneously enhancing wetting property and electrical conductivity of PEDOT:PSS for vacuum-free organic solar cells, Sol. Energy Mater. Sol. Cells. 137 (2015) 311–318. doi:10.1016/j.solmat.2015.02.024.

[22] J.P. Thomas, K.T. Leung, Defect-minimized PEDOT:PSS/planar-si solar cell with very high efficiency, Adv. Funct. Mater. 24 (2014) 4978–4985. doi:10.1002/adfm.201400380.

[23] W. Meng, R. Ge, Z. Li, J. Tong, T. Liu, Q. Zhao, S. Xiong, F. Jiang, L. Mao, Y. Zhou, Conductivity Enhancement of PEDOT:PSS Films via Phosphoric Acid Treatment

for Flexible All-Plastic Solar Cells, ACS Appl. Mater. Interfaces. 7 (2015) 14089–14094. doi:10.1021/acsami.5b03309.

[24] Y. Xia, K. Sun, J. Ouyang, Solution-processed metallic conducting polymer films as transparent electrode of optoelectronic devices, Adv. Mater. 24 (2012) 2436–2440. doi:10.1002/adma.201104795.

[25] N. Kim, H. Kang, J.H. Lee, S. Kee, S.H. Lee, K. Lee, Highly conductive all-plastic electrodes fabricated using a novel chemically controlled transfer-printing method, Adv. Mater. 27 (2015) 2317–2323. doi:10.1002/adma.201500078.

[26] H. Zhao, D. Xie, T. Feng, Y. Zhao, J. Xu, X. Li, H. Zhu, T. Ren, Enhanced performance of PEDOT:PSS/n-Si hybrid solar cell by HNO<inf>3</inf> treatment, Appl. Phys. Express. 7 (2014) 8–11. doi:10.7567/APEX.7.031602.

[27] E. Vitoratos, S. Sakkopoulos, E. Dalas, N. Paliatsas, D. Karageorgopoulos, F. Petraki, S. Kennou, S.A. Choulis, Thermal degradation mechanisms of PEDOT:PSS, Org. Electron. Physics, Mater. Appl. 10 (2009) 61–66. doi:10.1016/j.orgel.2008.10.008.

[28] A.A. Farah, S.A. Rutledge, A. Schaarschmidt, R. Lai, J.P. Freedman, A.S. Helmy, Conductivity enhancement of poly(3,4-ethylenedioxythiophene)- poly(styrene sulfonate) films post-spincasting, J. Appl. Phys. 112 (2012). doi:10.1063/1.4768265.

[29] J. Ouyang, Solution-processed pedot:pss films with conductivities as indium tin oxide through a treatment with mild and weak organic acids, ACS Appl. Mater. Interfaces. 5 (2013) 13082–13088. doi:10.1021/am404113n.

[30] G. Haacke, G. Haacke, New figure of merit for transparent conductors New figure of merit for transparent conductors *, 4086 (2016). doi:10.1063/1.323240.

[31] F. Greco, A. Zucca, S. Taccola, A. Menciassi, T. Fujie, H. Haniuda, S. Takeoka, P. Dario, V. Mattoli, Ultra-thin conductive free-standing PEDOT/PSS nanofilms, Soft Matter. 7 (2011) 10642–10650. doi:10.1039/c1sm06174g.

[32] A.M. Nardes, On the conductivity of PEDOT: PSS thin films, 2007. doi:http://dx.doi.org/10.6100/IR631615.

[33] E. Vitoratos, S. Sakkopoulos, E. Dalas, N. Paliatsas, K. Emmanouil, P. Malkaj, S.A. Choulis, Correlation between thickness, conductivity and thermal degradation mechanisms of PEDOT:PSS films, AIP Conf. Proc. 1203 (2010) 178–181. doi:10.1063/1.3322407.

[34] Fridman, Technical applications for conductive polymers, Electrochim. Acta. 39 (1994) 1345–1347. doi:10.1016/0013-4686(94)E0057-7.

[35] L. Rayleigh, I. Raman, R. Thornton, R. Sec, Raman Scattering, 155 (2016) 2–4. doi:10.1016/B978-012342070-1/50013-9.

[36] Y.-S. Hsiao, W.-T. Whang, C.-P. Chen, Y.-C. Chen, High-Conductivity Poly(3,4-ethylenedioxythiophene):Poly(styrene sulfonate) Film For Use In ITO-Free Polymer Solar Cells, J. Mater. Chem. 18 (2008) 5948–5955. doi:10.1039/b813079e.

[37] L. Ouyang, C. Musumeci, M.J. Jafari, T. Ederth, O. Inganäs, Imaging the Phase Separation between PEDOT and Polyelectrolytes during Processing of Highly Conductive PEDOT:PSS Films, ACS Appl. Mater. Interfaces. 7 (2015) 19764–19773. doi:10.1021/acsami.5b05439.

Chapter 4

Free-standing, high conductive, dark PEDOT:PSS paste

In the previous Chapter, it has been seen that the direct acidification of a PEDOT:PSS solution with H_2SO_4 causes the polymer precipitation. Once deposited by spin coating, the resulting film shows higher electrical conductivity with respect to the pristine PEDOT:PSS. Starting from these promising results, this Chapter is focused on the consequences of the direct acidification of PEDOT:PSS with sulfuric acid until the complete polymer precipitation. This low cost and fast in-solution treatment leads to a conductive dark-PEDOT (d-paste). A deposition procedure, as easy as the ink pen scribing, is here described for obtaining a free-standing, mouldable and mechanically robust product, with electrical conductivity up to 1000 Scm^{-1}, All these characteristics can make this new material a good alternative to standard and expensive metal contacts.

4.1 - Introduction

Conductive polymers (CPs) have attracted a considerable scientific interest thanks to their great versatility, compatibility with many different substrates, low cost processability and interesting physical and tribological properties. Indeed, they exhibit useful optical and electrical characteristics, mechanical flexibility and light

weight. Among the others, black or opaque conductive polymers, also used in the form of flexible and free standing foils, are exploited in several fields such as barrier for drug permeability, thermoelectric devices, sensors, fuel cells, and photoactive layers or electrodes in solar cells [1-9]. Also in this scenario, PEDOT:PSS has found a great interest: aside its largely documented use as transparent electrode [10-18], it was also employed in the form of opaque and free-standing conductive material. This tendency was documented in many different advanced technologies, uppermost in textiles, thermal insulation, flexible supercapacitors, as well as in bulk-heterojunction solar cells, where it has been used as metal-like contact or as holes transport layer [14,19-24]. In the context of the opaque CPs, the results that will be presented in this Chapter will show a dark and highly conductive material, obtained with a novel, cost effective and fast approach.

This discussion takes place from the results already illustrated in the previous Chapter. It has been seen that the acidification of a pristine PEDOT:PSS solution with pure H_2SO_4, diluted at concentrations far from saturation, leads to a phase separation. This occurs through the formation of dark blue precipitates which separate from the starting aqueous solution and are made by a conductive blend of PEDOT and PSS, which segregate from the dielectric PSS matrix [20,25,26]. The density and size of the agglomerates increases with the amount of the acid added. The electrical characterizations and the measured transmittance of the obtained deposited films have shown that the doped material presents a sheet resistance two-orders of magnitude smaller than the undoped film and a good transparency in the visible range of the spectrum. Both these properties were also evaluated through the calculation of the Haacke's Figure of Merit (FOM) (Chapter 3) showing that a

good compromise between the optical and the electrical performances can be achieved for the highest acid-content (1% wt.) used.

This Chapter presents a continuation of the results shown in the previous one. The focus will be to study what happens when the acid content in the PEDOT:PSS aqueous solution is increased up to saturation. The mechanism of the reaction occurring for the direct acid addition to the PEDOT:PSS will be clarified and reported in the section 4.3 of this Chapter. The solubility tests in section 4.4, the electrical characterizations shown in the sections 4.5, 4.6 and Raman analysis in 4.7 will drive the reader to the insights of the mechanism of reaction, chemical composition and physical properties of the product obtained, then explaining the new arrangement of polymer chains following the acidification. The interpretation of the chemical composition and the arrangement of both components, PEDOT and PSS, will be supplied in the section 4.8, eventually providing a schematic and reiterative model of the material obtained. When explicitly mentioned, this will be indicated as *dark polymer paste* or, alternatively, *d-paste*.

4.2 - Samples Preparation

The procedures here described are similar to the ones used in the previous Chapter. PEDOT:PSS (Sigma Aldrich) aqueous solution, 1.1% wt. with PEDOT-to-PSS relative content of 1:2.5 and electrical conductivity of 2-4 S/cm, and high purity sulfuric acid, H_2SO_4 (96%) (Basf), were used as received and without any further purification. Glass substrates were used as supports for the successive deposition, since dielectric substrates are required for excluding electrical contributions coming from the supports. They were cleaned by sonication for 5 minutes in

acetone, isopropyl alcohol and deionized water respectively and finally dried under nitrogen flow. Pristine PEDOT:PSS solution was subjected to gentle stirring for 15 minutes at room temperature in order to homogenize the initial aqueous blend of PEDOT and PSS. After that, sulfuric acid was added to the pristine solution, leading to the instantaneous formation of microscopic blue agglomerates. For large amount of pure acid directly added to the pristine polymer blend, it is obtained a complete phase separation which leaves a dark blue, gelatinous precipitate, on one hand, and a transparent supernatant on the other side, as reported in the schematic representation shown in the Fig. 4.1:

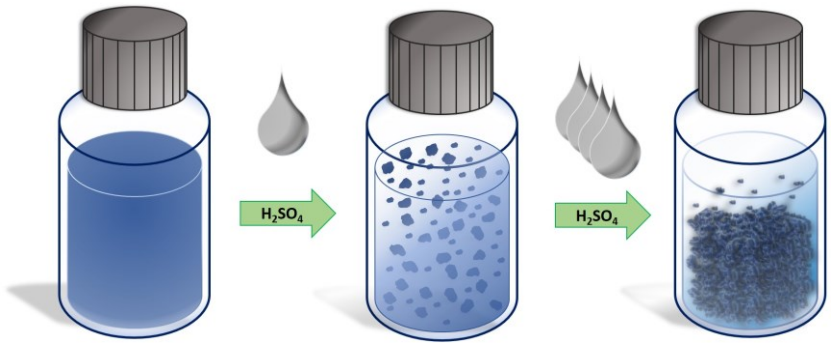

Fig. 4.1: Sketch of the effect due to the addition of H_2SO_4 directly to a pristine aqueous solution of PEDOT:PSS.

A minimum of C_s = 40% v/v of H_2SO_4 relative to the initial volume of PEDOT:PSS collected was found to lead to a dark precipitate after 24h of decantation, while a transparent and limpid supernatant appeared, as shown in Fig. 4.2a.

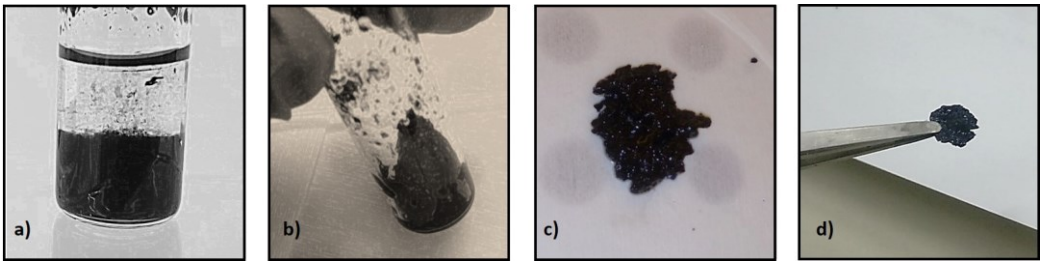

Fig. 4.2: a) Optical images of acid-saturate PEDOT solution after 24h of decantation; b) PEDOT wet gel obtained after separation from the transparent supernatant; c) d-PEDOT wet paste after rinsing by deionized water; d) free-standing d-PEDOT paste after dryin (apparent holes on the surface are reflections of the flash light used to take the pictures.).

C_s can be thus defined as the minimum acid amount to obtain the total phase separation of the polymer, while C_s > 40% vol. reduces the decantation time required for obtaining an effective phase separation between the precipitate and the supernatant. After the decantation, the precipitate was separated by its transparent supernatant and rinsed with deionized water, Fig. 4.2b. After rinsing, the precipitate appears as a dark and wet gel-like compound. This paste is easily manageable and transferable on surfaces within 30 minutes after the recovery (Fig. 4.2c). Differently, when if it is left to naturally dry for longer times, it gets hard to handle and its transfer in flask or deposition on surfaces becomes more difficult.

Before each deposition, glass substrates are pre-heated on a hot-plate at 170 °C for 10 minutes to remove any humidity trace. The paste deposition on the glass substrate is performed by inserting the wet PEDOT paste in a plastic syringe and then squeezing the material through a shadow mask onto the substrate. This procedure allows to control the shape and the initial thickness of the final layer. In this case, the mask used for the present experiment has a hole with 7 mm-size diameter and a thickness of 300 μm. After the deposition, the mask is detached from the substrate and it leaves a disk of dark blue PEDOT having 7 mm in

diameter and a nominal thickness of 300 µm. A scheme of this procedure is shown below in Fig. 4.3:

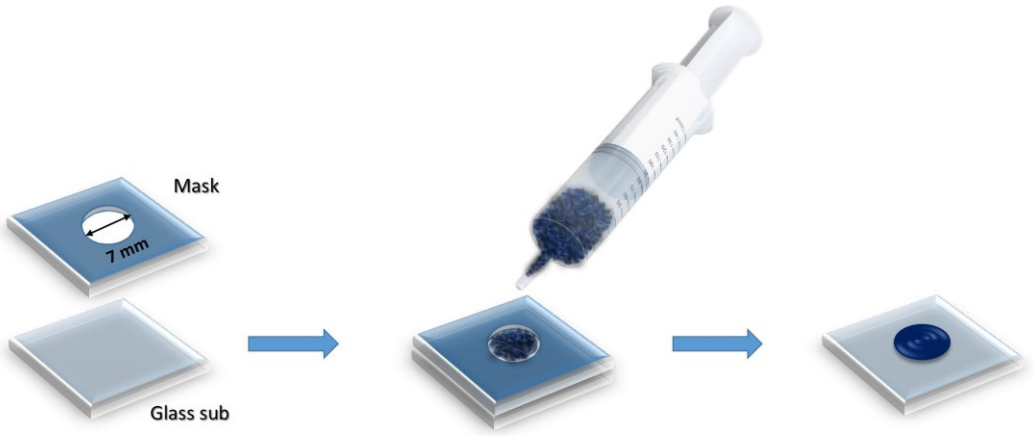

Fig. 4.3: Sketch of the paste deposition on glass substrate through a mask and by a syringe.

A thermal treatment subsequent to the paste deposition is done in order to remove the residual water retained by the polymer gel. In every case reported the thermal treatment (bake) was performed immediately after the deposition and in air. Time and temperature of the bake were increased until sample drying was observed, i.e. at 170°C for 2h.

The drying step has led to a strong reduction of the thickness due to the loss of residual water. The obtained PEDOT layer appears as a continuous, opaque dark disk with 7 mm size diameter and a final thickness of ≈33 ± 1 µm (Fig. 4.2d). The thickness of samples here reported was determined by a vertical Absolute Digimatic Indicator Mitutoyo 543-472B with accuracy of ± 1 µm. Interestingly, the disks are easily detachable from the substrate and result in flexible free-standing foils, easily transferable on other substrates. Since the purpose of this

work was not a systematic study of the rheological and mechanical response of the d-paste, stress-strain analysis was not performed. However, a qualitative clue of the flexibility and thus the mechanical potentials of the free-standing polymer paste is given in the Fig. 4.4. Here, it is possible to see that the paste can be easily bent without causing any damage in the material. Indeed, Fig. 4.4a shows a disk of the d-paste bent with tweezers. The release of the material returns the original disk without any visible sign of the bending and it stays flat. Fig. 4.4b shows that the dark polymer paste can be also bent until a half of the disk is overlapped on the other one, thus making a neat rotation of 180°.When the disk is released from this position, it remains bent by itself at an angle of about 31° without any external contribution (as shown in Fig. 4.4c). Forcing the sample against a surface with the help of tweezers, the re-open disk appears intact and without any cracks or holes on the surface, but only the bending sign along it, which is indicated by an arrow in the picture (Fig. 4.4d).

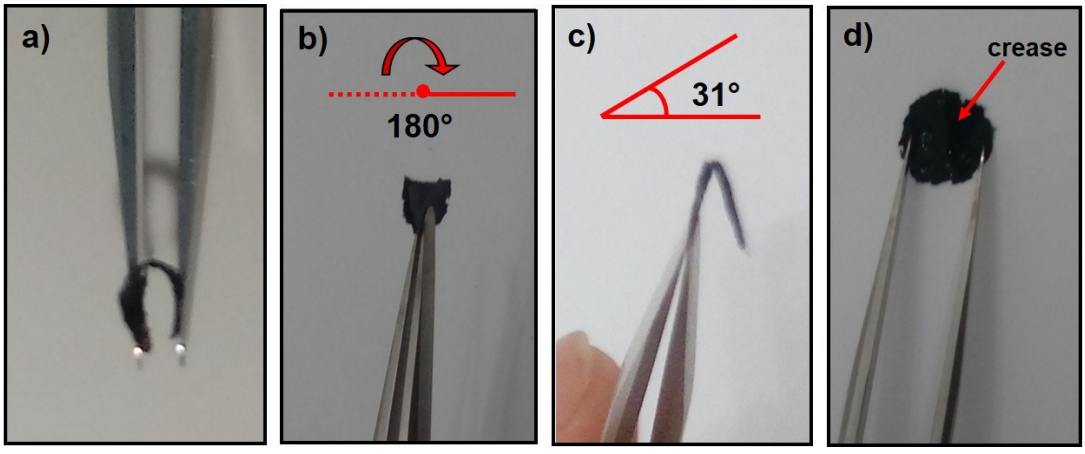

Fig. 4.4: Optical pictures showing the flexibility of the polymer foil obtained after baking carried at 170°C for 2h in air. a) Simple bending of the sample by the help of tweezers; b) total bending of the foil with an angle of 180°; c) release of the sample after the total (180°) bending. Sample naturally forms an angle of about 31°; d) re-

opened polymer disk. The hard bending seen in the b) leaves a straight crease crossing the entire disk.

4.3 - Insights of the Reaction Mechanism

From a chemical point of view, the appearance of the blue precipitates even for small acid amounts (Chapter 3), was attributed to the protonation of the anionic sulfonic groups on the PSS chains by the H^+ generated from the dissociation of the H_2SO_4 in the aqueous medium. A proposal of the reaction mechanism between the PSS and the sulfuric acid is thus shown in the schematic of the Fig. 4.5:

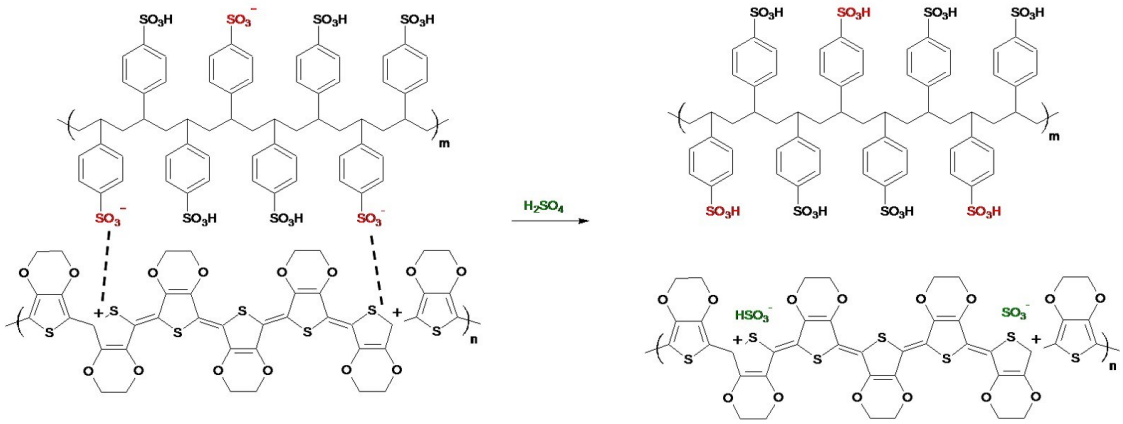

Fig. 4.5: Hypothetical scheme of reaction between PEDOT:PSS and sulfuric acid.

The mechanism here described is based on a process reported in other works [20,25-27]. As mentioned in the previous Chapters, the water solubility of PEDOT is given by the presence of the counter-anions placed along the PSS chains. Indeed, the non-protonated sulfonic groups in PSS retain a negative charge which balances the positive ones in the PEDOT species. Apart from the doping charges-balance which gives stability to the overall system, the anionic groups of PSS and the polarons of PEDOT give place to electrostatic interactions which have two main effects:

- On one side, they keep together the PSS chains with the PEDOT ones, which thus interact with the styrenic part through Coulomb forces;
- On the other hand, since the PSS manifests a good solubility in water (which shall depend on different parameters, such as chains length, sulfonation grade, pH, etc), it drags the insoluble PEDOT counter-part into the aqueous medium, thus keeping it as a water suspension.

According to the Ref. [27], the pK_α of the protonated sulfonic groups in the PSS can be estimated from that one found for the p-toluensulfonic acid, which in water is estimated to be around -2.8. The sulfuric acid, instead, has two protic dissociations, of which the first is strong and turns to completion, while the second has a pK_α = -6.4, as illustrated in the schematic below (Fig. 4.6):

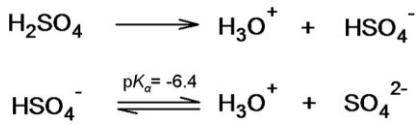

Fig. 4.6: Aqueous acid dissosiations of H_2SO_4.

As schematized in the Fig. 4.5, the mechanism that plays the main role in the polymer precipitation is the formation of a new chemical equilibrium in which PSS exchanges protons with those ones deriving from the acidic dissociation. The presence of these counter-anions coming from the acid dissociation of the H_2SO_4, together with protonated PSS groups, cause a sort of shielding effect which weakens the Coulomb attractions between PSS and PEDOT chains [28,29]. Therefore, in this process, the positive charges along the PEDOT due to the polarons are still maintained, as it will be explained later in this Chapter (sections 4.5 and 4.6). However, this time, it is more likely that the polarons are counterbalanced by the

anions left by the acid dissociation, in accordance with the reaction schematized in Fig. 4.5 and with the mechanism described in Ref. [20,25-27].

4.4 - Solubility Test

To understand if it was possible to re-dissolve the wet gel paste, the blue gelatinous precipitate recovered after the removal of the transparent supernatant and the water rinsing (see section 4.2) and also the dry paste, obtained after the bake, were used for the solubility tests. The criteria with which it was performed, are chosen according to different aspects, such as: 1) solvent polarity; 2) chemical equilibrium in acid-base reaction; 3) polar-apolar interactions; 4) hierarchical order in the reaction mechanism.

In the case of the wet paste, a small amount collected with the spatula was inserted into an Eppendorf test tube and then the chemical used for testing the product solubility was directly added to it. Analogously, once obtained the dark blue disk after the bake in air, this was cut in smaller pieces and inserted into the test tube, in which then a small quantity of each solvent used was added. Each test tube was stored for several days at 20°C. After that, test tubes were kept in water bath under sonication for 20 minutes at the maximum power achievable, both in ambient temperature and then with a mild heating, up to 60°C.

For each criterion mentioned above, a more detailed explanation and description of the procedure used, when required, is given here below:

1) first characteristic which must be investigated concerns the fact that the initial blend is formed by two kinds of polymer chains: their own structures drive to say that the polarity of PSS is quite different from that

of the PEDOT. Indeed, whether the PSS manifests a polar character that allows it to be solubilised in very polar solvent (i.e. water), PEDOT has a chemical structure which indicates itself as a hydrophobic compound. Therefore, since the behaviour of each of these species must respond differently to the surrounding solvent, six chemicals, having different relative polarity (rp.) [30], were used for this test. In particular, listed in order of the decreasing relative polarity, the solvents checked were: acetyl acetate (rp. 0,571), isopropyl alcohol (rp. 0,546), acetone (rp. 0,355), tetrahydrofuran (rp. 0,207) and toluene (rp. 0,099).

2) Since the precipitation occurs clearly by the effect of the acid addition, it is worth to wonder if it is possible to change the equilibrium by the addition of a base, such as potassium hydroxide, KOH. Indeed, if the protonation of the free sulfonic groups have occurred, the effect of a strong base in water could tear off the protons eventually bound to the sulfonic groups after the acidification, thus restoring the SO_3^- along the PSS and consequently the Coulomb interactions between these ones and the polarons along the PEDOT chains. For these purpose, aqueous solutions having a concentration of 1M and 2M, respectively, of KOH were used.

3) As documented in literature, some works [28] have previously schematized that the addition of some surfactants, such as GMS (glycerol monostearate), can lead to a separation phase between the PEDOT and PSS chains. This was explained by the fact that a surfactant can separate these two halves, merging them by its polar head on one side, which interacts with the styrenic part, and the apolar tail on the other hand, that instead can cooperate with the thiophenic one. In light of this, the presence

of these kind of compounds can reproduce the separation effect on the system which is here described. Therefore, in order to perform the test, hexadecyltrimethylammonium bromide ($C_{19}H_{42}BrN$), was used with an aqueous concentration of 1M.

4) The in-solution arrangement between PEDOT and PSS chains in the aqueous medium was supposed and widely schematized in literature [31-35] and also reported in Chapter 1. According to these works, woven random coils of PSS molecules interact with smaller chains of PEDOT. Differently, the effect of the direct acidification to the pristine solution has not been never investigated. About this, it is worth to remind that the solvation effect and some supramolecular interactions between polymer species can occur, eventually playing a role in the final solubility of the system. Moreover, not knowing how to predict the effect of the H_2SO_4 a priori, a hierarchical order in the acidification could eventually occur. In other words, this means that the order with which the chemicals listed above are added to the gel paste could also play a role in polymer precipitation. For this reason, each approach described so far was then replicated changing the order of the addition of the chemicals. This time, each solvents listed in the point 1) and the solution of hexadecyltrimethylammonium bromide of the point 3) were added to the solution of PEDOT:PSS before the acidification with H_2SO_4. Therefore, in this last case, the order with which chemicals are inserted in test tubes is the following: a small amount of the pristine polymer goes for first, followed by the pure solvent or basic/surfactant solution and finally the H_2SO_4. This experiment was not performed using the KOH solution since the pH variation spacing toward basic values, first, and then again to the

acid ones (because of the final acid addition), lied outside the scopes of this work. For each case here illustrated, the dark blue precipitate appears immediately after the addition of the acid.

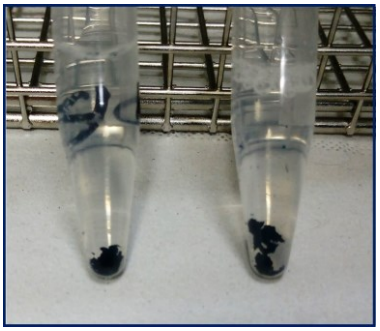

Fig. 4.7: Two examples of the solubility test performed on the paste obtained after 24h decantation, rinsing and removal of supernatant. In the picture, there are shown two Eppendorf test tubes containing the dark blue paste immersed respectively in 1M KOH (on the left) and in acetyl acetate (on the right).

For each situation described here above, both the dark blue wet gel and the dried paste obtained after baking have never solubilized again in none solvents or chemicals used. An example of this result is given in picture below, Fig. 4.7:

This result has two important implications, concerning the processing and the insight of the reaction, respectively.

On one side this suggests that, once precipitated, the paste obtained cannot be solubilized anymore, whatever the solvents or conditions used. This has a considerable implication in the successive processing methods of this material. Indeed, at a presence of a highly viscous, gelatinous paste, deposition techniques such as spin coating, drop casting, dip-coating, cast and spray coating and electrodeposition, have to be excluded. Instead, other methods must be taken in

consideration including, for instance, screen printing, doctor blade, inkjet printing and roll-to-roll techniques.

As second involvement, the results obtained by the solubility test give an important indication about the chemical composition of the paste. Indeed, the blue precipitate has to contain the PEDOT portion, thus excluding the possibility that is retained in the aqueous part. This can be asserted from what reported in Ref. [36-38]: first works for obtaining PEDOT have described it as a dark blue powder, infusible and insoluble after the polymerization. Indeed, the results obtained by the solubility test give us a clear indication about the chemical composition of the product obtained, which surely contains the conductive portion of the initial polymer blend. What concerning the PSS content in the precipitate cannot be yet discussed and will be investigated in the next sections (see 4.7 and 4.8).

4.5 - Two-Point Measurements

The d-paste was characterized by I-V curves performed with 2-point probes measurements, which were run immediately after the preparation of samples. Curves were obtained by sweeping the voltage in the range between -0.5 and +0.5V. In order to monitor any change in the electrical conductivity due to the electric field stress, the I-V measurements were performed for 10 consecutive times. Fig. 4.8 shows the results of this investigation. As observed, the trend of each curve is ascribable to a resistor-like behaviour, indicating a non-rectifying response. Interestingly, at 0.5V and -0.5V the measured current is of the order of 10^{-3} A, and precisely 3.2 mA. This same trend was already observed for thin films of PEDOT:PSS treated with a mixture of SDS and ethylene glycol [39].

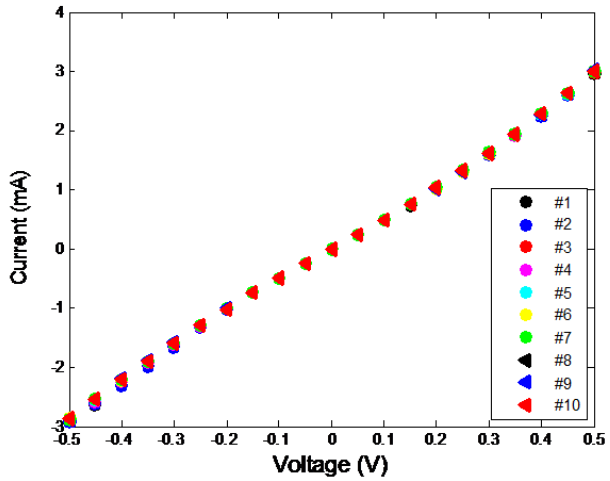

Fig. 4.8: I-V curves with sweep from -0.5V to +0.5V, ten measurements in sequence with interval time of 3 sec, performed on d-PEDOT

As reported in Fig. 4.8, the d-PEDOT paste does not show any relevant electrical modification during the voltage scans, thus indicating an apparent stability of the material to the electric field, even for several I-V measurements.

In order to exclude any possible effect of charge accumulation, I-V measurements by sweeping bias from -0.5 to +0.5V (i.e. in forward) and from +0.5 to -0.5V (reverse) were also performed. Each couple of sweeps was repeated for ten times. Fig. 4.9a shows the first couple of measurements, i.e. the sweep in forward (magenta curve) and reverse bias (blue) condition. It is possible to see that these curves are almost overlapped, thus suggesting that no charge accumulation effect is observable. This same behaviour is also confirmed by the successive results, in which each couple of measurements is overlapped with the others (Fig. 4.9b).

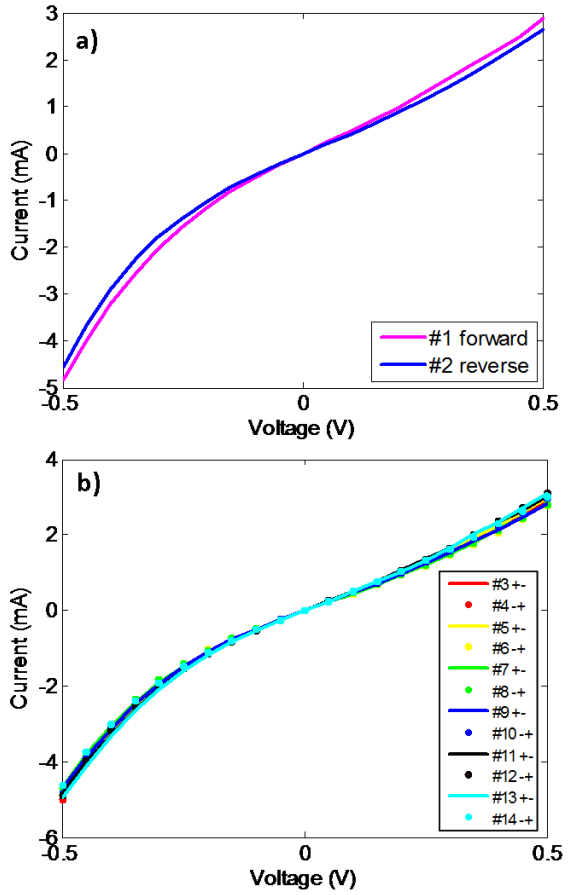

Fig. 4.9: (a) I-V sweeps in forward (magenta curve) and reverse (blue) conditions; (b) 2nd to the 7th sweep measurements, where forward and reverse scans are indicated by lines and dots, showing an insignificant hysteresis.

As it is possible to note, no significant hysteresis effects are exhibited. A rough calculation of the resistance which can be extracted from the I-V curves returns a resistance value in a range of 150-170 Ohm.

Seen the results at ± 0.5V, it is important to understand if the two-point measurements are affected by the contact resistance between the sample and probes.

For this reason, the electrical properties of the free-standing d-paste were investigated by 4PP measurements and shown more in detail in the next section.

4.6 - Four-Point Measurements

In order to understand if any contact resistance plays a role in the I-V curves seen so far 4PP measurements were also performed. The set-up of these measurements is shown more in detail in the Appendix B. Here again, metallic contacts were used for performing these measurements since they guarantee a good stability of the voltage outputs even at low current inputs and linear V-I responses. However, two measurements performed on the same sample with and without the metal contacts give back the same values of sheet resistance.

Since the paste obtained can have different applications in several technological fields [14,19-24], the response of the d-paste both in dark and under light conditions were investigated. Therefore, Voltage-Current (V-I) acquisitions were made in dark and under a standard light bulb irradiation, with an irradiance of 30 mW/cm^2 (1/3 SUN), measured by a photodiode. Sheet resistance values were acquired on several 30-33 μm thick samples and an example of the linear range of the V-I curves is shown in the Fig. 4.10. The graph shows the 4PP measurements performed on the same sample with two successive measurements in dark (black symbols) and light conditions (red symbols), respectively. 4PP measurements are acquired without moving the probes and with a delay of 5 seconds from the first and second measurement.

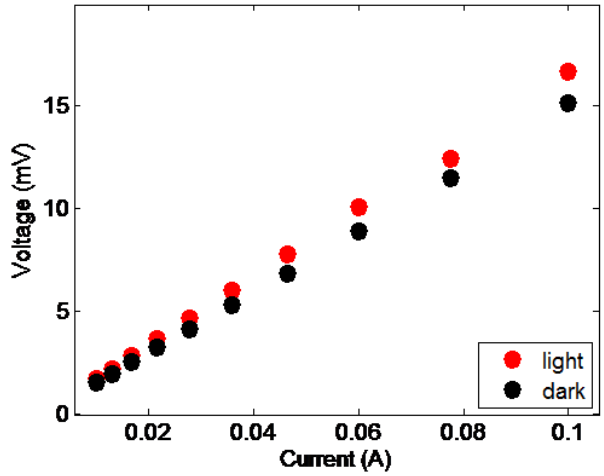

Fig. 4.10: V-I scan acquired in 4PP configuration on the d-PEDOT dried paste in dark (black data) and under light exposure (red).

In the examples shown in the Fig. 4.10, the sheet resistance measured gave an average result of 0.60 Ohm/sq (± 0.02) in dark, thus indicating a mean conductivity of 500 Scm^{-1}, while under light exposure the R_{sh} obtained was slightly different.

Whether this result is compared to that obtained by two points I-V curves, it is possible to see that the actual resistivity of the paste is much lower than the contribution of contact resistance given from the interface between the probes and the sample surface. This means that the contact resistance has a significant contribution in the two-contact measurements. For these reasons, 4PP analysis are more useful for better characterize the material and will be considered in the following.

For these scopes, several benches of samples were prepared and analysed with the 4PP technique. Moreover, for each sample set prepared, the stability of the material undergone to the electrical field was also tested. This last point was addressed with repeating each set of measurements up to ten consecutive times without moving the

four probes. The interval time between one acquisition and the successive one was of 30 seconds.

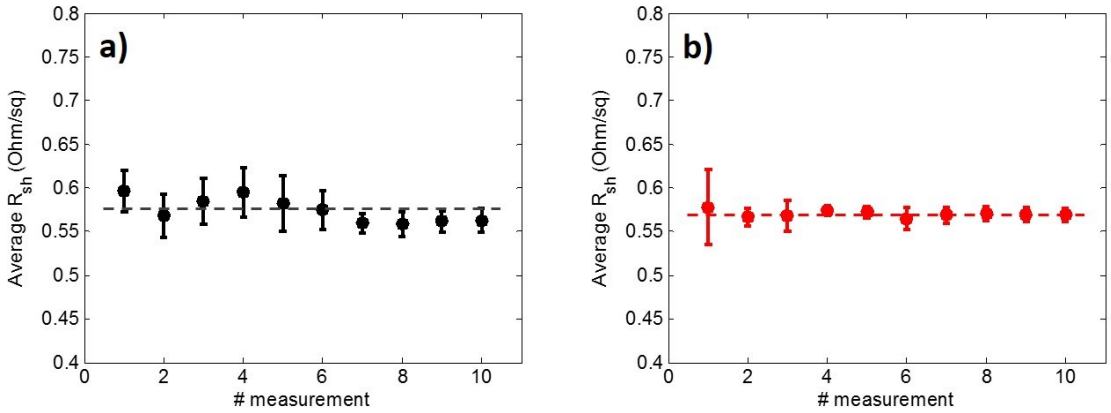

Fig. 4.11: Sheet resistance measured for samples prepared with bake in air at 170°C for 2h, respectively in a) dark and b) under light irradiation. Dashed lines in both images represent a guide to the eye.

Fig. 4.11 reports the sheet resistance measured for samples baked in air at 170°C for 2 hours. Fig. 4.11a and b show the results of the 4PP acquisition made in dark and under light conditions (1/3 SUN), respectively. Each point in the two graphs is given by a R_{sh} value averaged on three samples prepared in the same conditions, while error bars are calculated as standard deviations. From Fig. 4.11 it is possible to note that during the ten measurements performed, no great variations in the R_{sh} values are detected, and the global trend of the data appears substantially flat. From this, it can be asserted that each sample set shows a stability for both external conditions (dark/light) and also for the electrical field applied to the samples. Therefore, it is possible to conclude that, for samples prepared with only one

thermal treatment (i.e. bake in air at 170°C for 2h), the sheet resistance measured corresponds to ≈0.60 Ω/sq, thus returning a conductivity value of ≈500 S/cm.

In order to investigate the effect of the thermal conditions on the electric properties, another group of samples was prepared, exploring different and further thermal and environment conditions. Each sample underwent to the bake already described in the section 4.2 of this Chapter and it was then treated with an additional annealing as described in the Table 1. It has to be noted that the first air bake was required to evaporate most of the water entrapped in the samples and thus avoiding any damage to the vacuum equipment.

Second annealing performed in chamber at 0.01 mbar		
Samples	Annealing temperature	Annealing Time
Group A	170°C	10 min
Group B	170°C	1h
Group C	170°C	2h
Group D	170°C	4h
Group E	135°C	10 min

Table 4.1: Table of the samples treated with the annealing process in the vacuum chamber after the bake run in air at 170°C for 2h.

The vacuum condition corresponds to a pressure of 0.01 mbar. During the annealing, the pressure inside the oven chamber increased up to 2-3 mbar, because

of the samples degassing. For 2h and 4h annealing times, the internal pressure in the chamber goes back to its initial value of 0.01 mbar. Differently, for treatments of 10 minutes, the annealing duration is not enough for completely degassing the system and the regime pressure is not restored when the treatment is interrupted.

Here in the following, the results of the 4PP measurements for each case in the list above are shown.

Fig. 4.12 shows the average sheet resistance values of samples of Group A, acquired in dark and under light irradiation (Fig. 4.12a and b, respectively). Any detail regarding the experimental points and the error bars are analogous to those ones already described.

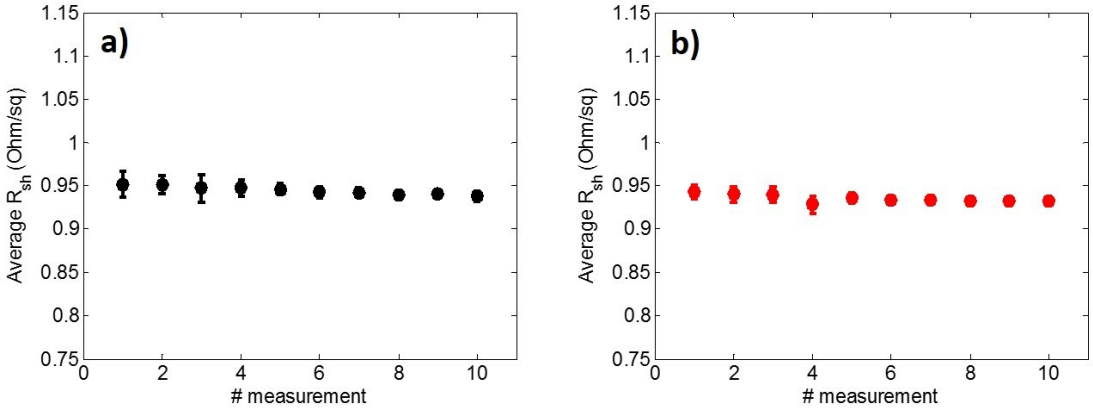

Fig. 4.12: Sheet resistance measured for samples prepared with bake in air at 170°C for 2h, and additional annealing in vacuum condition performed for 10 minutes at 170°C, respectively in a) dark and b) under light irradiation.

A good stability to electric field effect can be noted again, analogously to what was already reported in the Fig. 4.11. What it is worth to note, instead, is that the average value of the sheet resistance measured in this case is clearly higher with respect to that one obtained for samples undergone only to the bake in air (Fig.

4.11). No significant variations in the thickness of the foils were observed, neither in those ones measured before and after the vacuum annealing, nor after the bake. This result should indicate a variation in the conductivity of the paste. Later it will be investigated if it is correlated to a chemical or structural modification, or rather to a morphological re-arrangement.

Group B: since, as it was observed previously, no significant modification in R_{sh} values are observed when measurements are acquired in different ambient condition, only the results of the acquisitions made in dark condition will be reported from now on. Fig. 4.13 shows the sheet resistance obtained for 10 consecutive measurements on three samples prepared with the standard bake and the additional annealing performed at 170°C for 1h in vacuum. This time, our results display a mean sheet resistance of 0.66 Ω/sq with no variation observable in the thickness of the samples. Therefore, this result indicates that, as in the case of the samples of group A, a change in the conductivity of the material has occurred, leading to electrical performances comparable with those ones observed for samples only undergone to the bake.

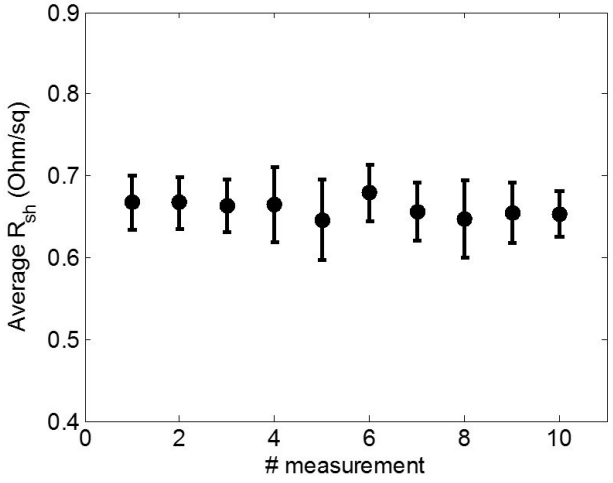

Fig. 4.13: Sheet resistance measured for samples prepared with bake in air at 170°C for 2h, and additional annealing in vacuum condition performed for 1h at 170°C. 4PP measurements performed in dark ambient.

Fig. 4.14 shows the sheet resistance acquired for 10 consecutive measurements on the three samples belonging to Group C, prepared with the standard bake and the additional annealing performed at 170°C for 2h in vacuum. This time, results display a mean sheet resistance of 0.40 Ω/sq. This indicates that a change in the conductivity of the material has occurred, leading to electrical performances which are even better than those samples described previously.

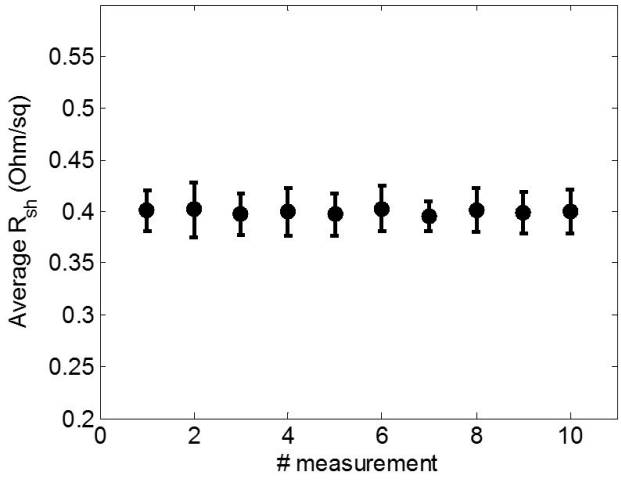

Fig. 4.14: Sheet resistance measured for samples prepared with bake in air at 170°C for 2h, and additional annealing in vacuum condition performed for 2h at 170°C. 4PP measurements performed in dark ambient.

In vacuum conditions, it is expected that any contaminant present in the environment that can eventually affect the conduction mechanism, is suppressed thus leading to better electrical performances. Moreover, longer duration of the thermal treatment probably leads to a re-arrangement of the polymer chains with respect to those samples belonged to the group A, thus approaching the conductive portions of the paste and decreasing the overall resistance.

However, a longer thermal process, even in vacuum, can lead to a deterioration of the material. This was observed for samples belonging to the Group D, annealed for 4h and for which it was not possible to acquire the 4PP measurements. In other words, long annealing times affect the electrical properties of the material under investigation, leading to a typical behaviour of an insulator. These results are reported in the Fig. 4.15:

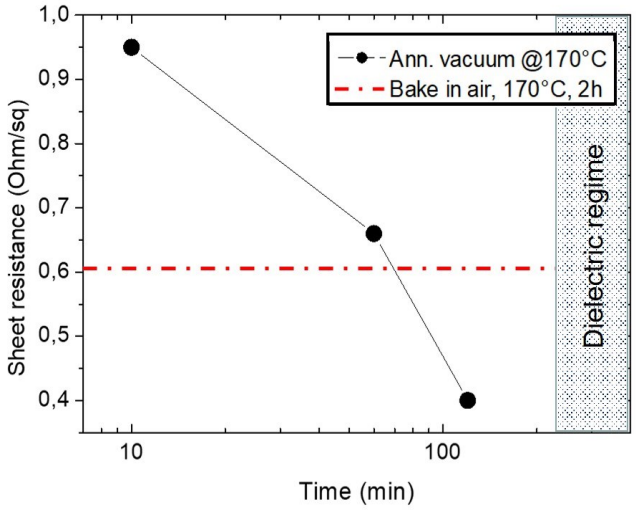

Fig. 4.15: Summary chart of the average sheet resistance as a function of the annealing time in vacuum chamber. Last point in the chart, corresponding to decades of kΩ/sq, is an arbitrary value for indicating the insulator-like behaviour of samples undergone to long vacuum annealing. Red line in the graph represents the mean value of R_{sh} acquired for the samples undergone only to the bake in air.

The annealing in vacuum performed at the same temperature with different duration, have proven that there is a dependence on the thermal budget on the load of duration. In order to find any other correlation to the thermal budget, we have also performed similar experiments on samples of group E that were prepared with an additional annealing in vacuum chamber at 135°C for 10 minutes. The results given from this last set of samples are reported in the Fig. 4.16

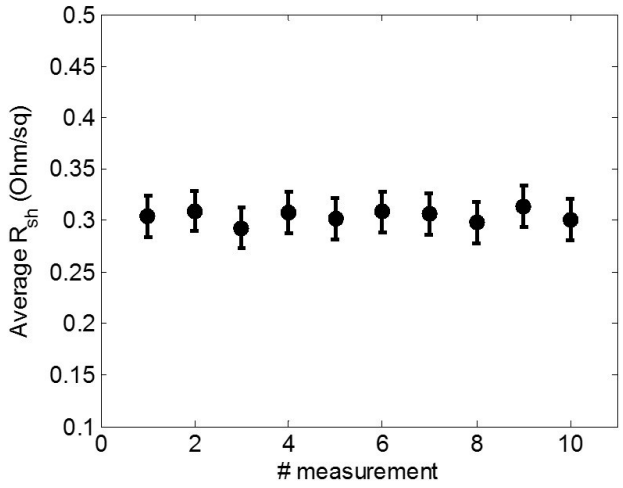

Fig. 4.16: Sheet resistance measured by 4PP in dark on samples prepared with bake in air at 170°C for 2h, and additional annealing in vacuum performed for 10 minutes at 135°C.

For this last group, the sheet resistance halves that one reported for samples baked in air, thus reaching an average value of 0.30 Ω/sq. Since also in this case no appreciable thickness variations are detected and the final depth of these samples is again of ≈30 μm ± 1, the final conductivity corresponds to ≈ 1000 S/cm. This was the best result achieved so far, in terms of electrical performances explicated. This result indicates that the thermal budget plays a clear role on the polymer paste. Previous results of Greco and co-workers [40] show the improvement of the electrical performances when the annealing is performed at lower temperature. Even if also in Ref. [40] an exhaustive explanation of this result was not provided, the authors have shown that an additional annealing at 170°C has slightly decreased the conductivity of their PEDOT:PSS films. In the same manner, the additional thermal treatment can thus have a beneficial effect when performed at lower temperature (e.g. 135°C) and can instead affects the properties of the

material probably because of a thermal degradation when higher temperatures for long times are used (such as in the case of Group D, 170°C for 4h). All these results are summarized in the Fig. 4.17:

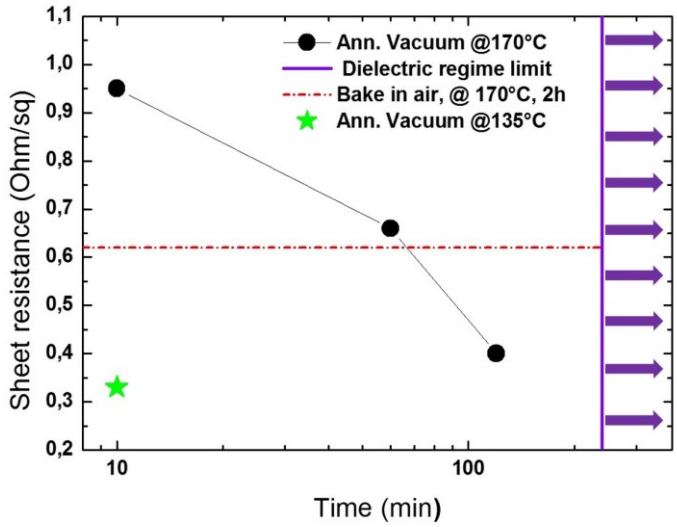

Fig. 4.17: Summary chart of the average sheet resistances as function of the annealing time and temperature in vacuum chamber. Axis of the graph are expressed in semilog scale. Red line in the graph represents the mean value of R_{sh} acquired for the samples undergone only to the bake in air.

For the sake of completeness, it is worth to do some considerations about the roughness and the chemical and physical uniformity of polymer paste.

The measurements of the vertical conduction of the samples could supply a valid indication of both the morphology of the polymer foil and also of the chemical and physical uniformity of the samples. However, as already explained previously in this section, I-V curves acquired on the d-paste have shown that the contact resistance has a significant contribution in the measurements. Indeed, the calculated conductivity of the polymer paste, obtained by the sheet resistance through the 4PP

method, ranges between 1010 and 340 S/cm. This means that the actual resistivity of the paste is much lower than the contribution of contact resistance given from the interface between the probes and the sample surface. Since the vertical conductivity should be performed by the two-points technique, the result would be affected by the contact resistance, thus underestimating the vertical conductivity of the paste. From these experimental findings, it is understood that it was not possible to measure the vertical conductivity through this technique.

However, it is reasonable to think that there should not be any significant variation between the conductivity measured in plan and the vertical one. This can be stated since the 4PP measurements performed on both sides of the paste have given the same values in each group of samples.

Moreover, some other considerations can be made on the paste roughness obtained, for which a coarse estimate is made by the depth of focus technique. It has been found that the top surface of the film presents an estimated roughness of about a few microns, while the rear side of the sample, at the interface with the substrate, is less than 1 micron. The surface roughness does not affect the electrical analysis anyway. Indeed, as reported above, the sheet resistance measured on the two sides of the samples returns the same value. This means that, whatever is the actual value of the roughness, it is negligible with respect to both the size of the probes and the overall depth of the samples.

4.7 - Raman Analysis

In order to shade light on the chemical composition of the conductive, dark paste obtained, Raman analysis on the sample only baked in air at 170°C for 2h was

performed. Differently to what already discussed in the previous Chapter, since the sample disk is quite thick (30 μm) and thus endures weakly the detection of the underlying substrate, in this characterization the d-paste is supported on glass slide instead of Si. This time, the acquisition is made by 785 nm-laser source. Indeed, it was observed that, using 532 nm as laser source it was not found any compromise between the quality of the spectrum obtained and the laser power used, and sample gets wrecked quickly under the laser spot. Unlike the case already seen in the Chapter 3, in which a laser source of 633 nm was used, for the polymer paste, poor quality in the spectrum acquired is obtained with this excitation wavelength, since signals are embedded and easily mistakable with the background noise. The best compromise was found using the 785 nm source with a laser power at ≈ 1 mW. When excited at this wavelength, spectrum shows a relevant fluorescence, which is then suppressed during the data analysis. The elaborated Raman spectrum is reported in the Fig. 4.18.

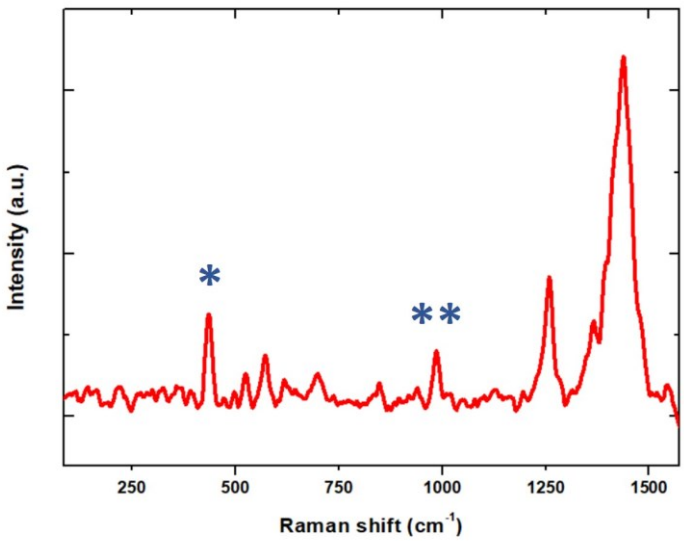

Fig. 4.18: Raman spectrum excited at λ_{ext}=785 nm and power laser source of ≈ 1 mW of the d-paste baked in air at 170°C for 2h, supported on glass slide.

It is possible to note that all signals, both related to the PSS (at ≈438 cm^{-1}) and PEDOT counterpart are present in the spectrum. Again and as already seen in the previous Chapter, spectral signals attribution is in agreement with those ones reported in the literature [41].

Signals related to the PEDOT are identified and listed here below: the asymmetric C_α=C_β stretching between 1563 and 1532 cm^{-1}, while at 1431 cm^{-1} large band is quite characteristic of the PEDOT and it is associated to the symmetric stretching of the C_α=C_β. Band at 1369 cm^{-1} is related to the stretching of the C_β=C_β, while band at 1260 cm^{-1} is attributed to the inter-ring stretching of the C_α=C_α and the region included between 1080-1160 cm^{-1} hosts the C-O-C deformation. Signals at 989 (which in the Fig. 4.18 is indicated with the double star) and 579 cm^{-1} are due to the oxyethylene ring breathing while 701 cm^{-1} band is attributed to the C-S-C deformation. Again, as already mentioned in the Chapter 3, the band appeared at ≈433 cm^{-1} (recognizable with symbol * in the Fig. 4.18) is the only signal which can be attributed to the PSS, since it is related to the SO_2 bending that can only come from the sulfonic group of the styrenic chain. Using the same criteria already seen previously (Chapter 3), we now take in consideration the signal related to the oxyethylene ring breathing of PEDOT (989 cm^{-1}) and the SO_2 bending (433 cm^{-1}) of PSS. The integrated intensity ratio for these two signals is here indicated as I_{438}/I_{989}, and it returns the value of 1.46. Apparently, this value is even higher than that one found for the undoped polymer reported previously (estimated to 1.09). However, these values should not be misleading: the sample presented as reference in the previous Chapter has a thickness in the order of hundreds of nanometers, while the paste under investigation is of ≈30 μm. This means that the sample depth, in this latter case, is more influenced by the bulk composition of the paste. Therefore, the

apparent higher amount of PSS does not indicate an actual higher concentration of this specie with respect to PEDOT, but it is related to a higher quantity of material sampled and detected by the source. In any case, what is worth to note is that after the process used for the sample preparation, thus acidification first and water rinsing after (check section 4.2 in this Chapter), the PSS portion of the original blend is not removed at all, but its signal is still clearly recognizable.

This result can suggest an important indication about the arrangement and the interaction of the PEDOT and PSS in water. The insight of the results obtained until here are thus better addressed in the next section (4.8).

4.8 - Discussion of the Results

It has been seen that the effect of the acid addition to the pristine PEDOT:PSS aqueous solution leads to the instantaneous formation of dark blue agglomerates which remain suspended in the aqueous medium [20,25,26]. The formation of this agglomerates is attributed to the establishment of a new equilibrium in which the protons released by the acid dissociation are repeatedly exchanged with the free sulfonic groups along the PSS chains (see section 4.3 of this Chapter) [27]. This phenomenon leads to a certain shielding effect between the anionic groups of the styrenic portion and the polarons present on the PEDOT chains [28,29]. The consequent decrease of the Coulomb interactions between these two species leads to the separation of one polymer from the other and the separation of both of them from the surrounding solvent, even for small amounts of acid, as sketched in the Fig. 4.19.

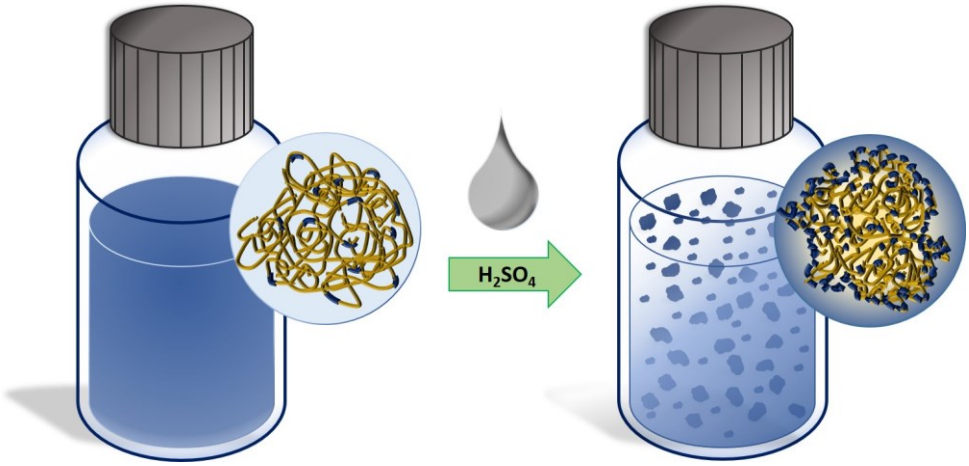

Fig. 4.19: Sketch of the re-arrangement between PEDOT and PSS chains following the addition of H_2SO_4 directly to the pristine aqueous solution. Pristine PEDOT:PSS is represented in the vial on left side, while flask containing small amount of acid in the polymer blend is depicted on the right. In each round, a schematic representation of the chains-arrangement is given (yellow lines represent PSS portion, while dark blue ones indicate the PEDOT chains).

In this phase separation, however, the styrenic portion, which is also more polar with respect to the PEDOT, is not retained in the aqueous medium, but precipitates together with its conductive counterpart. This is clearly evident by the Raman analysis from which the presence of PSS is detected by the typical signal related to the SO_2 bending at 433 cm^{-1} (section 4.7). If the PSS was completely retained in the supernatant or removed by the water rinsing, this signal should be less intense or even absent. However, the presence of the PSS chains should not surprise: with the addition of H_2SO_4 and the establishment of the protons exchange equilibrium mentioned above, the water solubility of PSS decreases. Therefore, two parallel effects due to the acidification manifest:

- On one hand the solubility of PSS lowers and thus it separates from the polar solvent;

- On the other side, the PEDOT cannot be kept anymore as water dispersion and thus precipitate. This clue is also given by the fact that the precipitate is insoluble in any solvent as proved by the solubility test performed (section 4.4).

These considerations justify the presence of both the polymer species in the precipitate. However, this process must lead toward a re-arrangement of the entire blend with respect to the pristine one. This assertion is due to the fact that we attend to a significant increase in the material conductivity which, start from some 2-4 S/cm of the pristine solution (Chapter 2), and achieves ≈1000 S/cm as form of dark paste in the best case here reported (check section 4.6). These results strongly suggest that the precipitation mechanism, and consequently the paste formation, leads to agglomerates in which a core made of PSS and PEDOT is surrounded by a PEDOT-based shell and this structure represents the unit-base of the precipitate (see scheme in Fig. 4.20).

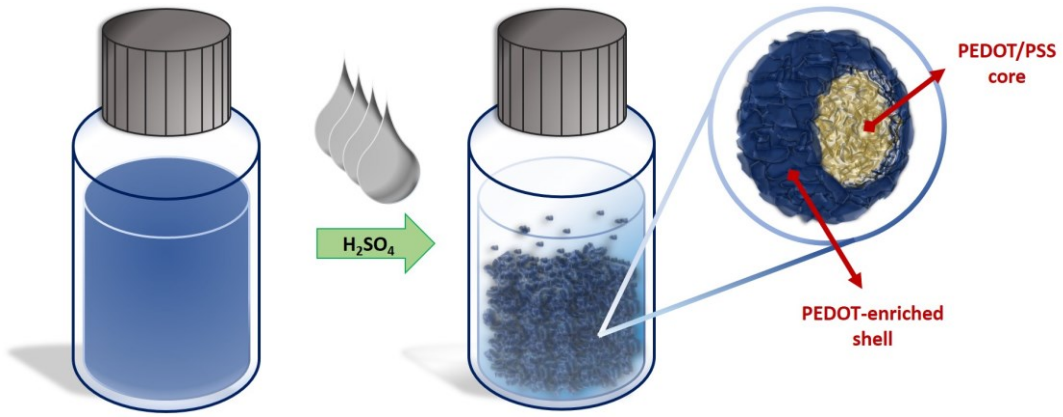

Fig. 4.20: Sketch of the hypothetical arrangement and composition of an agglomerate formed as a consequence of large amount of acid added to the pristine PEDOT:PSS solution. In the round, a schematized agglomerate formed by a PSS-core and a PEDOT-enriched shell.

The global conduction of the paste is given by a sort of percolation path in which each unit-base is surrounded and interconnected to its neighbours by PEDOT domains, thus allowing the charge transfer within the material, as schematized in the picture below (Fig. 4.21).

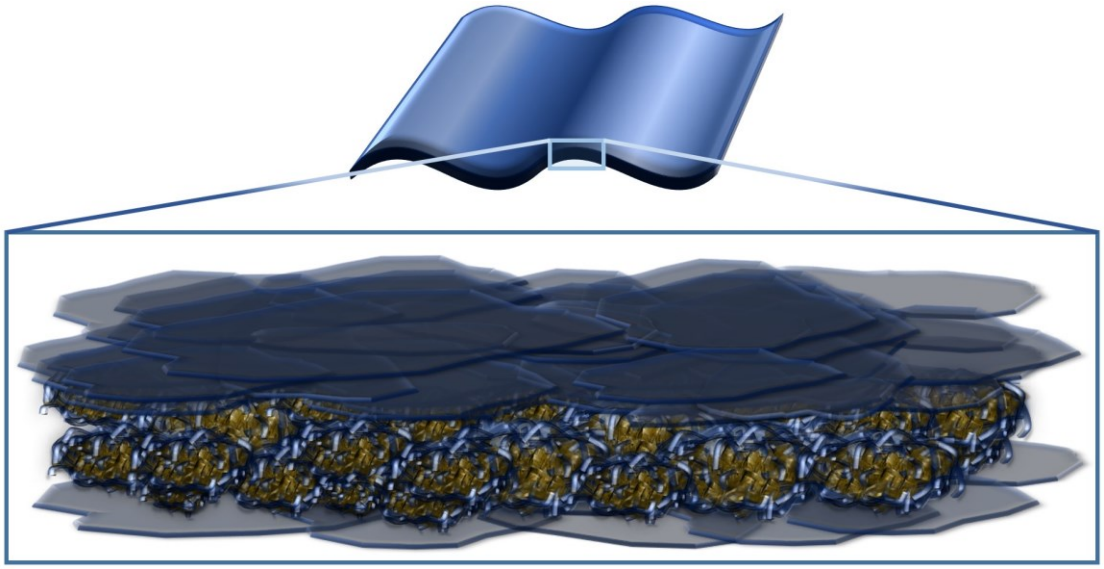

Fig. 4.21: Sketch of the hypothetical disposition of the agglomerates made of blend of PEDOT:PSS in the free-standing foil obtained after annealing. Legend of colours: yellow represents PEDOT/PSS domains, while blue corresponds to the conductive PEDOT.

The bake allows the removal of the dielectric solvent which otherwise would kill the charges transport, while a successive annealing in vacuum conditions leads to a further improvement of the global conductivity, probably caused by a more efficient solvent removal and the consecutive approaching of the conductive portions. However, as already discussed in the section 4.6 of this Chapter, this delicate mechanism is directed by a fine balance related to the thermal budget supplied. The

best performances are guaranteed by lower temperature (135°C) and short annealing time (10 minutes).

4.9 - Conclusions

In this Chapter, it was described a low cost and fast method to obtain a free-standing, flexible, thick and conductive polymer foil from a mouldable paste. The procedure is based on the phase separation of PEDOT from PSS, induced by acidification of the solution until its complete saturation. The method is as easy as writing by an ink-pen. The samples have been electrically characterized by four-point probe measurements. The results have shown a sheet resistance ranging between 0.90 and 0.30 Ohm/sq, depending on the thermal treatment. These values correspond to conductivities within 370 and 1000 S/cm. The chemical characterization has been carried through Raman analysis. The interpretation of all the results has led to imagine the material as an arrangement of agglomerates constituted of both PEDOT and PSS species. These results have demonstrated that the synthesized material can be considered competitive and a good alternative to the standard metallic contacts thanks to its flexibility and good electrical performances. Moreover, the preparation method can be easily scalable by techniques such as screen printing, doctor blade, inkjet printing and roll-to-roll techniques, which typically lend themselves to be used for highly viscous solutions and paste. Therefore, in future perspectives, it is worth to image our d-paste as a competitive alternative with other organic conductive materials and also as a valid alternative to the common and more expensive metallic contacts.

4.10 – Bibliography

[1] B. Anothumakkool, R. Soni, S.N. Bhange, S. Kurungot, Environmental Science Novel scalable synthesis of highly conducting and robust PEDOT paper for a high performance fl exible solid supercapacitor †, Energy Environ. Sci. 8 (2015) 1339–1347. doi:10.1039/C5EE00142K.

[2] K.L. Bhowmik, K. Deb, A. Bera, R.K. Nath, B. Saha, Charge Transport through Polyaniline Incorporated Electrically Conducting Functional Paper, (2016). doi:10.1021/acs.jpcc.5b08650.

[3] Y. Du, K. Cai, S. Chen, H. Wang, S.Z. Shen, R. Donelson, T. Lin, Thermoelectric Fabrics : Toward Power Generating Clothing, (2015) 1–6. doi:10.1038/srep06411.

[4] H. Farrokhzad, T. Van Gerven, B. Van Der Bruggen, Preparation and characterization of a conductive polyaniline / polysulfone film and evaluation of the effect of co-solvent, Eur. Polym. J. 49 (2013) 3234–3243. doi:10.1016/j.eurpolymj.2013.06.027.

[5] M. Kyotani, S. Matsushita, M. Goh, T. Nagai, K. Akagi, Entanglement-free fibrils of aligned polyacetylene films that produce single nanofibers, (2010). doi:10.1039/b9nr00254e.

[6] H.P. De Oliveira, S.A. Sydlik, T.M. Swager, Supercapacitors from Free-Standing Polypyrrole/Graphene Nanocomposites, (2013). doi:10.1021/jp400344u.

[7] V.A. Online, G. Qi, Z. Wu, H. Wang, Journal of Materials Chemistry C, (2013) 7102–7110. doi:10.1039/c3tc31340a.

[8] C.H. Park, S.K. Jang, F.S. Kim, Applied Surface Science Conductivity enhancement of surface-polymerized polyaniline films via control of processing conditions, Appl. Surf. Sci. 429 (2018) 121–127. doi:10.1016/j.apsusc.2017.09.031.

[9] D. Taylor, F.S. Gittleson, D.J. Kohn, X. Li, Improving the Assembly Speed ,

Quality , and Tunability of Thin Conductive Multilayers, (2012) 3703–3711. doi:10.1021/nn204384f.

[10] D. Alemu, H.-Y. Wei, K.-C. Ho, C.-W. Chu, Highly conductive PEDOT:PSS electrode by simple film treatment with methanol for ITO-free polymer solar cells, Energy Environ. Sci. 5 (2012) 9662. doi:10.1039/c2ee22595f.

[11] L. He, C. Jiang, H. Wang, H. Lei, D. Lai, Rusli, 11.3% efficient planar Si-PEDOT: PSS hybrid solar cell with a thin interfacial oxide, Conf. Rec. IEEE Photovolt. Spec. Conf. (2012) 2785–2787. doi:10.1109/PVSC.2012.6318170.

[12] Y.-S. Hsiao, W.-T. Whang, C.-P. Chen, Y.-C. Chen, High-Conductivity Poly(3,4-ethylenedioxythiophene):Poly(styrene sulfonate) Film For Use In ITO-Free Polymer Solar Cells, J. Mater. Chem. 18 (2008) 5948–5955. doi:10.1039/b813079e.

[13] S. Jäckle, M. Liebhaber, C. Gersmann, M. Mews, K. Jäger, S. Christiansen, K. Lips, Potential of PEDOT:PSS as a hole selective front contact for silicon heterojunction solar cells, Sci. Rep. 7 (2017). doi:10.1038/s41598-017-01946-3.

[14] Q. Jiang, C. Liu, H. Song, J. Xu, D. Mo, H. Shi, Z. Wang, Free-standing PEDOT : PSS Film as Electrode for the Electrodeposition of Bismuth Telluride and Its Thermoelectric Performance, 9 (2014) 7540–7551.

[15] B.J. Kim, S.H. Han, J.S. Park, Sheet resistance, transmittance, and chromatic property of CNTs coated with PEDOT:PSS films for transparent electrodes of touch screen panels, Thin Solid Films. 572 (2014) 68–72. doi:10.1016/j.tsf.2014.08.015.

[16] W. Meng, R. Ge, Z. Li, J. Tong, T. Liu, Q. Zhao, S. Xiong, F. Jiang, L. Mao, Y. Zhou, Conductivity Enhancement of PEDOT:PSS Films via Phosphoric Acid Treatment for Flexible All-Plastic Solar Cells, ACS Appl. Mater. Interfaces. 7 (2015) 14089–14094. doi:10.1021/acsami.5b03309.

[17] K.T. Park, H.J. Kim, M.J. Park, J.H. Jeong, J. Lee, D.G. Choi, J.H. Lee, J.H. Choi, 13.2% efficiency Si nanowire/PEDOT:PSS hybrid solar cell using a transfer-

imprinted Au mesh electrode, Sci. Rep. 5 (2015) 1–9. doi:10.1038/srep12093.

[18] H. Wang, J. Wang, L. Hong, Y.H. Tan, C.S. Tan, Rusli, Thin Film Silicon Nanowire/PEDOT:PSS Hybrid Solar Cells with Surface Treatment, Nanoscale Res. Lett. 11 (2016) 311. doi:10.1186/s11671-016-1527-1.

[19] M. Bansal, M. Sharma, C. Bullen, D. Svirskis, Materials Science & Engineering C Free standing PEDOT fi lms prepared by vapour phase polymerisation as electrically tuneable barriers to drug permeability, Mater. Sci. Eng. C. 84 (2018) 248–253. doi:10.1016/j.msec.2017.12.002.

[20] Z. Li, G. Ma, R. Ge, F. Qin, X. Dong, W. Meng, T. Liu, J. Tong, F. Jiang, Y. Zhou, K. Li, X. Min, K. Huo, Y. Zhou, Zuschriften Energy Conversion Hot Paper Free-Standing Conducting Polymer Films for High-Performance Energy Devices Zuschriften Angewandte, (2016) 991–994. doi:10.1002/ange.201509033.

[21] Y. Liu, B. Weng, J.M. Razal, Q. Xu, C. Zhao, Y. Hou, High-Performance Flexible All- Solid-State Supercapacitor from Large Free-Standing Graphene- PEDOT / PSS Films, Nat. Publ. Gr. (2015) 1–11. doi:10.1038/srep17045.

[22] S. Matter, F. Greco, A. Zucca, S. Taccola, A. Menciassi, T. Fujie, H. Haniuda, S. Takeoka, V. Mattoli, Soft Matter, (2011) 10642–10650. doi:10.1039/c1sm06174g.

[23] H. Song, C. Liu, H. Zhu, F. Kong, B. Lu, J. Xu, J. Wang, F. Zhao, Improved Thermoelectric Performance of Free-Standing PEDOT : PSS / Bi 2 Te 3 Films with Low Thermal Conductivity, 42 (2013) 1268–1274. doi:10.1007/s11664-013-2587-y.

[24] M.J. Kye, J. Cho, J.C. Yu, Y.W. Chang, J. Han, E. Lee, H.S. Lim, J.A. Lim, “Drop-on-textile” patternable aqueous PEDOT composite ink providing highly stretchable and wash-resistant electrodes for electronic textiles, Dye. Pigment. 155 (2018) 150–158. doi:10.1016/j.dyepig.2018.03.024.

[25] V. Lombardo, S. Di Franco, A. La Magna, A. Terrasi, R.A. Puglisi, Conductive free standing polymer paste synthesized by acid induced phase separation, (n.d.) 1–5.

[26] V. Lombardo, L.D. Urso, G. Mannino, S. Scalese, Transparent conductive polymers obtained by in-solution doping of PEDOT : PSS, (n.d.).

[27] Y. Xia, K. Sun, J. Ouyang, Solution-processed metallic conducting polymer films as transparent electrode of optoelectronic devices, Adv. Mater. 24 (2012) 2436–2440. doi:10.1002/adma.201104795.

[28] W. Zhang, B. Zhao, Z. He, X. Zhao, H. Wang, S. Yang, H. Wu, Y. Cao, High-efficiency ITO-free polymer solar cells using highly conductive PEDOT:PSS/surfactant bilayer transparent anodes, Energy Environ. Sci. 6 (2013) 1956–1964. doi:10.1039/c3ee41077c.

[29] Y. Xia, H. Zhang, J. Ouyang, Highly conductive PEDOT : PSS films prepared through a treatment with zwitterions and their application in polymer photovoltaic cells, (2010) 9740–9747. doi:10.1039/c0jm01593h.

[30] Christian Reichardt, Solvents and Solvent Effects in Organic Chemistry , Wiley-VCH Publishers, 3rd ed., 2003, (2003) 2003.

[31] J. Ouyang, Q. Xu, C.W. Chu, Y. Yang, G. Li, J. Shinar, On the mechanism of conductivity enhancement in poly(3,4- ethylenedioxythiophene):poly(styrene sulfonate) film through solvent treatment, Polymer (Guildf). 45 (2004) 8443–8450. doi:10.1016/j.polymer.2004.10.001.

[32] U. Lang, E. Muller, N. Naujoks, J. Dual, Microscopical investigations of PEDOT:PSS thin films, Adv. Funct. Mater. 19 (2009) 1215–1220. doi:10.1002/adfm.200801258.

[33] L. Ouyang, C. Musumeci, M.J. Jafari, T. Ederth, O. Inganäs, Imaging the Phase Separation between PEDOT and Polyelectrolytes during Processing of Highly Conductive PEDOT:PSS Films, ACS Appl. Mater. Interfaces. 7 (2015) 19764–19773. doi:10.1021/acsami.5b05439.

[34] J. Ouyang, Solution-processed pedot:pss films with conductivities as indium tin oxide through a treatment with mild and weak organic acids, ACS Appl. Mater.

Interfaces. 5 (2013) 13082–13088. doi:10.1021/am404113n.

[35] J. Ouyang, "secondary doping" methods to significantly enhance the conductivity of PEDOT:PSS for its application as transparent electrode of optoelectronic devices, Displays. 34 (2013) 423–436. doi:10.1016/j.displa.2013.08.007.

[36] F. Jonas, POLYMERS, 39 (1994) 1345–1347.

[37] F. Jonas, Z.F. Uerdingen, B. Ag, W. Krafft, A. Ag, 100, 169-173 (1995), 173 (1995) 169–173.

[38] B.Y. Palladium, O.R. Nickel, Elsevier Sequoia S.A., Lausanne - Printed in The Netherlands, J. Organomet. Chem. 5 (1979) 121 – 145. doi:10.1016/0022-5088(68)90136-7.

[39] J. Suárez-Vargas, M. Calderón, W. Brämer-Escamilla, S. Briceño, I. Sánchez, P. Bolaño, C. Caputo, Electrical Characterization and Electrogenic Cell Stimulation Using a Conductive Polymer Composite Based on Pedot:Pss/Pva/Eg., Caracter. Eléctrica Y Estimul. Células Electrogénicas Usando El Polímero Conduct. Pedot Comb. Con PedotPss/Pva/Eg. 35 (2015) 70–77. http://search.ebscohost.com/login.aspx?direct=true&db=a9h&AN=99220797&lang=es&site=ehost-live.

[40] F. Greco, A. Zucca, S. Taccola, A. Menciassi, T. Fujie, H. Haniuda, S. Takeoka, P. Dario, V. Mattoli, Ultra-thin conductive free-standing PEDOT/PSS nanofilms, Soft Matter. 7 (2011) 10642–10650. doi:10.1039/c1sm06174g.

[41] A.A. Farah, S.A. Rutledge, A. Schaarschmidt, R. Lai, J.P. Freedman, A.S. Helmy, Conductivity enhancement of poly(3,4-ethylenedioxythiophene)- poly(styrenes ulfonate) films post-spincasting, J. Appl. Phys. 112 (2012). doi:10.1063/1.4768265

.

Chapter 5

Block copolymer self-assembly with novel solvents

Hitherto, it has been reported a systematic study concerning PEDOT:PSS and its chemical doping through sulfuric acid. This material and its perspective uses are not restricted to a specific technological field, but it can find a wide range of possible applications in the electronics. One of these, e.g. photovoltaics, can involve the doped PEDOT:PSS in the formation of heterojunction interfaces between it and nanostructured silicon surface. As an example of possible application of the developed conductive polymers, it has been studied a synthesis protocol to fabricate quasi-1D nanostructures. In this Chapter, it is presented a block copolymer self-assembly strategy by using novel deposition solvents as alternative to toluene, classically used in this process. An opportune selection made on different chemicals has led the choice on ethyl acetate and tetrahydrofuran. In these following sections, an accurate study carried by SEM analysis and images elaboration run with ImageJ program has led to promising results achieved for those polymer solutions deposited from ethyl acetate, in terms of uniformity of geometrical features, ordered areas extension and homogeneity of the pattern obtained. The following discussion thus presents ethyl acetate as a good and efficient alternative to the toluene.

5.1 – Introduction

In the last decades, the fabrication of nanostructures on metals and semiconductor have represented one of the most important aim achieved in the technology. The

surface engineering has led to the employment of new concepts, such as photonic, which requires surface template with geometrical features in the micro or nano scale. The realization of surface nanostructures can be made through two different approaches, i.e. top-down and bottom-up methods. Among these latter, there is a plethora of techniques allowing for the construction of nanostructures embedded into the substrates, usually identified with the term of holes or pores. Depending on the technique used for this purpose and the intended use of the pattern realized, the system obtained can size in different ranges of dimensions, spacing from hundreds of micrometres to few nanometres.

Block copolymer (BCP) lithography is one of the most promising and interesting for the realization of nanoholes, NHs. It is based on the self-assembly (SA) of di- or tri-block copolymers which generate a microphase separation toward well-defined and self-organized motifs. This phenomenon occurs when a suitable thermal budget is supplied to the entire system, thus promoting the chain motions for microdomains formation. The exposition to UV light and the successive development in a suitable chemical lead to porous template which acts as a soft shadow mask for dry etching. This latter transfers the template realized to the underlying substrate, usually SiO_2/Si, through a series of dry etching based on Bosch process [1]. With this procedure, a specific hexagonal array of silicon nanoholes with diameter of ≈20-30 nm and aspect ratio ≈1, are obtained [2]. The success reached by this technique in the last ten years is mainly due to its features, since it praises easiness, low cost, and suitability for the semiconductor industry [1,3]. Moreover, the appealing of this method is due to the ability of overcoming the resolution limitations of the common lithographic techniques [4]. The most used BCP-SA exploits binary species, i.e. co-polymers made with two different linear blocks, covalently bonded to each other. Whether enough mobility is

provided to both these species, e.g. suppling a suitable thermal budget, and if these two blocks manifest such a chemical incompatibility, they exhibit a de-mixing tendency. This causes a microphase separation with the appearance of domains entirely made by only one polymer block.

The driving force of the BCP SA is the minimization of the surface free energy of block copolymers [5-7]. In a BCP thin film, the total free energy F can be expressed by a phenomenological description [8-9], which can be written in the following way:

$$F = F_{mix} + F_{interface} + F_{elast}$$

In the equation above, F_{mix} represents the interaction term within polymer blocks and described by the Flory–Huggins parameter that, in its turn, can be expressed as a function of the polymerization degree and block length ratio. $F_{interface}$ determines the surface wetting forces in polymer/substrate interface and affects the orientation of the homopolymer microphase. Finally, F_{elast} describes the elastic free energy of the stretched polymer chains including their conformation [8,9]. A more detailed discussion about the first two terms of the equation above is faced up in the next sections.

5.1.1 – Blocks Compatibility and Flory-Huggins Parameter

The microphase separation occurs when the entire BCP system has enough mobility for allowing intra- and inter-chain motions. In other words, for trigging the de-mixing of polymer species, A and B, the entire system has to be in its molten state. This means that the microphase separation occurs when glass

transition temperatures of both polymer blocks are overcome, thus allowing the migration of A and B chains in their respective domains. However, the de-mixing process occurs only if a poor chemical affinity exists between the polymeric blocks. The tendency to a separation phase is estimated through the Flory-Higgins parameter [10]. It is given by the following expression:

$$\chi_{AB} = \left(\frac{Z}{k_B T}\right)\left[\varepsilon_{AB} - \frac{1}{2(\varepsilon_{AA} + \varepsilon_{BB})}\right]$$

which describes the free-energy cost for each monomer. In this definition, T and k_B are the system's temperature and Boltzmann's constant respectively, Z is the number of the monomers nearest to the copolymer cell configuration, while ε_{AB} is the interaction energy between A and B monomers. When χ_{AB} is positive, there is a strong repulsion between A and B species while, if negative, it indicates a strong driving force leading to the mixing. Apart the consideration made so far, when polymers are in their molten state, the elastic chain forces due to covalent bonds have to be taken in regard the microphase separation. Indeed, the polymer chain tends to assume an extended configuration for minimizing the unfavourable interactions between A and B. This mechanism generates a strength of "entropy restoring" that leads the polymer toward a random coil configuration, thus causing the effective separation between A and B blocks. The formation and growth of these phases can be controlled by two parameters: (1) the polymerization total grade, N, i.e. the total number of monomers into a macromolecule and (2) the polymer fraction f_A=N_A/N, where N_A is the number of monomers A per each macromolecule. When f_A=f_B=1/2, the two blocks are perfectly symmetric, and both A and B blocks organize in alternating lamella-like configuration. Differently, in

the case of a linear AB copolymer with f_A >1/2, cylindrical microdomains of B are formed into a matrix of A. This is usually obtained in the case of the PS:PMMA (70:30) block copolymer that is commonly used for the BCP-SA [3]. The highest order achievable with this polymer is a repetitive hexagonal pattern in which the fundamental unit is represented by 6+1 cylindrical domains, oriented vertically to the substrate and arranged along the six vertexes of a regular hexagon and the seventh in its centre. Whether the PMMA fraction is in 0.3-0.5 range, it would be possible to observe the formation of microdomains with different shapes, such as the gyroidal or the lamellar-porous mixed configuration.

Once established the chain composition of the block copolymer, the geometrical features are influenced by the molecular weight of the BCP. General tendency is that the higher the weight of polymer specie, the bigger the geometrical size in the pattern obtained. Aside the copolymer chemical composition, many other parameters can influence the self-assembly process.

5.1.2 – Substrate Interaction and Influence of the Film Thickness

Hitherto, it has been seen that BCP-SA and the final pattern obtained are ruled by the chemical composition, the relative blocks fraction and the length (i.e. molecular weight) of the macromolecules used. These three characteristics are the most relevant in the bulk configuration. Nevertheless, when applied in thin films, two further features play a role in the SA mechanism, such as the interaction between the block copolymer and the underlying substrate, the BCP film thickness, as well as time and temperature of the annealing. By properly changing these parameters,

different pattern can be realized, such as lamellas-like motif or cylindrical hexagonal domains.

Lamellas are easily obtained when BCP film thickness are >40 nm [11]. As an example, when PS-b-PMMA 70:30 is spun onto silicon oxide, it tends to form a sort of labyrinth of lamellas in which each polymer portion alternate parallelly to the substrate. Thin BCP films tend instead to create some micro domains in which lamellas arrange in random microdomains, surrounded by a phase in which no pattern or order can be observed.

Differently to the lamellar pattern, obtained by direct BCP deposition on the substrate and finely tuned by layer thickness, the cylindrical configuration requires further process steps. Indeed, the hexagonal pattern in which PMMA cylinders are vertically aligned to the substrate and surrounded by a matrix of PS, can be obtained only by a preliminary neutralization step of the underlying substrate. This is required since the pattern formation is highly influenced by the wettability between polymers and surface, i.e. $F_{interface}$ term. In fact, whether one of the two blocks has a better chemical affinity with the surface, it tends to preferably interact with the substrate, leading to alternating, parallel lamellas [12]. For realizing the cylindrical configuration, a random copolymer (RCP) film, having the same chemical composition of the BCP used for SA, has to be preliminary deposited onto the substrate. This process step is called “neutralization” and minimizes the effect due to the surface interaction by excluding the free energy contribution of the polymer/substrate interface. Mansky et al. [13] have reported that the surface neutralization is obtained by depositing an OH-ended PS-random-PMMA synthesized through radical living polymerization from by (2,2,6,6-Tetramethylpiperidin-1-yl) oxyl, TEMPO. The hydroxyl group is needed for grafting random PS-PMMA polymer to an OH- terminated silicon oxide substrate.

Weak interactions, i.e. hydrogen bonds, between random copolymer and substrate leaves a thin layer of buffer film which thus isolates the following block copolymer film. This suppress the influence due to the silicon oxide and allows the correct orientation to the vertical cylindrical pattern of PMMA into the styrenic matrix.

The PS content in the random copolymer has also a certain influence on the arrangement obtained on the PS-b-PMMA deposited on it. Indeed, when the styrenic fraction in the random copolymer chains is less than 48%, the microdomains obtained in the overlying layer are parallel to the substrate, similarly to a lamellar configuration. Instead, when the buffer film is deposited from a random co-polymer which contains at least 64% of PS, microdomains spontaneously orients vertically to the substrate, thus creating the PMMA cylinders embedded in the PS matrix [8,13]. Recently, Braessat at al. [9] have demonstrated that the surface neutralization step can be skipped if the silicon oxide substrate is replaced by titanium dioxide or gold, thus modifying the surface polarity.

Whatever the substrate used, once that interfacial tension between the two polymer blocks and the surface has been compromised, the hexagonal template can be influenced by the film thickness, *t*. When block copolymer used has a composition 70:30 PS:PMMA, with average pores diameter of 18 nm and centre-centre distance of 36 nm, there is only a window of BCP film thickness, between 18 and 42 nm, in which the regular hexagonal pattern formation is observed. Instead, out of this range, too thin films lead to a broad distribution in terms of dimensions and average distance, thus returning a pattern with poor order. Vice versa, too thick films, form holes with elongated 2D shape and the system tends to the lamella-like configuration, at most [14]. This discussion is efficiently summarized in the Fig. 5.1.

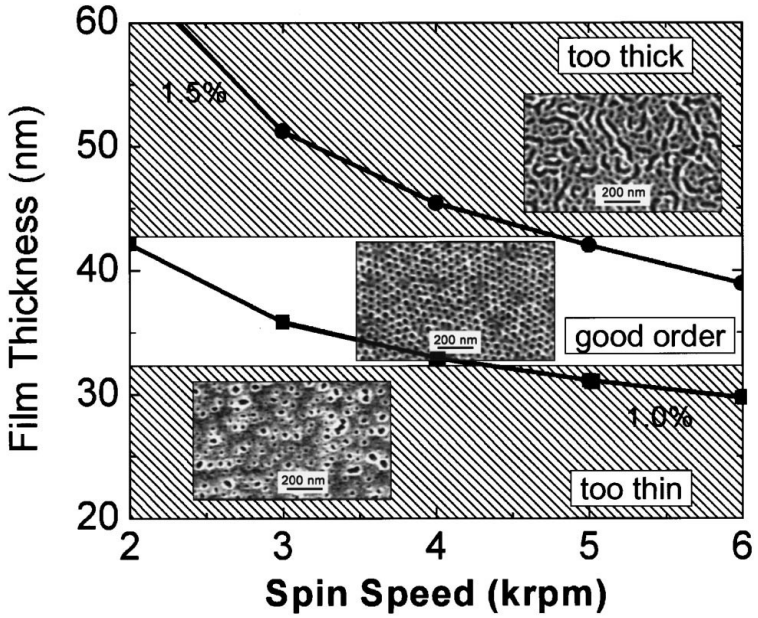

Fig. 5.1: Ellipsometric film thickness as a function of the deposition spin speed and different concentration solutions of PS-PMMA di-block copolymer (*Mn* 567 000 g/mol) diluted in toluene (percent by weight). Shaded regions indicate where film is too thin or too thick to achieve proper ordering of the polymer block domains. SEM images superimposed on the graph show representative film morphologies (after exposure and development) for the different film thicknesses. Image reprinted from Ref. [12].

5.1.3 – Influence of Annealing and Solvent Evaporation on BCP

Thermal treatment of the BCP layer is the fundamental stride to allow for BCP-SA, since it supplies enough energy for promoting the chain motions and the microphase separation. This concept requires that both blocks have to be in their molten state, i.e. over their glass transition temperatures. Then, the effective annealing conditions, in terms of temperature and duration, can influence the BCP pattern. As an example, when the annealing is performed at 160°C, the order of

pattern and film uniformity tend to improve with increasing the duration of the thermal treatment [12], as reported in Fig. 5.2.

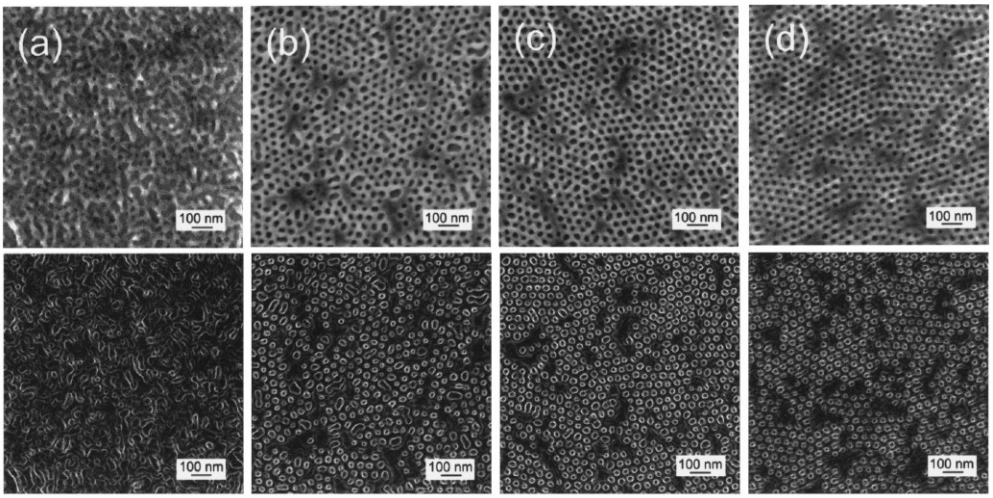

Fig. 5.2: SEM micrographs of exposed and developed PS template for different annealing times. Each sample was annealed undisturbed at 160 °C in vacuum for total time of a) 3.5 h, b) 6 h, c) 15 h, and d) 34 h. Lower images have been filtered to enhance edges. Image reprinted from Ref. [12].

When the annealing is performed at a fixed time, a template with a superior order is obtained with at 180°C instead 160°C [14]. This result is due to a higher mobility of the co-polymer chains achieved at higher temperature, which drives the pattern toward the most stable configuration. Nevertheless, this tendency has not a linear trend-dependence on the temperature. In fact, annealing performed at 200°C leads abruptly to a less ordered array than the expected one, suggesting that 180°C is the limit temperature for achieving the highest packaging and ordered template before a thermal degradation of the polymers.

Aside the specific influence given by the annealing conditions, some authors have also found that the vertical orientation of the cylinders can be also controlled by an external field force, such as that one supplied by the solvent evaporation [15]. In-solution copolymers are in a swollen state in which the solvent mediates the non-favourable interactions between the two blocks in the co-polymeric chain. When BCP solution is spun on a substrate, solvent starts to evaporate from the free surface of the polymeric layer and the mediation of non-favourable interactions between the two blocks in the chain does not occur anymore, thus causing the phase separation. This process results in the exclusion of one polymeric block from the other, forming domains of the minor quantity polymer into a matrix of the major one. In this specific case, the gradual solvent evaporation is the driving force which gradually transfers the free surface order to the entire depth of the polymeric film.

5.2 – Motivations

The parameters which influence the formation of nanopatterns from the block copolymer self-assembly are manifold. Apart the characteristic features of both random and block copolymers used, such as molecular weight and composition, film thickness and heating conditions also can play a crucial role. Hitherto, it has been seen that the optimization of these control-parameters leads to the formation of patterns, specific features. Many works in literature aimed for the obtainment of long-range ordered pattern by changing the polymer composition, substrates and annealing conditions [11,16–18]. Differently, the purpose of this work is related to the effects of the solvent substitution. As it was previously mentioned, the various steps which leads to the SA mechanism involve a routine of spin coating deposition

of RCP and BCP solutions and thermal treatments. Hitherto, toluene is the only solvent used for performing BCP lithography with PS-b-PMMA and it leads to excellent results, in terms of order and geometrical features. Indeed, its chemical and physical features well fit with both random and block PS-PMMA copolymers, such as its volatility and the effective solvent-power of both polymer species.

Nevertheless, some of its intrinsic characteristics do not match with the increasing tendency of many electronic industries to use chemicals with limited toxicity, low health/environmental risk and reduced hazard due to chemical wastes. Indeed, toluene is catalogued as mutagen and cannot satisfy eco-friendly requirements, thus limiting an industrial cost-effective scale-up of the BCP lithography. Moreover, the high hygroscopicity of toluene needs to adopt some specific precautions for not affecting the results.

In order to meet the new industrial protocols and overcome these technological issues and increase the knowledge about the kinetics and the mechanism which rule BCP-SA, the aim of this work was the replacement of the toluene with some novel chemicals. Some preliminary results were already reported in previous work, where acetone was used as alternative to toluene for depositing BCP films, showing the real possibility to obtain the BCP ordering with solvents different from toluene [1]. Moreover, the self-assembling kinetics with novel chemicals are not presently known in literature Criteria for choosing the substitutional solvents were based on the relative eco/operator-compatibility, industrial protocols affinity and appropriate physical characteristics, such as volatility, polarity and hygroscopicity. Based on these requirements, the survey has led the choice to ethyl acetate (Et. Ac.) and tetrahydrofuran (THF). The long-term aim is the entire replacement of the toluene in all steps of BCP-SA procedure, thus producing both the initial RCP solution and BCP one. Nevertheless, seen the complexity of the whole process, a step-by-step strategy was planned. For this reason, , the work is focused on the solubilization of

PS-b-PMMA in ethyl acetate and THF and its effects on the BCP self-assembling mechanisms, while RCP deposition was carried out from toluene in each case. Therefore, for the first time a systematic study on the BCP-SA realized with novel solvents as alternative to toluene was run. The scope of this work was to identify the kinetics aspects due to the evaporation of the deposition solvents and their characteristics on the BCP pattern formation. The effects due to the new solvents were investigated also as a function of the different BCP film thickness. A detailed description of the procedure adopted is discussed, while the characterization of the BCP films were carried through scanning electron microscopy. Images and data elaboration about the geometrical features of the templates obtained were acquired by Scanning electron Microscopy (SEM) and analysed by suitable software and protocols set up to appropriately convert the grey scale microscopy images to black and white ones. Our results have shown the real possibility to replace toluene with other solvents. In particular, ethyl acetate gave very promising results in term of homogeneity of the pattern obtained and extension of the ordered area. This paves the way for further investigation, giving new clues and ideas for future research in the BCP-SA field, as well as opening the way to a real industrial exploitation.

5.3 – Sample Preparation

BCP patterns were obtained by di-block copolymer PS-b-PMMA, M_n=67 kg/mol with PS fraction of 70% and polydispersity of 1.1, while random copolymer PS-r-PMMA, OH-terminated, with a PS fraction 62% and M_n=5.3 kg/mol was used for substrate neutralization. Both polymers were purchased as powders from Polymer Source Inc. Solutions with about 1% wt. concentration were prepared by dissolving polymer powders in the investigated solvents. For the purpose of this work, four

months-aged toluene, ethyl acetate and tetrahydrofuran (Sigma Aldrich), respectively, were used. Each dispersion was kept under a gentle stirring at room temperature for about 24h before use. This strategy ensures the perfect dissolution and homogenization of the solutions prepared. Substrates used for preparing copolymer films were square c-Si <100> samples of 1 cm side covered with a stoichiometric oxide of 20 nm, grown by rapid thermal annealing. Before use, silicon supports were cleaned by sonication in acetone, isopropyl alcohol and deionized water for 5 minutes each and finally dried under nitrogen flow. Random copolymer solution with a concentration of 1.5% wt. in toluene was kept under gentle stirring for 30 minutes before each deposition and then spun onto SiO_2 substrates for 60 seconds, obtaining polymer film thickness of about hundred nanometres, measured by ellipsometry. Films were thermally treated in vacuum chamber (0.01 mbar) at 140°C for 48h. During this annealing step, a complete removal of the solvent and the establishment of weak interaction forces between OH-terminated RCP and the SiO_2 substrate occur. At the end of this step, a grafted layer of PS-r-PMMA layer adheres to the SiO_2. The excess of the unreacted polymer is removed by immersing samples into pure toluene and left under a gentle stirring for 30 minutes and finally dried under nitrogen flow. This process leaves a very thin film of ≈3-4 nm of grafted random copolymer [19,20]. BCP solutions were thus deposited by 60 seconds spin coating on neutralized surfaces. Three solutions were prepared by dissolving PS-b-PMMA in four-months aged toluene, used ad reference, ethyl acetate (Et. Ac.), and tethrahydronfuran (THF), and keeping them under stirring for 30 minutes at room temperature before each deposition. Solution concentrations were around 1% wt. and carefully chosen in each case according to calibration curves previously obtained by ellipsometer film thickness measurements. Samples were prepared by depositing toluene, Ac. Et. And THF solutions through spin coating at different speeds, obtaining a final

thickness 27-29, 30-32 and 34-35 nm respectively. Samples were finally annealed in vacuum chamber (0.01 mbar as regime pressure), at 180°C for 2h. During this thermal treatment, self-assembly between the styrenic and acrylic part occurs, pushed by both the solvent evaporation and the thermal budget which supplies the needed force for generating the segregation phase. In order to allow this process, polymer chains require high mobility into the film for achieving reptation modes motion. For this reason, the BCP annealing temperature, 180°C, is chosen for overcoming the glass transition temperature (T_g) of both polymer blocks i.e. 95°C of polystyrene and 105°C for polymethylacrylate, thus ensuring the chains motion and avoiding at the same time the thermal degradation of both PS and PMMA. After thermal treatment, samples are exposed to UV-lamp with source 254 nm for 20 minutes for allowing the reticulation of PS chains and light-degradation of the acrylate ones. Samples are developed by rinsing in a degassed glacial acetic acid, for removing the degraded PMMA parts, leaving a styrenic cross-liked network, which was finally washed in deionized water and dried under nitrogen flow.

5.4 – Results and Discussion

As seen previously, since the self-assembly of block copolymers is influenced by different parameters, including the thickness films described hereinafter were prepared with three different thicknesses of the PS-b-PMMA layer, 29-27, 32-30 and 34-35 nm respectively. Characterizations were prevalently based on SEM analysis. For a wider vision of the results obtained, SEM images with different magnification will be supplied in the next sections. Finally, results obtained with the new solvents used will be compared by a statistical survey of the features obtained.

5.4.1 – Effects Due to Thickness and Solvent

The aim of this study was to verify if a solvent, different from toluene, can allow the self-assembly of block polymer. BCP films obtained by the standard polymer solution in aged-toluene were used as reference. Fig. 5.3 shows in-plane SEM images for samples deposited from toluene solution and with three different thickness, 35, 32 and 29 nm (± 1 nm) in Fig. 5.3a, b and c respectively. SEM Images show that for higher film thicknesses, two phases coexist in the same film, one identified as lamellar and the second in which nanopores are formed. Fig. 5.3a shows that lamella do not follow a preferential orientation into the film and the space between one of this and its neighbours is quite constant, estimating the centre-centre lamellas distance to be around 42 ± 2 nm. Vice versa, in those areas in which pores are the main features, neither a regular shape nor a defined size are observed. Some small pores, with circular shape and diameters ranging between 10 and 20 nm can be observed, but in the case of bigger species, ellipse-like shapes are sometimes distinguished with size of about 40 and 20 nm, depending on the axis measured. These elliptical pores are usually obtained by the collapse of two or more near pores. In this case, edge-edge distance is hard to be established because of the non-well defined form of the pores. Some of these considerations can be applied for sample reported in Fig. 5.3b. Again, both lamellas and pores can be distinguished, but the area occupied by the first ones slightly decreases in favour of the seconds. In some regions, lamellas vanish turning to circle-like shape, achieving undefined silhouettes. In Fig. 5.3c, finally, no lamellas are still present on the sample surface, which this time shows only pores.

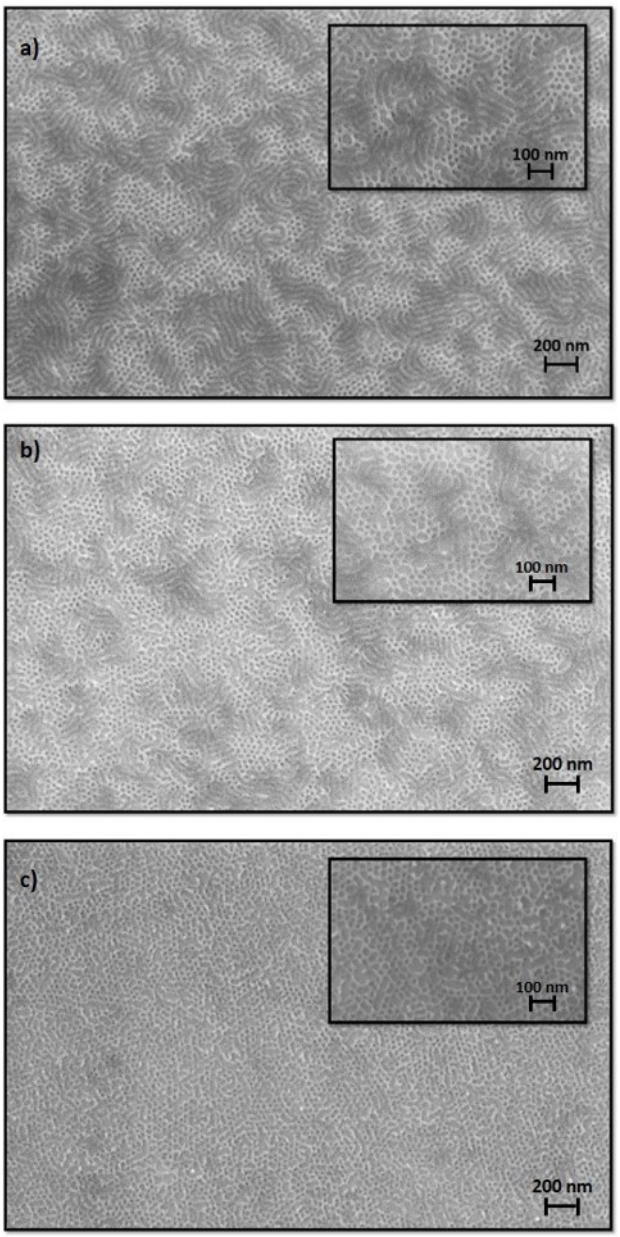

Fig. 5.3: In plane SEM images acquired on BCP samples prepared from the same PS-b-PMMA toluene solution. Three samples reported in the picture have a thickness of a) 35, b) 32 and c) 29 nm, respectively.

Once again, these do not have regular feature in size and shape and regular domains with a hexagonal pore-packaging are observed only occasionally. As expected, the film thickness clearly influences the pattern obtained. According to the literature [19.20], for higher film thickness, lamellas-like pattern prevail on other shape, while pores are the preponderant specie in the case of thinner films. In Fig. 5.3a and b, these pattern both coexist, probably because of a borderline region of film depth in which a real distinction of the two species obtained cannot be observed [18]. The pores obtained on the 29 nm-thick sample do not represent an optimal condition since the ordered pattern is not achieved anyway. Indeed, the window thickness in which films are formed is very narrow and do not allow the achievement of the right condition for establishing the hexagonal pattern formation. The same routine discussed so far was replicated for three different film thickness, again 35, 32 and 29 nm each (error bar ± 1 nm), obtained from a solution of PS-b-PMMA in ethyl acetate. The SEM analysis results are shown in Fig. 5.4. Very similarly to the toluene case, the films obtained from ethyl acetate show the coexistence of both lamellas and pores arrangement for thickness of 35 and 32 nm, while the thinnest film, i.e. 29 nm, shows only the pore-like features. In this latter, both phases appear to have more regular shape and repetitiveness as well as 35 nm-thick film shows some areas with highly ordered pores pattern, regular shape and diameter, defined edge-edge distances and ordered hexagonal pattern. These ordered regions are separated from the lamellas by a sort of border area in which some pores with no order are formed, as shown in Fig. 5.4a. Lamellas are prevalently formed very close to round polymer particles deposited onto the film and characterized with high brightness in Fig. 5.4b. This somehow justify the existence of both phases in these samples. About this, it is supposed that residual polymeric particles, not perfectly solubilized in the solvent used, are dragged onto the solid-state film deposited.

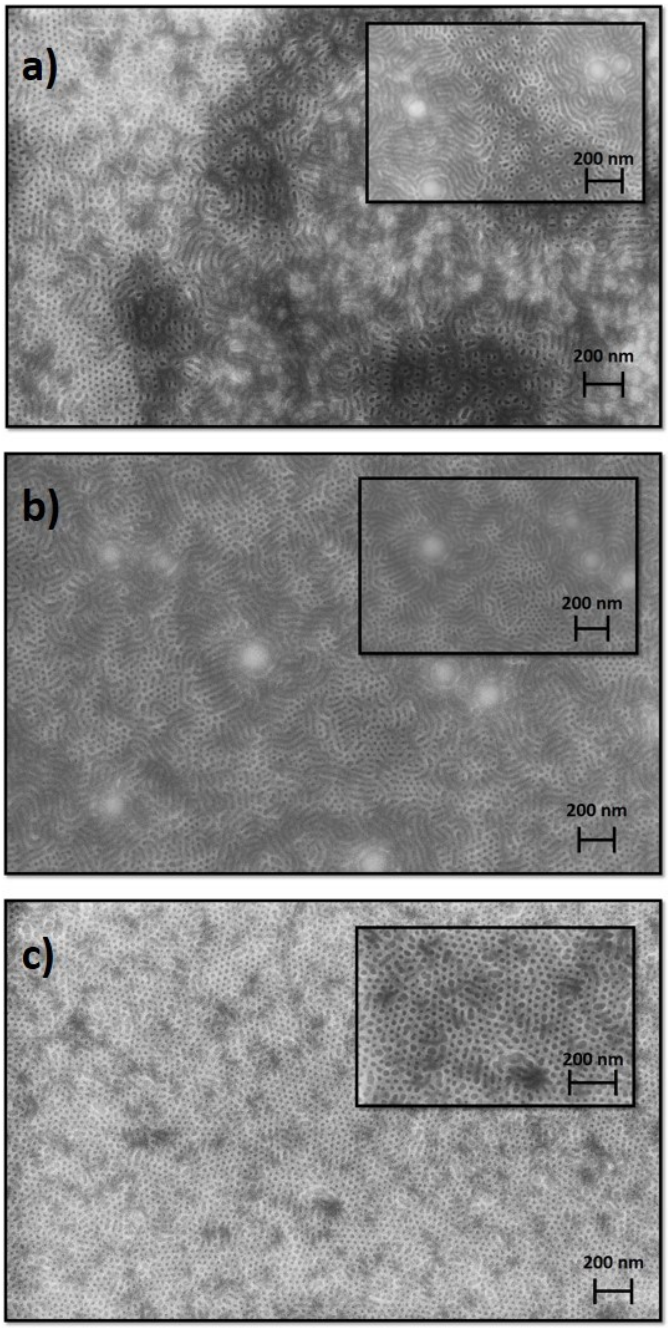

Fig. 5.4: In-plane SEM images acquired on BCP samples prepared from the same PS-b-PMMA ethyl acetate solution. Film thickness are a) 35, b) 32 and c) 29 nm, respectively.

This creates some local thickness variation causing a slight slop from the particle down the flatten polymer PS film. Therefore, it assists to a gradual phase change, passing from lamellar arrangement in those zones in which thickness is higher, i.e. very close to particles, to porous features where the layer is thinner. For this reason, and also because of the average thickness reached, no phase prevails.

A more interesting result is instead achieved for 29 nm-thick sample, Fig. 5.4c. In this last case, only nanoholes are present along the entire film obtained, while lamellas totally disappear. This result is in perfect agreement to what already seen previously for BCP toluene solution and what expected from the thickness-dependence of the pattern [19,20]. Surprisingly, pores with a more regular size and edge-edge distance, arranged in a hexagonal pattern, are obtained, thus achieving a better result than that obtained with toluene solution. For understanding this assertion, the planar SEM images obtained on 29 nm-thick samples deposited from toluene and ethyl acetate are reported, in Fig. 5.5a and b respectively.

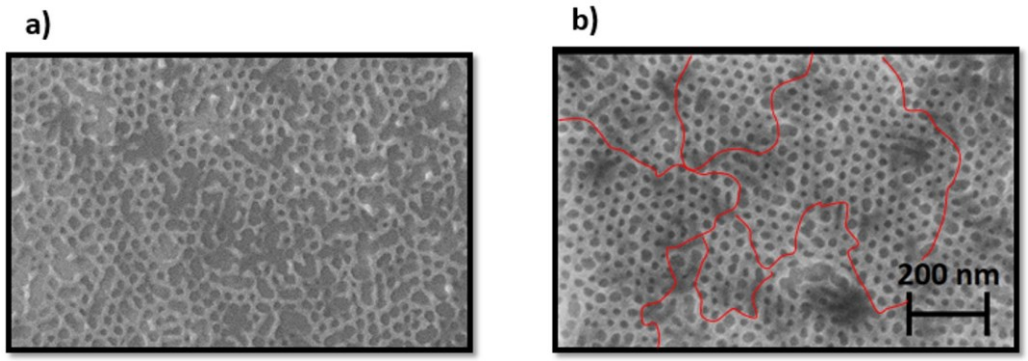

Fig. 5.5: Direct qualitative comparison between 29 nm-thick porous PS films obtained with depositing PS-b-PMMA from 1% wt. solution of a) toluene and b) ethyl acetate. In this figures, red lines roughly demarcate zones of film in which the hexagonal arrangement is recognized.

Same experiments were finally replicated with PS-b-PMMA dispersed in THF with concentration 1% wt. For three samples prepared, film thicknesses reached are 34, 30 and 27 nm (error bar ± 1 nm) respectively. The results obtained are quite different with respect to those discussed so far. Fig. 5.6 shows SEM image of 34 nm-thick film deposited from THF. An overview of the sample, Fig. 5.6a, shows an uneven surface, characterized by very large deposits with lighter brightness, surrounded by dark zones. Using higher magnification, Fig. 5.6b, bright areas are revealed to be polymer agglomerates with undefined shape, while regions of the film with dark contrast show the pores formation.

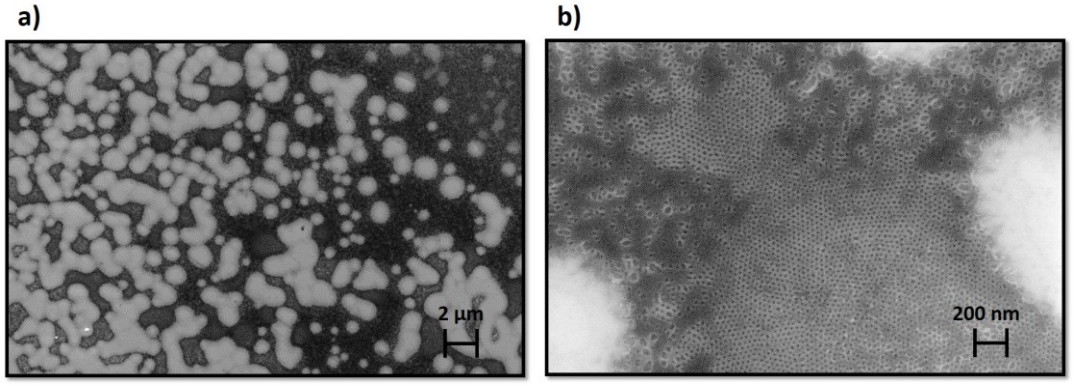

Fig. 5.6: PS-b-PMMA film obtained from 1% wt. THF solution and final thickness of 34 nm. a) in-plane SEM image of the film obtained at low magnification; b) SEM acquired at magnification with 100k.

This time, no lamella-like arrangement is detected on the film surface, while two different porous patterns are recognizable. Fig. 5.7 shows more in detail these arrangements. Fig. 5.7a shows large areas with pores having no regular shape and randomly positioned between each other. In these areas, some small islands with a more ordered package are revealed, as shown in Fig. 5.7b.

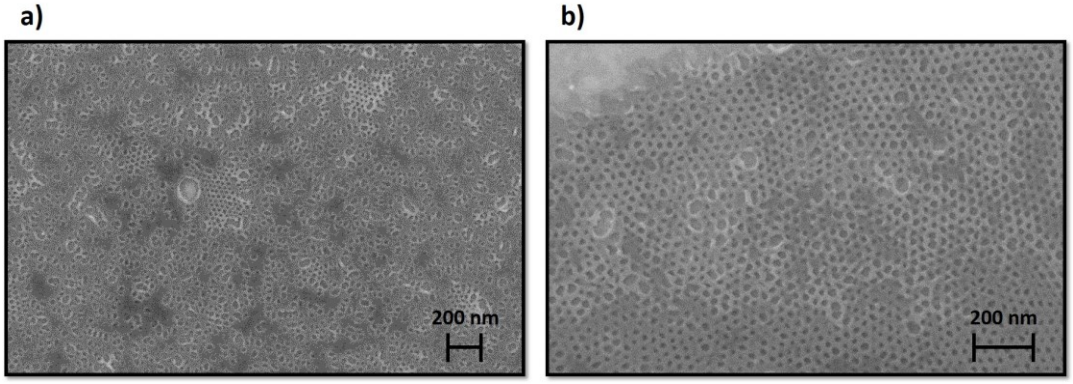

Fig. 5.7: PS-b-PMMA film obtained from 1% wt. THF solution and final thickness of 34 nm. In-plane SEM image acquired with magnification of a) 100k and b) 200k.

As previously reported, small film thickness variations influence the pattern formation, but here the transition is not enough for causing a phase permutation and only leads to more regular pores. Fig. 5.8 shows a rough demarcation of these areas in which small thickness variations manifest. Red area represents a large bright agglomerate on the film thickness that, as asserted before, corresponds to a polymer agglomerate. In this region, the material accumulation does not lead to any pattern formation. Green area corresponds instead to a sort of transition region, having a thickness lower than the previous but higher than the successive one. Here pore formation starts to be recognizable, showing some ordered domains with the hexagonal holes-packaging, occasionally interrupted from larger porous. As mentioned before, these are caused by the collapse of two or more neighbour holes.

Fig. 5.8: replication of Fig. 5.5b in false colours, evidencing three different areas: red as a polymer agglomerate, green as a portion with middle order and blue with regular pore formation.

Finally, blue domain in Fig. 5.8 corresponds to a thinner portion of the PS porous film, in which higher order in term of holes size, reciprocal distance and hexagonal arrangement are distinguished. Interestingly, pore order does not enhance when thinner PS-b-PMMA films are obtained. Fig. 5.9a and b report respectively SEM images of film thickness of 30 and 27 nm respectively. As seen in the previous case, very large bright polymer agglomerates with lateral size of the order micrometres are easily recognizable. These are surrounded by a sort of concentric areas in which probably thickness decreases by enhancing the distance from the agglomerate. When a suitable layer depth is reached, pore formation is observed for both film thickness, but no defined geometrical features and total absence of a regular arrangement are evidenced. Moreover, pore density slightly decreases for the thinnest film prepared. This effect is probably attributed to an anomalous solvent retention.

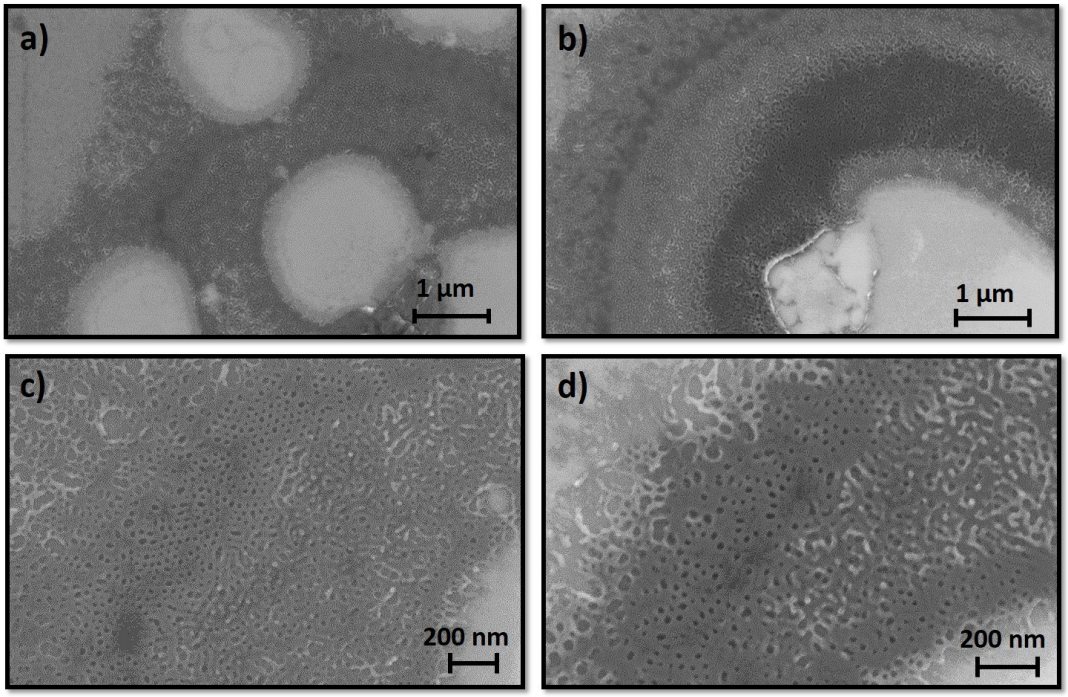

Fig. 5.9: SEM images of films deposited from THF solution with thickness of 30 and 27 nm. Figures a) and b) correspond respectively to layer of 30 and 27 nm, acquired both at a magnification of 50k; c) is a magnification of 100k of a region reported in a), while d) in a 150k magnification of 27 nm-thick film in b).

Hitherto, it has been seen a qualitative analysis of films obtained from PS-b-PMMA dispersed in three different solvents, toluene, ethyl acetate and THF. Now, the aim is to quantitatively relate the solvent effect to the porous pattern formation. In particular, a direct comparison between the two new solvents used for SA, ethyl acetate and THF, is required to better understand the effects and role played by the deposition solvent.

In order to start a statistical analysis on the samples discussed so far, for each solvent used, those ones which have shown an ordered-pattern were selected. For this purpose, in the case of the copolymers deposited from ethyl acetate, 32 and 29

nm-thick films were selected, while for those prepared from THF solution, polymer layers with thickness of 34 ad 30 nm were chosen.

In the following discussion, a statistical analysis won't be carried for polymer film thickness obtained with toluene. For results about statistical features obtained according with a more classical procedure, it is referred to discussions reported elsewhere [18-20].

5.4.2 – Statistical Survey of Morphological Parameters

The effects on the pattern obtained by the BCP self-assembly from both ethyl acetate and THF used as solvents of deposition were studied by a statistical survey. This was carried through the analysis of pore diameter and circularity expressed as a function of the film thickness obtained and the solvent used. The analysis of both these features is done via a routine carried by an open source program for scientific multidimensional images, Imagej. After choosing a SEM image of a given sample, a wide square area is selected from it, on which Fast Fourier Transform (FFT) is calculated. Some specific filters are applied on the FFT image in order to partly suppress the noise, thus returning a clearer image. This is obtained by re-transforming the FFT filter image and passing back from frequencies to space domain. The intensity distribution of pixels composing the image under study is calculated by selecting a suitable threshold. All intensities lower this limit value are posed equal to 0, while all higher values correspond to the unity. In this way, it is possible to convert the image from grey-scale to binary, in which pixel under threshold are black and while those higher are depicted white. In binary image obtained with this routine, black areas correspond to the holes in the original image, while white background is related to the PS network. Once obtained the

binary image, the statistical analysis can start. The routine explained so far is summarized in the Fig. 5.10.

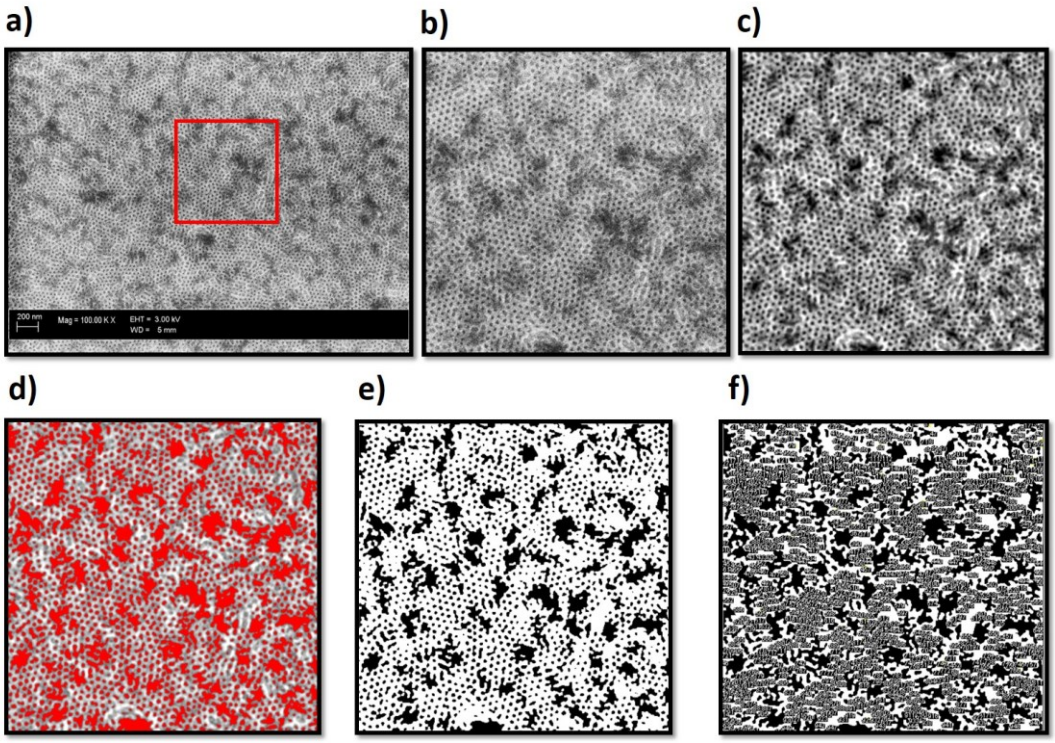

Fig. 5.10: Example of the routine used in ImageJ for carrying the statistical survey on morphological features: a) on the original SEM image, a square and representative area is selected in which b) contrast and brightness are opportunely adjusted and balanced; c) a suitable filter is applied on the FFT image, thus returning a reverse FFT figure which has less background noise; d) pixel intensity threshold is established for selecting only those portions of the image which corresponds to porous zones. These are then converted in the binary image shown in e); f) finally, by imposing a suitable shape/size filter, count of porous with on the specification of their roundness and dimension are performed, with excluding those areas without any pattern revealed.

From this analysis it is possible to obtain the pores number within the selected area, also measuring their relative surface and circularity (which corresponds to

$4\pi \cdot \text{area/perimeter}^2$). The pore diameter from each area is calculated and once normalized for the sample area under investigation, returning the distribution curve. With this strategy, it is also possible to calculate both the integral density, expressed as number of pores per square centimetre, i.e. $n°/cm^2$, and the average centre-centre (c-c) distance for each analysed image. Table 1 summarizes the results obtained in terms of pores density and c-c distance as a function of the solvent used and relative film thickness explored.

Solvent	*Film Thickness (nm)*	*Pores density ($n°/cm^2$)*	*c-c pores distance (nm)*
Ethyl acetate	29 ± 2	7.1×10^{10}	43 ± 2
	32 ± 2	4.3×10^{10}	44 ± 2
Tetrahydrofuran	34 ± 2	6.7×10^{10}	42 ± 2
	30 ± 2	3.9×10^{10}	44 ± 2

Table 5.1: summary of the most important morphological features for each solvent used and as a function of the film thickness investigated.

From Table 1, it is possible to note a different behaviour with changing the deposition solvent. Indeed, the nanopores density decreases with increasing the BCP film thickness obtained from ethyl acetate, while an opposite trend is observed in the case of films deposited from THF. Moreover, a similar trend, for both of deposition solvent, is also observed for the variation of the c-c distance, which slightly enhances with increasing the film thickness, still remaining within its error bar. In Fig. 5.11, for samples obtained both with ethyl acetate and THF,

the pores fraction having a certain diameter, *d*, is reported with respect to the total pores density, thus obtaining the pores diameter distribution curve for each solvent. In this case, diameter interval range are analysed each two nanometres up to the highest value of 58 nm. This threshold was chosen since no pores with larger diameter were detected.

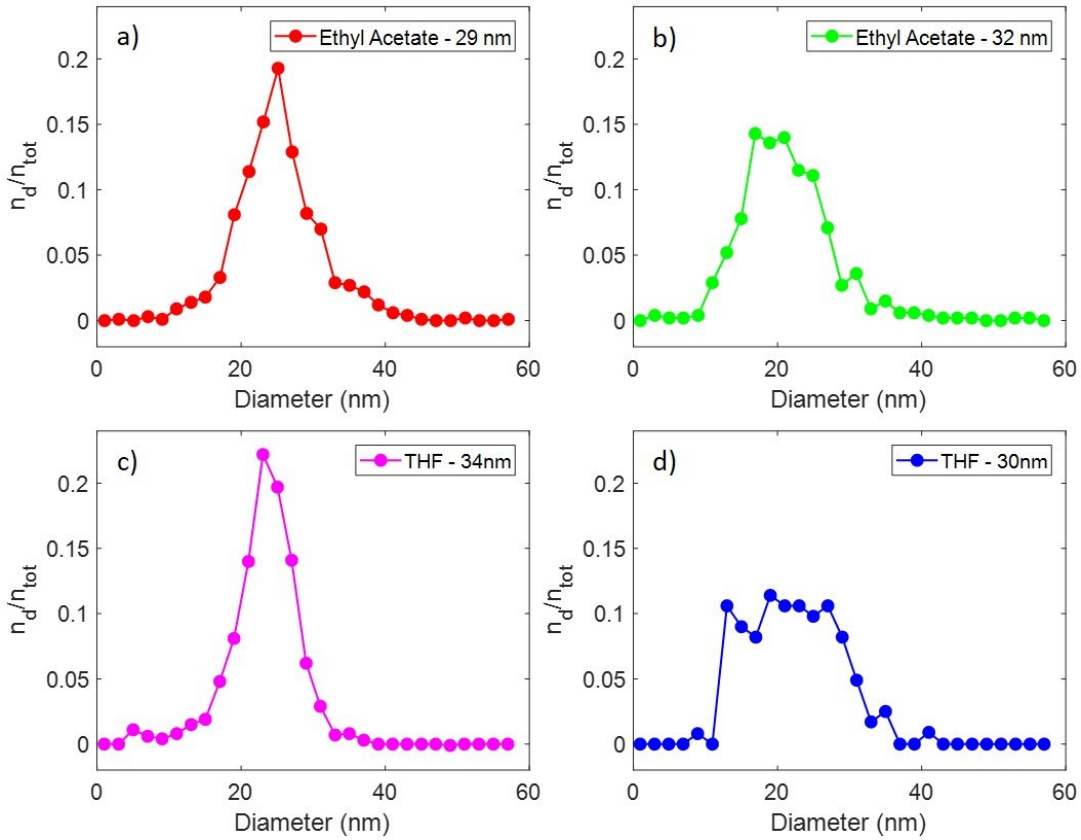

Fig. 5.11: Pores diameter distribution normalized for the area under study; n_d/n_{tot} represents the number of elements having diameter d with respect to the integral density n_{tot}. a) and b) distribution curves of BCP samples obtained from ethyl acetate solution and with thickness 29 and 32 nm respectively. c) and d) distribution curves of BCP samples deposited from THF solution and with thickness 34 and 30 nm respectively.

Copolymer film deposited from ethyl acetate and with thickness of 29 nm is reported in Fig. 5.11a, showing a narrow distribution curve centred at 25 nm, while 32 nm-thick film obtained from the same solution, Fig. 5.11b, shows a broader curve with maxima placed within 18 and 22 nm. Fig. 5.11c and d show diameter distribution curves for BCP films deposited from THF and with thickness of 34 and 30 nm respectively. Analogously to what observed in the previous case, thicker sample shows a narrow peak at 22 nm, while a broader curve is obtained for 30 nm-thick BCP film, with maxima ranging between 18 and 30 nm. As reported in the previous section, this trend is due to a significant lack of uniformity in the nanopores distribution, thus indicating that the self-assembly process on these samples is more defective. As a general consideration, fraction of nanopores having the same diameter never overcomes 25% and this result does not depend on the sample thickness investigated.

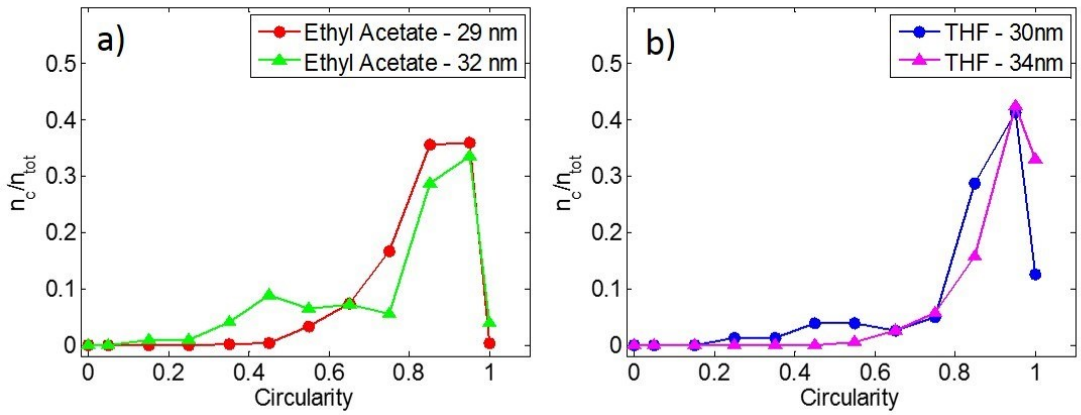

Fig. 5.12: Distribution comparison of pores circularity for ethyl acetate and THF. In each graph it is reported the fraction n_c/n_{tot} of elements with a given circularity with respect to the total number of elements present in the investigated area. a) Distribution curves of BCP samples obtained from ethyl acetate with sample thickness of 29 and 32 nm and b) distribution cure of 34 and 30 nm-thick films deposited from THF.

Fig. 5.12 reports the nanopores circularity distribution for both solvents used. Fig. 5.12a shows that, for both films deposited from ethyl acetate, circularity trends are quite similar, and both achieve their higher values in a range of 0.85-0.95, indicating that this feature is not affected from the film thickness. Moreover, in the case of 29nm-thick film, no pore with a circularity lower than 0.5 is revealed while for film thickness of 32 nm a very small fraction of nanostructures with circularity even lower than 0.35 is found. This means that the thicker sample obtained from ethyl acetate solution has a major content of pores with both irregular shape and dimensions, caused by the presence of collapsed holes. A better trend is instead detected for 29 nm-thick BCP sample, since this exhibits a more uniform and regular morphology. Fig. 5.12b shows circularity distribution calculated for BCP samples deposited from THF. In this case, both samples show a quite similar distribution, peaked around 0.95, and the presence of pores which reach the circularity unit. This indicates the presence of perfect round shape objects, with a higher density than those obtained from the ethyl acetate. From these calculations, it is possible to deduce that circularity distributions have a dependence with the solvent used, but it is not affected by the film thickness. In Fig. 5.13, both pores diameter and circularity distributions are compared for the best representative film obtained from ethyl acetate and THF deposition, i.e. 29 nm in the first case and 34 nm in the latter.

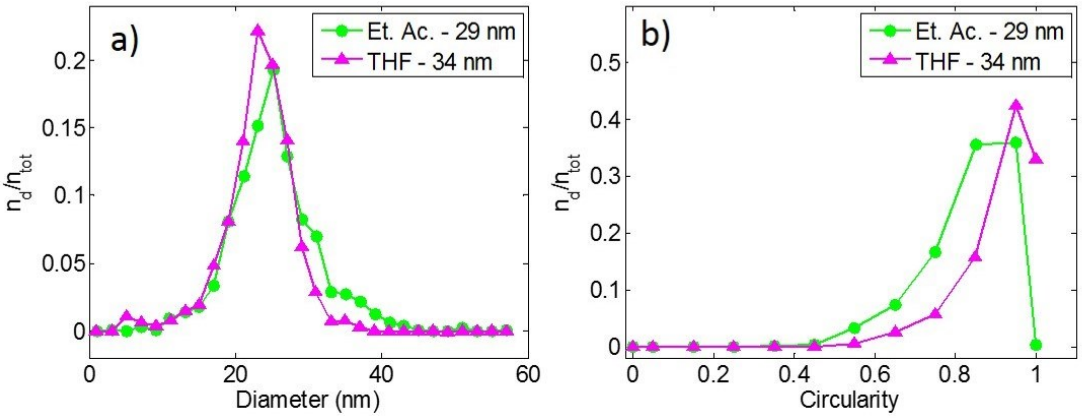

Fig. 5.13: Comparison of distribution graphs of a) pores diameter and b) circularity.

The trend of diameter distributions for both solvents show a certain similarity, with curves peaked at slightly different values, i.e. 25 nm in the case of ethyl acetate and 22 nm for THF, Fig. 5.13a. Instead, circularity trends are overlapped in the two cases up to 0.45 while, above this value, curves show a different behaviour, with ethyl acetate manifesting higher pore density with respect to THF for the same circularity value. These results indicate that samples obtained from THF solution exhibit a major regularity in term of roundness, while in the case of ethyl acetate pores manifest a more irregular silhouette. However, as seen in the previous section, while the 34 nm-thick sample obtained from ethyl acetate shows the nanopattern formation onto a wide area, films prepared by the THF solution have very ordered islands surrounded by random regions or deposits of polymer particles. For this reason, in order to understand which solvent gives the best performance in term of ordered pattern obtained, it is required to estimate the percentage area of each sample which exhibit a certain regular arrangement of porous pattern formation. The histograms in Fig. 5.14 reports the % ordered area for each solvent and thickness investigated. As somehow predicted with observing

the SEM analysis in the previous section, BCP films obtained by ethyl acetate exhibit an ordered pattern on a much wider areas with respect to samples prepared from THF dispersion.

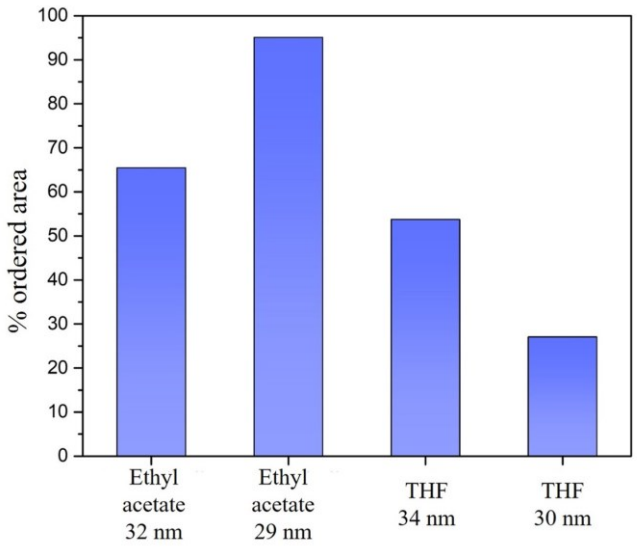

Fig. 5.14: Histograms showing the percentage of ordered area for each solvent investigated.

Indeed, while ordered areas reach 95% for 29 nm-thick sample deposited from ethyl acetate, THF does not overcome 53% for the thickest sample prepared. Therefore, even if this latter solvent has led to pores with better geometrical features, has to be taken in regard that this effect was obtained only in very small regions with respect to the lateral dimension of the substrate.

Considering the integral density calculated for each sample, a better diameter distribution for each solvent is obtained for those samples with a higher integral density. This consideration indicates that the solvent effectively plays a role in the BCP self-assembly. In particular, some physical features, such as boiling point

(b.p.) and volatility, are a crucial aspect in this process and these parameters have been considered for both ethyl acetate and THF. The first one has a p.b. or around 77°C and a vapour tension of 9700 Pa at 293 K, while THF exhibits a b.p. of 66°C with a vapour tension of 17300 Pa. It means that, in the same conditions of external pressure and temperature, ethyl acetate has slower evaporation rate with respect to THF. Seen the low boiling points for both the solvents used, it is possible to suppose that the major amount evaporates from the film during the spin coating deposition. However, in the case of a more volatile solvent, this process is faster. Too fast solvent removal from films affect the pattern formation, since in this case solvent leaves the film before that polymer solution is uniformly spread on the substrate with the rotation imprinted from the spinning. This causes a non-uniform solvent evaporation which leads to local material concentration and thus changes the film thickness underlying. Moreover, also the solvent power has such an influence on the uniformity film thickness since, in the case of THF, insolubilized polymer particles, then deposited onto the solid film, cause some variation in layer depth, thus compromising the arrangement of nanostructures obtained. These drawbacks are overcome with the use of ethyl acetate which, having a less volatility and a superior solvent power with respect to THF, firstly solubilizes better the copolymer chains and secondly gives place to a more uniform evaporation along the film surface, thus leading to a better arrangement reported on a broader substrate's area.

5.5 – Conclusions

In this Chapter, it has been demonstrated the possibility to efficiently replace the traditional BCP-SA solvent, toluene, with chemicals such as ethyl acetate and THF.

This important result can lay the fundamentals for the substitution of toluene in the block copolymer lithography routine, giving some new and important implications both in technology and in the industrial scale production of BCP nanostructures. Experiments were carried by solubilizing 67 kDa PS-b-PMMA in toluene, ethyl acetate and THF and depositing them on random copolymer layer, obtaining film with thickness around 30 nm. After deposition, annealing was performed in each case for allowing the SA process. Experiments performed in analogous conditions have shown that there is a dependence of the pattern obtained on the BCP film thickness. In particular, in the cases of those BCP films deposited from ethyl acetate solution, it has been assisted to an improvement of the features' homogeneity of the nanopores formed with decreasing the layer depth. Vice versa, for BCP films obtained from THF dispersion, the uniformity of SA obtained has shown an opposite trend in term of uniformity pattern-dependence and film thickness and, in this last case, better results were obtained for thicker polymer films. This result has suggested that the solvent used for the BCP-SA has actually a role on the order of nanostructures, which can be related to the chemical/physical characteristics of the solvent used, such as vapour tension and relative polarity. Any eventual inhomogeneities and particulates detected on the deposited film were indeed attributed to some non-negligible solvent-power effects. At the same time, different solvent volatility can establish competitive mechanism in the solvent evaporation: indeed, chemical with lower vapour tension, i.e. ethyl acetate, can be removed only by the effect of spin coating deposition and leads to a general more uniform BCP film with an improved morphology in thinner layers. Vice versa, THF, with a higher vapour tension, generates competitive evaporation mechanism which leads to BCP films with less uniformity and limited ordered pattern, which further worsens with reducing film thickness.

Aside the study on the morphology, a statistical survey was made on the most representative BCP films obtained by ethyl acetate and THF solution. The routine, made with analysing SEM images by ImageJ software, was run for counting porous structure obtained within specific and representative areas, extrapolating also their geometrical features, such as dimensions and circularity. Distribution curves were obtained by these data and results were compared. It has been found that when a better morphological homogeneity was achieved, this was also associated to sharp distribution of the geometrical features. In other words, for the same diameters, it was revealed a higher pore density. BCP layers obtained from ethyl acetate solution and THF have shown that, in both these cases, curves trend was consistent, reporting lower values for BCP pattern obtained from THF. The ordered, patterned area obtained was also calculated in both cases, finding that ethyl acetate solution gives the best results in term of ordered zones (up to 95%), with any dependence on the film thickness. Vice versa, in the case of films deposited by THF, ordered area was found to badly achieve 50% at most. Even if this latter one has returned better results in term of geometrical features achieved, SA was obtained only on very limited and small areas, while very promising results were achieved by using ethyl acetate, which has led up to 95% of ordered zones. This important result can lay the fundamentals for toluene-replacement in the BCP lithography, giving some new and important implications both in technology and in the industrial scale production of nanostructures

5.6 – Bibliography

[1] R.A. Puglisi, Towards Ordered Silicon Nanostructures through Self-Assembling Mechanisms and Processes, J. Nanomater. 2015 (2015). doi:10.1155/2015/586458.

[2] K.W. Guarini, C.T. Black, Y. Zhang, H. Kim, E.M. Sikorski, I. V. Babich, Process integration of self-assembled polymer templates into silicon nanofabrication, J. Vac. Sci. Technol. B Microelectron. Nanom. Struct. 20 (2002) 2788. doi:10.1116/1.1521730.

[3] F.S. Bates, G.H. Fredrickson, Block copolymers-designer soft materials, Phys. Today. 52 (1999) 32–38. doi:10.1063/1.882522.

[4] Rosaria Anna Puglisi, Valentina Lombardo and Sebastiano Caccamo (2017), "Silicon quasi-1Dimensional nanostructures for photovoltaic applications", Review Chapter, number 7, pages 131-153, in the Book: "Nanowires - New Insights", ISBN 978-953-51-5257-6, Ed, (2016). doi:10.5772/711.

[5] E.A. Men'shikov, A. V. Bol'shakova, I. V. Yaminskii, Determination of the Flory-Huggins parameter for a pair of polymer units from AFM data for thin films of block copolymers, Prot. Met. Phys. Chem. Surfaces. 45 (2009) 295–299. doi:10.1134/S2070205109030058.

[6] P.J. Flory, Themodynamics of high polymer solutions, J. Chem. Phys. 10 (1942) 51–61. doi:10.1063/1.1723621.

[7] M.L. Huggins, Solutions of long chain compounds, J. Chem. Phys. 9 (1941) 440. doi:10.1063/1.1750930.

[8] A. Andreozzi, E. Poliani, G. Seguini, M. Perego, The effect of random copolymer on the characteristic dimensions of cylinder-forming PS-b-PMMA thin films, Nanotechnology. 22 (2011). doi:10.1088/0957-4484/22/18/185304.

[9] K. Brassat, D. Kool, J. Bürger, J.K.N. Lindner, Hierarchical nanopores formed by block copolymer lithography on the surfaces of different materials pre-patterned by nanosphere lithography, Nanoscale. 10 (2018) 10005–10017. doi:10.1039/c8nr01397g.

[10] P. J. Flory, Principles of Polymer Chemistry, Cornell Univ. Press, 1953., (n.d.).

[11] C.T. Black, O. Bezencenet, Nanometer-scale pattern registration and alignment by directed diblock copolymer self-assembly, IEEE Trans. Nanotechnol. 3 (2004) 412–415. doi:10.1109/TNANO.2004.834160.

[12] K.W. Guarini, C.T. Black, K.R. Milkove, R.L. Sandstrom, Nanoscale patterning using self-assembled polymers for semiconductor applications, J. Vac. Sci. Technol. B Microelectron. Nanom. Struct. 19 (2001) 2784. doi:10.1116/1.1421551.

[13] P. Mansky, Y. Liu, E. Huang, T.P. Russell, C. Hawker, Controlling polymer-surface interactions with random copolymer brushes, Science (80-.). 275 (1997) 1458–1460. doi:10.1126/science.275.5305.1458.

[14] K.W. Guarini, C.T. Black, S.H.I. Yeuing, Optimization of diblock copolymer thin film self assembly, Adv. Mater. 14 (2002) 1290–+. doi:Doi 10.1002/1521-4095(20020916)14:18<1290::Aid-Adma1290>3.0.Co;2-N.

[15] S.H. Kim, M.J. Misner, T. Xu, M. Kimura, T.P. Russell, Highly oriented and ordered arrays from block copolymers via solvent evaporation, Adv. Mater. 16 (2004) 226–231. doi:10.1002/adma.200304906.

[16] Mat. Res. Soc. Symp. Proc. Vol. 728 © 2002 Materials Research Society, 728 (2002) 1–8. doi:10.1557/PROC-728-S4.9.

[17] A. Checco, A. Rahman, C.T. Black, Robust superhydrophobicity in large-area nanostructured surfaces defined by block-copolymer self assembly, Adv. Mater. 26 (2014) 886–891. doi:10.1002/adma.201304006.

[18] K.G. Yager, E. Lai, C.T. Black, Self-assembled phases of block copolymer blend thin films, ACS Nano. 8 (2014) 10582–10588. doi:10.1021/nn504977r.

[19] K.W. Guarini, C.T. Black, S.H.I. Yeung, Optimization of diblock copolymer thin film self assembly, Adv. Mater. 14 (2002) 1290–1294. doi:10.1002/1521-4095(20020916)14:18<1290::AID-ADMA1290>3.0.CO;2-N.

[20] K.W. Guarini, C.T. Black, K.R. Milkove, R.L. Sandstrom, Nanoscale patterning

using self-assembled polymers for semiconductor applications, (2001) 2784–2788. doi:10.1116/1.1421551.

.

Appendix A

Spin-coating deposition

In the wide panorama of deposition techniques, liquid-phase approaches, such as spin-coating, spray-coating and dip-coating, are considered to be some of the most versatile and cheapest. These techniques are suitable for depositing liquid materials or solution, i.e. high molecular weight polymer dissolved in an organic solvent [1]. In all this technique, the main step are the dropping of solutions or liquids onto the substrate and the solvent evaporation. Usually, this leads to a solid-state thin film which appears uniform, adherent, defect-free, and covers the entire surface of the underlying substrate. Among the three mentioned approaches, spin coating in certainly the most used, especially for in-solution dispersed polymeric materials.

A schematic representation of the spin coating technique is shown in Fig. A.1:

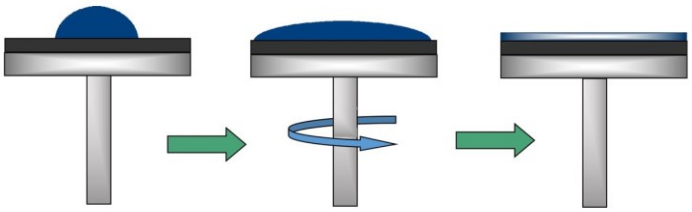

Fig. A.1: Sketch of the spin-coating deposition.

In a common spin coating deposition procedure, the substrate is held in a vacuum chuck and it can be sometimes pre-treated or pre-heated for increasing the adhesion of the adhesion between its surface and the spun material. The deposition process stars when the solution is pipetted at the centre of the substrate ad then spread out toward the substrate's edges because of a rotation applied. At the very beginning, the rotational velocity is approximately 500 min^{-1}, but is then increased up to 2000-4000 min^{-1}. It is in this condition that the desired film thickness of the material is formed [2].

Film thickness obtained by spin coating can be rationalized through an empirical equation supplied by Thompson [1]. Given a liquid polymer system with a constant molecular weight, solution concentration etc., the film thickness can be calculated by the following equation:

$$t = k\omega^{\alpha}$$

In which ω is the rotational velocity and both k and α are constants. A graph reporting a log-log pot of the film thickness as a function of the rotational velocity, must return a linear curve in which slop is represented by α value. In the case in which the concentration of depositing solution changes, the thickness of the obtained film will be given by:

$$t = k'C^{\beta}$$

Where this time both k' and β are constants. In this case the linear curve as slope equivalent to β when graph of log(t) as a function of log(ω) is presented.

Molecular weight (obtained by measurements of the intrinsic viscosity) of the deposited polymer has also a certain influence of the film thickness. This dependence can be expressed as:

$$t = k''\eta^{\gamma}$$

With k'' and γ are constants. The three equations listed above can be combined in a unique one, thus expressing the film thickness as a function of spinning speed, the solution concentration and the molecular weight, thus writing the following:

$$t = \frac{KC^{\beta}\eta^{\gamma}}{\omega^{\alpha}}$$

Where parameter K includes all constant values.

Bibliography

[1] Thompson LF (1994) Resist processing. In: Thompson L, Willson GC, Bowden MJ (eds), Introducing into microlithography, 2nd edn. America Chemical Society, Washington.

[2] Gatzen HH, Saile V, Leuthold J, Micro and Nano Fabrication. Tools and Process. Springer-Verlag Berlin Heidelberg 2015.

Appendix B

Electrical measurements

One of the most important features to electrically characterize a material is the resistivity, ρ. This is an inherent parameter, which means that it does not depend on the sample shape, size or thickness, but it is proper of a given material, and gives a measure of how much it opposes to the crossing electrical flow. Being an inherent characteristic, resistivity depends on free charges density, both electrons and holes, indicated with *n* and *p* respectively, and on their mobility, μ_n and μ_p, according to the following relationship:

$$\rho = \frac{1}{q(n\mu_n + p\mu_p)}$$

From the resistivity value it is possible to calculate the conductivity of a material, σ, which in its turn is also an inherent feature. These two parameters are related with each other by the following:

$$\sigma = \frac{1}{\rho}$$

The resistivity of a material, in principle can be measured by the two-point probe method. A linear voltage-current, V-I, graph allow to calculate the resistance of the entire system by applying the Ohm's law:

$$V = RI$$

In which the slop of the linear curve corresponds to the material resistance, R. Nevertheless, this value cannot be related directly to the resistivity of the material, since it corresponds to a total resistance, R_T, which is given by the contribution of three variables: R_w, relative to the wire or probe resistance, R_c the contact resistance and R_{DUT} which indicated the real resistance of the material under investigation. The relationship between them can be summarized in the following formula:

$$R_T = \frac{V}{I} = 2R_w + 2R_c + R_{DUT}$$

From this last one, it can be deduced that when R_w and R_c are much larger with respect to the resistance of the material, they can significantly affect the final value R_T, which could be significantly different from R_{DUT}. In order to exclude the contribution coming from the contact resistance and those ones relative to the probes used, it is worth to use the so-called four-point probe method, 4PP. In this approach, two more probes are present in the measuring system, and terminals which supply current to the material under investigation are not the same of those ones which measure the bias. Even if the terminals measuring the voltage contain both probe and contact resistance in their turn, the current which flow into the voltage path is low thanks to the high input impedance of the voltmeter. This let fall the contribution coming from R_w and R_c, and thus the resistance measured corresponds to the actual resistance of the material, R_{DUT}.

In the four-point probe method, however, the relationship which binds R, V and I is not so intuitive. For a complete discussion on how to derive the resistivity formula in 4PP method, we refer to more specific texts [1]. Here we instead report the final formula which allow to calculate the electrical parameter of the material. For 4PP

method used with the four probes in a linear configuration and equal probe-probe spacing, s, the resistivity is obtained as in the following:

$$\rho = \frac{\pi}{\ln(2)} t \frac{V}{I} = 4.532\, t \frac{V}{I}$$

Where t is the thickness of the material under investigation. Dividing both members of the equation above for the investigated thickness t, the equation can be written as:

$$R_{sh} = \frac{\rho}{t} = 4.532 \frac{V}{I}$$

R_{sh} is defined as the sheet resistance, and virtually represents the value of resistance for an infinitely thin, uniformly doped layer. When required, the sheet resistance calculated by voltage-current measurements must be opportunely corrected by some correction factors related to the sample thickness, the lateral sample dimensions, probe spacing shape of sample under investigation, probes placement relative with respect to the sample edges. Sheet resistance formula including the corrections factor can be written as:

$$R_{sh} = 4.532 F \frac{V}{I}$$

Where F represents the arithmetic product of all the needed correction factors. For this purpose, in all the cases reported in which sheet resistance was measured, we used the following graphs for deriving the appropriate correction factors, Fig. B.1a and b from Ref. [2]:

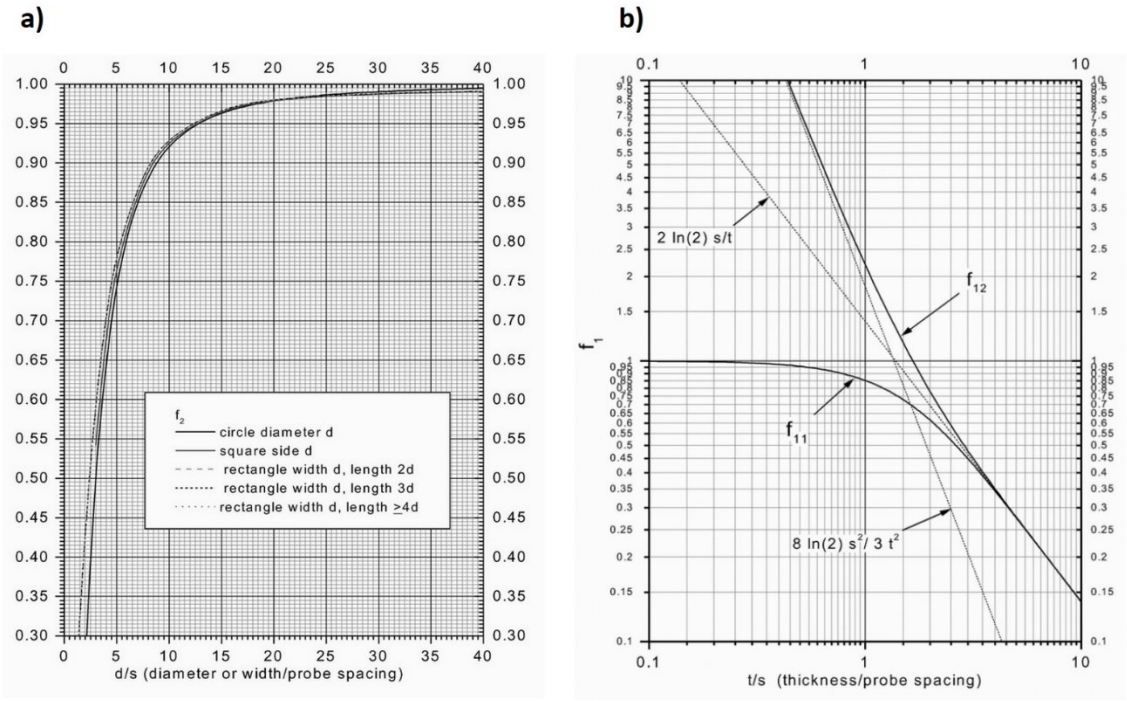

Fig. B.1: Graphs for obtaining the sheet resistance correction factors relatively to a) lateral size, probe spacing and sample shape and b) sample thickness, probe spacing and insulating/conducting bottom boundary conditions.

Film conductivity, always expressed as S/cm in this thesis, was obtained according to the following formula:

$$\sigma = \frac{1}{\rho} = \frac{1}{tR_{sh}}$$

Bibliography

[1] D.K. Schroeder, Semiconductor Material and Device Characterization, Wiley 1990

[2] F.M.Smits, "Measurement of Sheet Resistivities with the Four-Point Probe", The Bell System Technical Journal 37, 711-718 (1958)

Appendix C

Scanning Electron Microscopy

Scanning Electron Microscopy (SEM) is a high-resolution technique which allows to acquire images by scanning in a raster scan pattern a sample through an electron focused beam. This technique leads to information concerning the topography, morphology and elemental composition of the sample. The most common detection mode used in a SEM exploits the secondary electrons emitted by the excitation of the sample's atoms with the probe electrons. In this way, the pixel by pixel image is acquired, recorded and displayed in real time showing the topography of the sample surface [1]. A scanning electron microscope is normally equipped with a source of electrons, a column of electromagnetic lenses in which the electron beam coming from the source is driven and finely focused on the sample, secondary electron detector, sample chamber, computer interfaced and monitor on which the image is displayed, vacuum system (Fig. C.1). The probe electrons are produced by the cold-emission cathode source at the top of the column. Electrons are then accelerated through the column thanks to a combination of electromagnetic lenses and apertures, thus producing a focused beam which interacts with the sample's surface. Sample is placed on a moving stage, which allows to tilt it when required. Both sample and stage are located in a chamber which is evacuated by a pump system, reaching value of internal pressure below than 10^{-7} mbar. The movements of the electron beam are allowed thanks to scan coils, situated above the objective

lens. The powerful electrons sent to the sample are able to penetrate its surface for a certain depth which can is a function of the accelerating voltage, the density of the sample and its composition [1].

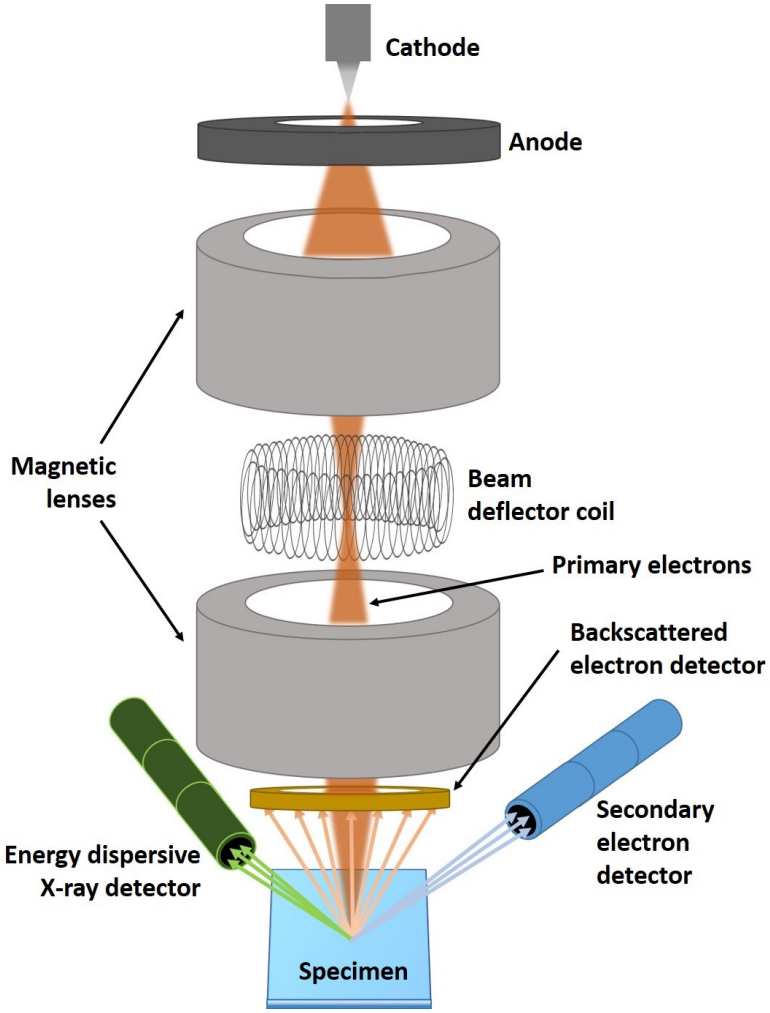

Fig. C.1: schematic representation of the main components of a scanning electron microscope.

The resulting interaction between these probe electrons and the sample's surface produces different species which can be detected as different signals and that

supply information about the sample. They are mainly backscattered, secondary and Auger electrons. In parallel, X-ray signals which are characteristic of the elements which compose the sample, are also produced. Using opportune detectors for all these species, it is possible to obtain some specific information about the sample under investigation. They include topography (through primary and secondary electrons emitted from the sample), surface characteristics (supplied by the Auger electrons) and specimen elemental composition (which exploits the X-rays collected). The scanning electron microscope used in this thesis was field emission Scanning Electron Microscope (Zeiss Supra35 FE-SEM) equipped with energy dispersive X-ray (EDX) microanalysis system (Oxford Instruments, X-MAX, 80 mm^2). The instrument has usually operated with an EHT not exceeding 3kV for avoiding any damage to the polymer species under investigation in this work. Elemental composition of sample was obtained by using the EDX detector. When dielectric polymer samples, such as BCP were investigated, a silver track was deposited on them by silver paste. This was made in order to prevent any resolution losses due to charging effects of the sample's surface.

Bibliography

[1] W. Zhou, Z. Lin Wang, Scanning Microscopy for nanotechnology: techniques and applications, Springer 2006

Appendix D

Raman spectroscopy

Raman spectroscopy is a technique which exploits the vibrational modes occurring in molecules in order to identify the chemical specimen or the crystal structure of the sample under investigation.

Its working principle is based on the excitation of the vibrational, rotational, and other low-frequency modes in a system as a consequence of the interaction with a laser source (Fig. D.1a). Usually, for providing the information concerning the fingerprint signals of a chemical specie, the excitation wavelength of the laser source has to be within the near infrared and the near ultraviolet range. When a chemical specimen interacts with the electromagnetic radiation, the electron clouds is distorted and generates a virtual state, which is unstable and leads to immediate relaxation of the photon toward less energetic vibrational levels. This phenomenon can occur through three different paths. In the first one, the electron is excited from the vibrational ground state and falls into a virtual one. When it loses its energy, going back to the starting level, the radiation emitted has the same characteristics, in terms of energy, wavelength and frequency, of the incident one. This mechanism thus conservers the whole energy of the system, the scattering is elastic, and the radiation emitted is called "Rayleigh scattered light" (Fig. D.1b). Vice versa, when the emitted radiation has different characteristics than the incident one, the light

scattering involves through an inelastic process (Raman scattering). This can take place by two mechanisms: when the electron is excited from the ground state (V_{GS}) and falls in the virtual one and then relaxes into a vibrational level ($\neq V_{GS}$), it involves energy absorption by the molecule. In this case, the radiated light has less energy than the incident one. The radiation generated in this case takes the name of "Stokes Raman scattering" (Fig. D.1c). By contrast, if the light emitted during the relaxation process has higher energy than the incident source, the scattered light obtained is called "anti-Stokes Raman scattering" (Fig. 1d).

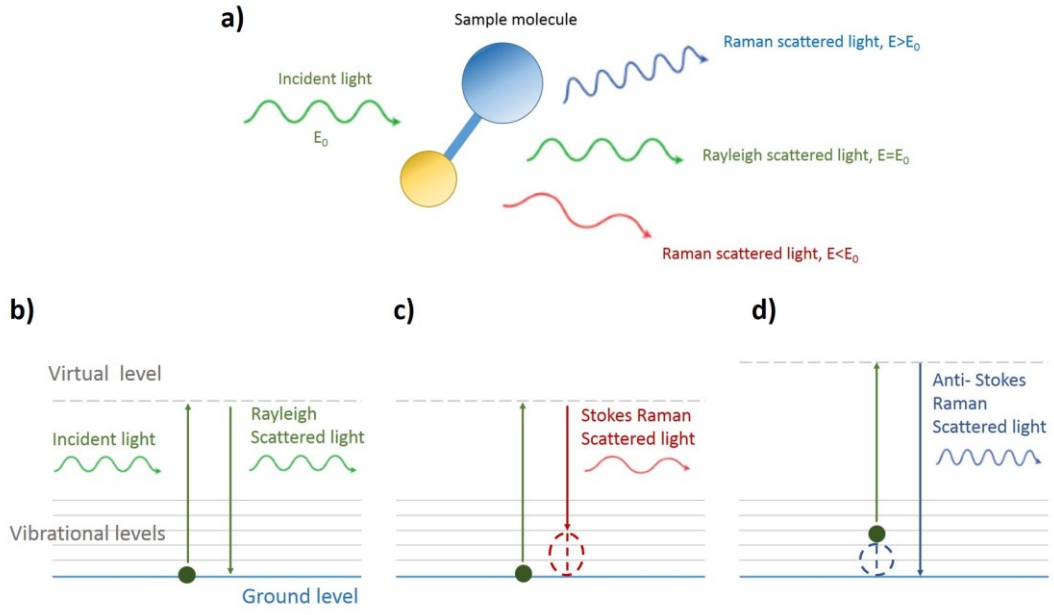

Fig. D.1: Schematic representation of the Raman scattering. When a specific radiation intercepts a molecule, three different radiations are produced, as represented in a); b) representation of the Rayleigh scattering light and of Raman c) Stokes and d) anti-Stokes light.

It has to be considered that the predominant contribution is always given by the Rayleigh scattering, while the Raman mechanism contributes for only the

0.000001%, thus returning very weak radiations. By considering only the inelastic process, the ratio of Stokes and anti-Stokes Raman scattering is a function of the population of the various states of the molecule. At room temperature, this ratio is in favor of the first one, since the number of molecules in an excited vibrational state is smaller that of the ground level, thus generation more intense Stokes Raman light. For this reason, standard Raman measurements are performed by only acquiring the Stokes Raman scattering, while Rayleigh scattered light is reject by an opportune filter. Alternatively, since the increase of the temperature causes a change of the population state of vibrational levels, it allows the measurement of the sample temperature of trough the intensity ratio of the anti-Stokes and Stokes emissions.

The main interesting related to a Raman analysis mainly lies on the fact that it is non-destructive and does not need any preliminary sample preparation, also offering a high spatial resolution up to a sub-micron scale.

In this thesis, Raman analysis was performed in order to observe if any change occurs after the chemical modification due the acidification. Moreover, peak identification was used in order to recognize PEDOT and PSS, thus giving an estimation of the relative amount of these two components in the pristine blend and in the modified polymer. The excitation wavelength is specified time by time in the spectra reported in Chapter 3 and 4. The laser power was opportunely chosen in order to avoid any sample damage or chemical decomposition. It was started from low laser power LP1 (Fig. D.2) and then slightly increasing up to reaching a clear Raman spectrum without causing any modification in the sample (LP3 in Fig. D.2). The value of laser power found for LP3 was ≈1.3 mW and was kept constant in all the characterization, in order to make all the results between each other. All Raman

analysis were performed by a WITec Alpha 300 RS instrument in the backscattering mode.

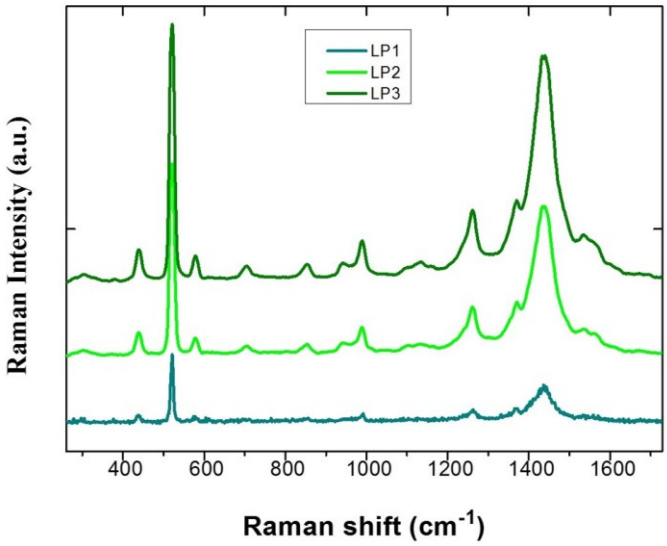

Fig. D.2: Raman spectra of a pristine PEDOT:PSS thin film deposited on a silicon substrate. Laser power is indicated as LP and is reported as LP1<LP2<LP3. LP3 was measured by a power meter and estimated to be ≈1.3 mW.

Bibliography

[1] Challa S. S. R. Kumar, "Raman Spectroscopy for Nanomaterials Characterization", Springer-Verlag Berlin Heidelberg 2012

Closing Remarks

All the images displayed in this thesis are original and were designed by the author (Valentina Lombardo), specifically for this manuscript (this statement is not applied for literature data in which is clearly indicated the source reference within the caption).

The experimental data and the schemes reported in this thesis were performed and collected by the author, with the following exceptions:

- **Chapter 1:** Fig. 1.12 can be found in Ref. [23], "A.M. Nardes, M. Kemerink, R.A.J. Janssen, J.A.M. Bastiaansen, N.M.M. Kiggen, B.M.W. Langeveld, A.J.J.M. Van Breemen, M.M. De Kok, Microscopic understanding of the anisotropic conductivity of PEDOT:PSS thin films, Adv. Mater. 19 (2007) 1196–1200. doi:10.1002/adma.200602575".
- **Chapter 1:** Fig. 1.13 belongs to Ref. [43], J. Ouyang, Q. Xu, C.W. Chu, Y. Yang, G. Li, J. Shinar, On the mechanism of conductivity enhancement in poly(3,4- ethylenedioxythiophene):poly(styrene sulfonate) film through solvent treatment, Polymer. 45 (2004) 8443–8450. doi: 10.1016/j.polymer.2004.10.001.
- **Chapter 5:** Fig. 5.1 and Fig 5.2 were both reproduced from the Ref.[12], K.W. Guarini, C.T. Black, K.R. Milkove, R.L. Sandstrom, Nanoscale patterning using self-assembled polymers for semiconductor applications, J.

Vac. Sci. Technol. B Microelectron. Nanom. Struct. 19 (2001) 2784. doi:10.1116/1.1421551

Section dedicated to PhD candidate

Publications

- Rosaria Anna Puglisi, **Valentina Lombardo** and Sebastiano Caccamo (2017), "Silicon quasi-1Dimensional nanostructures for photovoltaic applications", Review Chapter, number 7, pages 131-153, in the Book: "Nanowires - New Insights", ISBN 978-953-51-5257-6, Editor: Dr. Khan Maaz, Intech.

- **Valentina Lombardo**, Luisa D'Urso, Giovanni Mannino, Silvia Scalese, Daniele Spucches, Antonino La Magna, Antonio Terrasi, Rosaria A. Puglisi, "Transparent conductive polymer obtained by in-solution doping of PEDOT:PSS", *Polymer 155 (2018) 199–207*

- **Valentina Lombardo,** Salvatore Di Franco, Luisa D'Urso, Antonino La Magna, Antonio Terrasi, Rosaria A. Puglisi. "Conductive free-standing polymer paste synthesized by acid induced phase separation", IEEE Conference, RTSI 2018

- **Valentina Lombardo,** Salvatore Di Franco, Luisa D'Urso, Antonino La Magna, Antonio Terrasi, Rosaria A. Puglisi, "Highly conductive, free-standing PEDOT:PSS paste obtained by in-solution process", *submitted*

- **Valentina Lombardo,** Luisa D'Urso, Francesca Lo Presti, Silvia Scalese, Antonino La Magna, Rosaria A. Puglisi, "Block copolymer self-assembling with novel solvents", *under review*

Poster presentations

"Deposition of PEDOT:PSS layers for application in homojunction Si solar cells"

R. A. Puglisi, **V. Lombardo**, G. Mannino, S. Scalese, A.Terrasi, A. La Magna

Materials.it 2016

12-16th December 2016 - Aci Castello (Catania), Italy

Oral communications

- "Polymeric Transparent electrodes obtained by in solution-doping of PEDOT:PSS", **Valentina Lombardo**, Luisa D'Urso, Giovanni Mannino, Silvia Scalese, Daniele Spucches, Antonino La Magna, Antonio Terrasi, Rosaria A. Puglisi

  International Conference on Semiconductors, Optoelectronics and Nanostructures

  20-21st August 2018 – Paris, France
- "Conductive free-standing polymer paste synthesized by acid induced phase separation"

Valentina Lombardo, Salvatore Di Franco, Luisa D'Urso, Antonino La Magna, Antonio Terrasi, Rosaria A. Puglisi

4th International Forum on Research and Technologies for Society and Industry

10-13th September 2018 – Palermo, Italy

Schools

- "Joint EPS-SIF International School on Energy 2017",
  21-26th July 2017, Villa Monastero, Varenna, Lago di Como, Italy.
- "Erice Energy School 2016",
  13-19th July 2016, Erice (Trapani), Italy

Lectures

- 16-19 May 2016, CNR-IMM, Strada VII, Z.I., Catania
  - Dr. Antonino La Magna: "La simulazione dei sistemi complessi nella scienza dei materiali", 16 hours
  - Dr. Sabrina Conoci: " Le micro e le nano tecnologie nell'analisi del DNA ", 16 hours

- 16-20 January 2017, Viale delle Scienze, Palermo

- Prof. Francesco Giannici: "Spettroscopia di assorbimento dei raggi X nello studio dei materiali.Concetti di base ed analisi di dati sperimentali", 8 hours
- Prof. Rosalinda Inguanta: "Metodi elettrochimici per la deposizione e caratterizzazione di semiconduttori per celle solari", 8 hours
- Prof. Francesco Ferrante: "Spettroscopia computazionale", 12 hours

- 23-27 January 2017, Via Archirafi, Palermo
  - Prof. Simone Agnello: "Spettroscopia Raman e microraman: Applicazioni allo studio dei materiali", 10 hours
  - Prof. Marco Cannas: "Spettroscopia di emissione risolta in tempo. Applicazioni allo studio dei materiali", 10 hours

- "Functional nanostructures: from microelectronics to biomedicine" at Scuola Superiore di Catania
  - Prof. Ausrine Bartasyte (1-3 February 2017, 14 hours)
  - Prof. Adolfo Speghini (8-9 Febbraio 2017, 10 hours)
  - Prof. David Munoz Rojas (13-15 Febbario 2017, 10 hours)

Seminars and Forums

- "Scientific Writing", 9-10th July 2016, Dr. Maria Bellantone
- 10 PhD Days at Scuola Superiore di Catania, June-September 2016
- Prof. Valeria Nicolosi, "New frontiers opened by the world's thinnest materials", 19th December 2016, Dipartimento di Scienze Chimiche, Catania.

- Prof. Leon Gradon, “Formation of nanostructured functional particles”, 29-30th June 2017, CNR-IMM HQ, Catania.
- Dr. Felice Torrisi, "Nanostructured films of Graphene and Two-dimensional Materials: electronic transport, non-linear optics and THz photonics", 2nd October 2017, Dipartimento di Fisica e Astronomia, Catania
- Agilent forum: “Tecnologie del vuoto. Forum per la ricerca e l’industria”, 20th September 2017, INFN - Laboratori Nazionali del Sud, Catania.

Acknowledgements

As a wise person* (and friend) said once, PhD is not just an academic title but, more than other things, it is a journey and an important piece of one's life. Whatever the research went, whatever the results obtained, PhD is a great opportunity for everyone to grow, to improve yourself as a scientist, as a worker, as a person. This complex path needed patience, devotion and the help of those people who were at my side and to whom I want to dedicate few lines.

I wish to thank my tutor, Prof. Antonio (Tony) Terrasi, for precious and paternal advices, for all the encouragements, for having helped and supervised me when I needed, with patience and affection.

My deepest gratitude goes to my co-tutor and supervisor, Dr. Rosaria Puglisi, for having given me the opportunity to do this path, for having welcomed, taught and always guided me, even in moments of discouragement. Thanks also for being a friend sometimes and for some very nice moments spent together, just drinking and chatting.

My most sincere thankfulness to all the amazing people met during these three years at the CNR! Thanks to all the staff of researchers and technicians: Antonino, Giovanni, Salvo (Pannitteri), Markus, Domenico, Simona, Stefania, Antonella, Alessandra, Francesco, Antonio and Corrado. A special thank has to go to Dr. Silvia Scalese (for having almost “adopted” me in her group, for her lovely way of speaking and for all the lunches and coffee times), to Salvo (Di Franco, who deserves a special note for advices, suggestions, for the time he had dedicated to me … and for gossip, as well) and to Alfio (who has always rushed when I needed

help, even for the most trivial things). Thanks also to the girls of the administrative staff: Anna, Francesca, Giovanna and Giusy.

Among the people met during these three years at the CNR, there are also those ones who I use to call friends, with which I shared smiles and tears, laughs and gripes, peaceful moments and arguments, trips and chats. Here, my warmest thanks to some special guys as Marziuccia (aka Marzia Ferragna), Daniele (DD), Lele (Lillo, sometimes), (Zu) Stefano, Salvuccio (Slombi), Rosa (never forgotten!), Francesca (my little padawan), Rossana (who is always in our thoughts, despite the distance), Michele, Gabriella (The Queen), Antonio (Mio), Seby, Monia, Enzo, Giovanni, Valentina, Francesca, Luca and to my "travel friends", Giacomo, Alice, Bernardo, Antonio, Anna and Vanessa (…her also for suppling Giulia as the mascot of this PhD!).

My gratitude goes to Simona*, my Wawa, friend and sister, for understanding me with sweetness, for believing in me and for being one of the greatest examples of strength. Thanks for all the time we spent together, for laughs, discussions, suggestions and for having taught to me that there is always a bright side in everything. Thanks for this Journey!!

Thanks to Mom and Dad, who have always understood my feelings (even when I was not able to explain them) and have supported me, always and with unconditional love and patience (… all well-seasoned with lots of feline affection).

Finally, thanks to Marco, my new family, for being always at my side, for being a friend, a partner and that person to discuss with, to learn from and a shoulder on which to lean. Thanks for having guided me in this journey. Thanks for the new one we have started together.